Functions of Myosin-X in Polarized Epithelial Cells

Katy C. Liu

A dissertation submitted to the faculty of the University of North Carolina at Chapel Hill in partial fulfillment of the requirements for the degree of Doctor of Philosophy in the Department of Cell and Molecular Physiology.

Chapel Hill
2012

Approved by:

Richard Cheney, PhD

John Rawls, PhD

Alan Fanning, PhD

Carol Otey, PhD

Mark Peifer, PhD

ABSTRACT

KATY LIU: Functions of Myosin-X in Polarized Epithelial Cells
(Under the direction of Dr. Richard E. Cheney)

Myosin-X (Myo10) is an unconventional myosin, known functions of which have been largely deduced through studies in non-polarized cells. Myo10 is well-known for localizing to the tips of filopodia and has important roles in filopodial formation. Myo10 is expressed at high levels in epithelial tissues such as kidney, yet relatively little is known about the functions of Myo10 in polarized epithelia. Here, we determine that Myo10 localizes to the basolateral domain of polarized epithelial cells and has important functions in junction assembly and epithelial morphogenesis.

Polarized epithelial cells have apical and basolateral domains, which are separated by the apical cell junction. Normal functions of polarized cell junctions, such as barrier formation and maintenance of cell polarity, are critical. Dysfunction is commonly observed in inflammatory diseases and infection where the epithelial barrier is breached, and in ischemic states and invasive cancers, where malignant cells undergo epithelial to mesenchymal transition. Thus, it is important to identify molecules that mediate these processes in polarized epithelia.

In kidney, we found that Myo10 is expressed at the basolateral domain. We then used MDCK cells as a cell culture model to generate stably expressing GFP-Myo10 and Myo10 knockdown lines. Consistent with our results *in vivo*, GFP-Myo10 localized to the lateral membrane during junction assembly. Importantly knockdown led to a delay in

junction formation and increased paracellular permeability. Furthermore, Myo10 knockdown resulted in abnormal multiple lumen formation during cystogenesis.

In fully polarized cells, GFP-Myo10 showed striking localization to the tips of basolateral filopodia. Intriguingly, GFP-Myo10 HMM (heavy mero-myosin, a construct lacking the tail) was found at apical microvilli. Yet, localization experiments using GFP-Myo10 and anti-Myo10 antibodies showed full-length Myo10 is not detected in microvilli. Moreover, knockdown studies indicated that Myo10 does not appear to function in the formation of microvilli. Nonetheless, the apical localization of GFP-Myo10 HMM led us to investigate apico-basal targeting of Myo10. The tail of Myo10 localized to the basolateral membrane, and deletion of the pleckstrin homology (PH) domains resulted in localization to the apical microvilli. Additionally, disruption of phosphatidylinositol binding partially redistributed Myo10 to apical microvilli. Our results suggest Myo10 targeting to basolateral filopodia is regulated by PH domains of the tail.

Recent studies have revealed that basolateral filopodia are critical for normal tissue patterning, yet relatively few proteins are known to localize to and function in basolateral filopodia. Given the importance of Myo10 in filopodia and the functions we have discovered here in polarized epithelia, it is likely that Myo10 mediates critical processes in basolateral filopodia, a subject that beckons further investigation.

ACKNOWLEDGEMENTS

The journey that has brought me to this point has been uncommon to say the least. Over the years, I have had amazing opportunities to study science, medicine, architecture and engineering. I have been privileged to learn from experts and pioneers in their fields. My journey has taken me to England (twice) and back. Graduate school has been a formative period of scientific and personal growth. With the help of colleagues and friends, it has been a positive experience that has helped shape me into the person who I am today.

I am privileged to have had excellent mentors along the way. Guided by these mentors, I have gained valuable scientific knowledge and skills, presentation skills and the mental capacity needed to pursue a career in science. I am most grateful for my advisor, Dr. Richard Cheney who has been a phenomenal scientific role model. I am always astounded by his boundless scientific knowledge, not only the facts, but also the methods, pitfalls and the history. Perhaps most importantly, Richard has instilled in me an ongoing passion and curiosity for scientific knowledge, which I feel speaks to the heart of why many of us chose to become scientists. Finally, I thank Richard for his continuous patience and support. Also, thanks to my committee, Drs. Alan Fanning, Carol Otey, John Rawls and Mark Peifer, for their guidance that aided my thesis project to succeed. I am also grateful to my college thesis advisor, Dr. Maria Garlock, whom I always look to as a female academic role model. She has been and continues to be supportive of me, taking a genuine interest in my

academic pursuits that have ranged from civil engineering to medicine. Finally, Dr. Michael Goy has been an excellent professor and a true friend.

I have also been extremely fortunate to have had amazing labmates – Melinda DiVito, Mike Kerber, Taofei Yin, Alex Raines, Brian Dunn and Damon Jacobs – who made for an extremely collaborative and enjoyable work environment. Our special group of "Cheneyites" not only worked well together but also became great friends, sharing countless laughs and memorable times in and outside of lab. I especially thank Damon who patiently and selflessly mentored me as a rotation student at the start of my project.

Thank you to the Department of Cell & Molecular Physiology, as it is a wonderful and supportive department. Ann Stuart and her Presentation Class are a unique aspect of our program that has instilled in me valuable skills I will use throughout my career. I am particularly appreciative of the administrative staff – Adriana Tavernise, Vicki Morgan and Jan McCormick were extremely helpful and made the students in the department feel comfortable and at home. Finally, I thank the UNC MD/PhD program for their gracious and unconditional support, particularly Dr. Eugene Orringer, Dr. David Siderovski, Dr. Kym Rathmell and Alison Regan, who are truly remarkable for their academic and career mentoring as well as their genuine caring and concern for my training.

Lastly, the continual love and support of my family and friends are priceless. I've relied on the amazing support and encouragement of my closest friends, Nikki Hastings and Monica Kim. Really, they're family to me. Finally, thank you to my parents and my brother, Tom, who are and will always be there for me. I only hope that, one day, I can give back to the incredible people and places that have supported me through these years.

TABLE OF CONTENTS

LIST OF FIGURES

LIST OF MOVIES

LIST OF ABBREVIATIONS

aa	amino acid
Ab	antibody
AJ	adherens junction
AQP1	aquaporin-1
AQP2	aquaporin-2
ATP	adenosine triphosphate
B	beads
bp	base pair
Caco-2	colon adenocarcinoma-2
CC	coiled coil
CD	Celiac disease
CLP	calmodulin-like protein
DN	dominant negative
ECM	extracellular matrix
EHEC	enterohemorrhagic E. coli
EPEC	enteropathogenic E. coli
F-actin	filamentous actin
FACS	fluorescence-activated cell sorting
FERM	band 4.1, ezrin, radixin, moesin
GFP	green fluorescent protein
HEK293	human embryonic kidney 293

HGF	hepatocyte growth factor
HMM	heavy mero-myosin
Ig	immunoglobulin
IP	immunoprecipitation
kD	kilodalton
L	lysate
LLC-PK1	porcine kidney cell line
LSB	loading sample buffer
M10	Myosin-X
MALDI-TOF	matrix-assisted laser desorption/ionization-time of flight mass spectrometer
MDCK	Madin-Darby canine kidney
MID	Microvillous Inclusion Disease
min	minutes
mRNA	messenger RNA
Ms	mouse
Myo10	Myosin-X
MyTH4	myosin tail homology 4
NI	non-immune
NS	non-specific
PBS	phosphate buffered saline
PFA	paraformaldehyde
PI	phosphoinositide

PI3K	phosphoinositide 3-kinase
PIP2	phosphatidylinositol-4,5-bisphosphate
PIP3	phosphatidylinositol-3,4,5-trisphosphate
PH	pleckstrin homology
pLL	pLentiLox
Rb	rabbit
rpm	rotations per minute
qrtPCR	quantitative real-time polymerase chain reaction
SDS	sodium dodecyl sulfate
SEM	scanning electron microscopy
s	seconds
SAH	stable alpha helix
sh	short hairpin
shRNA	short hairpin RNA
siRNA	small interfering RNA
Sup	supernatant
TBST	Tris buffered saline + Tween 20
TEM	transmission electron microscopy
TER	transepithelial electrical resistance
TIRF	total internal reflection fluorescence
TJ	tight junction
µg	micrograms

µl	microliters
µm	micron
WCL	whole cell lysate
ZO-1	Zonula Occludens-1

CHAPTER ONE

INTRODUCTION

Polarized Epithelia and Cell Junctions are Important for Normal Physiology and can be Compromised in Disease States

Polarized epithelial cells line organs in the body such as the kidney tubules and the small and large intestines. These specialized cells function to absorb nutrients, ions and water, and to provide a protective barrier against luminal antigens and pathogens. These functions are made possible by the polarized structure and uneven distribution of proteins and lipids in polarized epithelial cells. The polarized structure consists of the apical domain which faces the lumen, and the basolateral domain where cell-cell interactions and cell-substrate interactions occur. The apical domain includes microvilli and the terminal web. Microvilli are actin-rich, finger-like projections that are directed toward the lumen. The roots of the microvilli terminate in a dense meshwork of actin called the terminal web. The apical and basolateral domains are separated by cell junctions. The cell junction is a structural complex comprised of the tight junction and adherens junction. The paracellular barrier is maintained by the tight junction, which blocks the translocation of most solutes, microorganisms and luminal antigens. The basolateral domain can be further divided into lateral and basal surfaces. The lateral membrane is the site of cadherin-based cell-cell adhesion, while the basal surface facilitates integrin-mediated cell-substrate adhesion.

Polarized epithelial cells organize into cell sheets and are crucial for organ development; during development, polarized epithelial cells organize into complex three-dimensional cysts and tubules in a process called epithelial morphogenesis. Furthermore, maintenance of polarized epithelial cells is important, as compromises to polarity are characteristic in certain disease states such as ischemia, inflammatory diseases, bacterial infection and cancer. Thus, the establishment and maintenance of polarized epithelial cells is critical for normal physiology.

During ischemic injury in the kidney, loss of oxygen perfusion leads to depletion of cellular ATP and rearrangements in epithelial polarity. Following ischemic injury, the polarized distribution of proteins is lost; the normally basolateral Na^+-K^+ ATPase appears at the apical domain, and the apical leucine aminopeptidase is found at the basolateral membrane (Molitoris, 1991). Ischemic injury can also result in the loss of polarity of integrins (Goligorsky et al., 1993) as well as a compromised tight junction barrier; both can cause increased membrane permeability and back-leak of filtrate into the underlying basement membrane (Goligorsky et al., 1993).

In the gut, increased epithelial permeability can result from defects in the cell junctions, as is seen in Crohn's disease or infections with intestinal parasites or bacteria (Laukoetter et al., 2006). Crohn's disease is an inflammatory bowel disease that is characterized by transmural inflammation of the intestine, most commonly in the distal small intestine. Tissue from Crohn's patients shows tight junction proteins are disrupted (Oshitani et al., 2005), and junctional protein expression and mRNA are down-regulated (Gassler et al., 2001). This junctional dysregulation contributes to increased intestinal

epithelial permeability (Laukoetter et al., 2006). Evidence suggests that alterations in epithelial permeability in Crohn's may precede the onset of disease (Irvine and Marshall, 2000; Podolsky, 2002); moreover, damage to the apical domain of intestinal epithelial cells is compounded by the overproduction of pro-inflammatory cytokines (Bruewer et al., 2003).

Additionally, intestinal parasites and bacteria such as enteropathogenic and enterohemorrhagic *E. coli* (EPEC, EHEC), *Vibrio cholerae*, and *Giardia lamblia* disrupt polarized epithelia as a host infection mechanism (Chatterjee et al., 2004; Muza-Moons et al., 2004; Troeger et al., 2007). For instance, EPEC disrupts the tight junction *in vivo* (Shifflett et al., 2005), and the increase in epithelial permeability allows for bacterial translocation and activation of host inflammatory responses. EPEC can also cause microvillar effacement, which can be mediated by an effector protein, EspB, that inhibits myosin function (Iizumi et al., 2007).

Finally, in cancer, the uncontrolled growth of epithelial cells is evident in over 90% of malignant tumors (Fish and Molitoris, 1994). A defect in normal cell-cell adhesion or cell-substrate adhesion programs can result in high degree of invasiveness in a malignant tumor. Consistent with this mechanism, E-cadherin expression is decreased in a subset of esophageal, gastric and breast carcinomas (Fish and Molitoris, 1994).

It is clear that the establishment and maintenance of polarized epithelial cells are important for normal epithelial physiology, while dysfunction contributes to disease states characterized by loss of epithelial polarity and increased membrane permeability. In order to develop treatments for diseases of polarized epithelial cells, it is essential to understand the underlying mechanisms that regulate epithelial polarity and cell junctions by identifying

and exploring key mediators of these processes. This thesis will define the roles of myosin-X in polarized epithelial cells, a subject that is completely unexplored, and will identify new functions for myosin-X in polarized epithelial cells.

The Actin Cytoskeleton is an Essential Component of Polarized Epithelial Cells

Filamentous actin (F-actin) forms the structural backbone of polarized epithelial cells. Actin-based structures can be divided into several classes (Figure 1.1). At the apical domain, microvilli have a core of actin filaments with the plus ends of the filaments oriented toward the tips of the microvilli (Figure 1.1A). The actin filaments are cross-linked by actin-binding proteins such as villin and fimbrin, and the actin is surrounded by and attached to the plasma membrane by myosin-1a. The cell junctions are also associated with the actin cytoskeleton (Figure 1.1B); a circumferential ring of bundled actin filaments connects to the adherens junction, while a loose meshwork of actin associates with the tight junction (Ivanov, 2008). Actin is necessary for the formation of the apical domain as cytochalasin D, an actin polymerization inhibitor, results in the loss of microvilli (Kellerman et al., 1990) and junctional proteins (Shen and Turner, 2005; Stevenson and Begg, 1994) as well as increased membrane permeability (Madara et al., 1986; Stevenson and Begg, 1994). Along the basolateral domain of most epithelial cells, sheet-like protrusions at the lateral membrane extend into neighboring cells (Figure 1.1C) (Demontis and Dahmann, 2007), and at the basal surface, dynamic filopodia are embedded within lamellipodia (Figure 1.1D) (Georgiou and Baum, 2010). In fact, both types of basolateral protrusions are dynamic,

although basal filopodia showed quicker rates of extension and retraction than lateral protrusions by live cell imaging (Georgiou and Baum, 2010).

Filopodia are Implicated in the Establishment of Polarized Epithelia

Filopodia have been proposed to function at key steps in the formation of microvilli and cell junctions. Filopodia are slender, actin-rich projections located at the cell periphery and are involved in cell motility, migration and adhesion. As an actin-based structure, filopodia are structurally related to microvilli, but filopodia are generally more dynamic, have fewer actin filaments, and filopodia vary considerably in length.

Given the structural similarities between filopodia and microvilli, filopodia have been theorized to precede microvillar formation (Peterson and Mooseker, 1993) (Figure 1.2A). However, an alternate theory conjectures that microvilli elongate from shorter microvillar 'pimples' (DeRosier and Tilney, 2000; Tilney et al., 2004) (Figure 1.2B). While several proteins are capable of inducing formation of microvilli (Baas et al., 2004; Chiba et al., 2006; Nielsen et al., 2007), the proteins necessary for microvillar formation are largely unidentified (Hanono et al., 2006). Surprisingly, microvilli-specific proteins such as villin and ezrin are not required for formation of microvilli *in vivo* (Ferrary et al., 1999; Saotome et al., 2004), although ezrin is necessary for normal microvillar morphology (Saotome et al., 2004).

During polarization and junctional assembly, filopodia are theorized to form nascent junctions by initiating 'actin cable' contacts between adjacent cells (Vaezi et al., 2002; Vasioukhin et al., 2000) (Figure 1.3). At the sites of filopodial contact, 'puncta' of adherens junction proteins, like E-cadherin, and tight junction proteins, like occludin and ZO-1, have

been observed (Ivanov et al., 2005; Takai and Nakanishi, 2003). Importantly, assembly by actin cables has been detected in cultured polarized epithelial cells (Ivanov et al., 2005). As nascent junctions mature, junctional complexes are established, and puncta of junctional proteins at filopodial contacts become a continuous adhesive belt (Ivanov et al., 2005).

Myosin-X is Required for Filopodial Formation but its Role in Polarized Epithelial Cells is Unknown

Myosin-X (Myo10) is a 237 kD molecular motor with a head, neck and tail domain (Figure 1.4A). The conserved head domain binds to actin and generates motor activity through ATP hydrolysis. The neck region consists of three IQ motifs and is hypothesized to regulate motor activity. The neck region is followed by a length of stable alpha helix (SAH), which may dimerize the myosin motor (Knight et al., 2005). Most intriguing is the tail domain of Myo10 which may allow the protein to take on unique functions within the apical domain. The tail includes three PH (pleckstrin homology) domains, a MyTH4 (myosin tail homology 4) domain and a FERM (band 4.1, ezrin, radixin, moesin) domain. The PH domains may provide a means for regulation of microvillar dynamics and junctional assembly, as they function as binding sites for inositol phospholipids in phosphatidylinositol 3-kinase signaling pathways necessary for cell motility (Berg et al., 2000) and junctional integrity (Balda et al., 1991; Laprise et al., 2002). Additionally, the FERM domains of the tail region bind integrins and would potentially allow Myo10 to interact with integral membrane proteins (Berg et al., 2000).

By Northern blot, Myo10 is expressed at highest levels in the kidney (Berg et al., 2000), and immunohistochemistry indicates Myo10 is expressed most abundantly in

epithelial cells (Uhlen et al., 2005). Nonetheless, the role of Myo10 in polarized epithelial cells remains completely unexplored. From our lab's work in fibroblast cells, Myo10 localizes to the tips of filopodia, which I have also observed in unpolarized Caco-2 and MDCK cells (Figure 1.4B). Importantly, it is clear that Myo10 is necessary for filopodial formation; Myo10 knockdown in HeLa cells dramatically reduces the number of dorsal filopodia (Bohil et al., 2006).

Since filopodia are structures implicated in the formation of the polarized epithelia and Myo10 is required for filopodial formation, my graduate work has investigated the role of Myo10 in polarized epithelial cells, and specifically, in the formation of microvilli and cell junctions. Finally, I explored the apico-basal localization of Myo10 and the requirement of the PH domains for proper apico-basal localization.

The following describes the contents of the next chapters in this dissertation. Chapter 2 is a review on myosins in cell junctions, in preparation for submission to the journal BioArchitecture. Chapter 3 is a published article: Liu KC, Jacobs DT, Dunn BD, Fanning AS and Cheney RE. 2012. Myosin-X Functions in Polarized Epithelial Cells. *Mol Biol Cell*. 23:1675-1687. For this published work, I performed all of the experiments and wrote the majority of the manuscript. Chapter 4 is a work in progress on the targeting of Myo10 in polarized epithelial cells. The Appendix is unpublished data that does not support a role for Myo10 in microvilli.

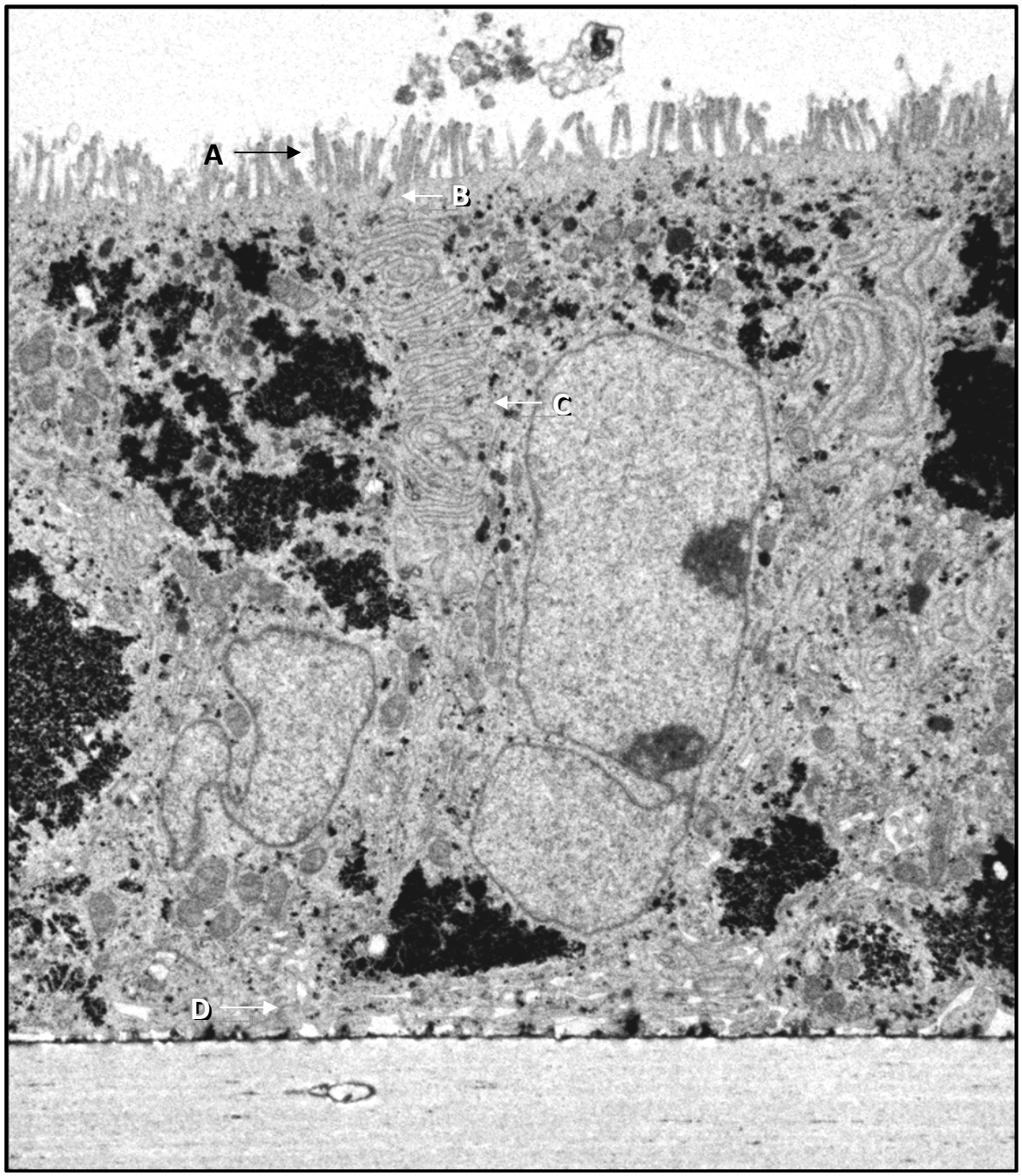

Figure 1.1 The actin cytoskeleton of polarized epithelia (Caco-2 cells) as viewed by transmission electron microscopy. (A) The apical domain is composed of microvilli and the terminal web. (B) Cell junctions, the tight junction and adherens junction, have actin components. (C) At the lateral domain, sheet-like actin-based protrusions are present. (D) At the basal surface, filopodia-like protrusions contact the underlying surface. Image was acquired using a Gatan Orius SC1000 CCD Digital Camera and Digital Micrograph 3.11.0 (Microscopy Services Laboratory, UNC Department of Pathology).

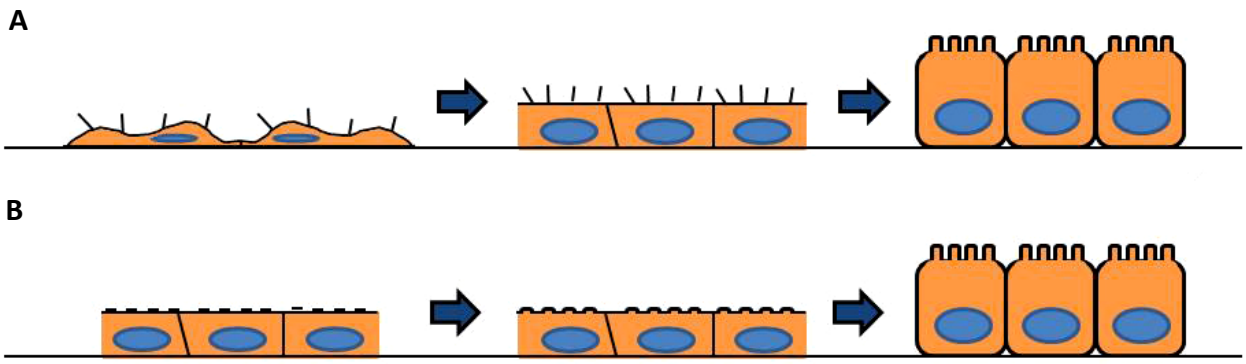

Figure 1.2 Filopodia are theorized to precede formation of microvilli. (A) Filopodia-precursor hypothesis: Mature microvilli form from filopodia-like precursors. (B) Alternate hypothesis: Microvillar 'pimples' extend to form mature microvilli.

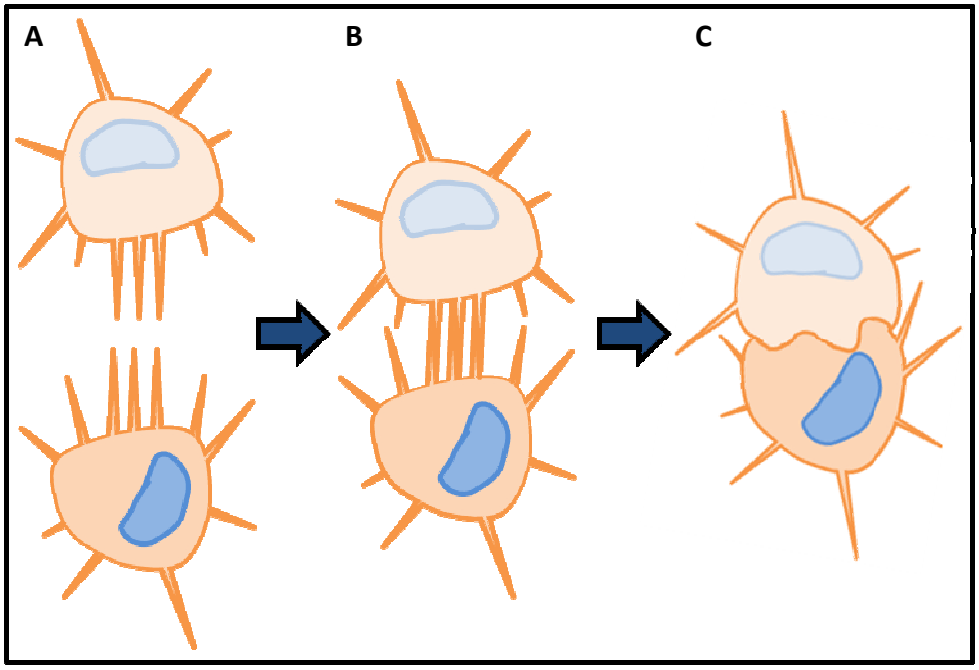

Figure 1.3 Filopodia are theorized to function in junctional assembly. (A) Filopodia of spreading cells (B) contact to form nascent junctions. (C) Mature linear junctions form.

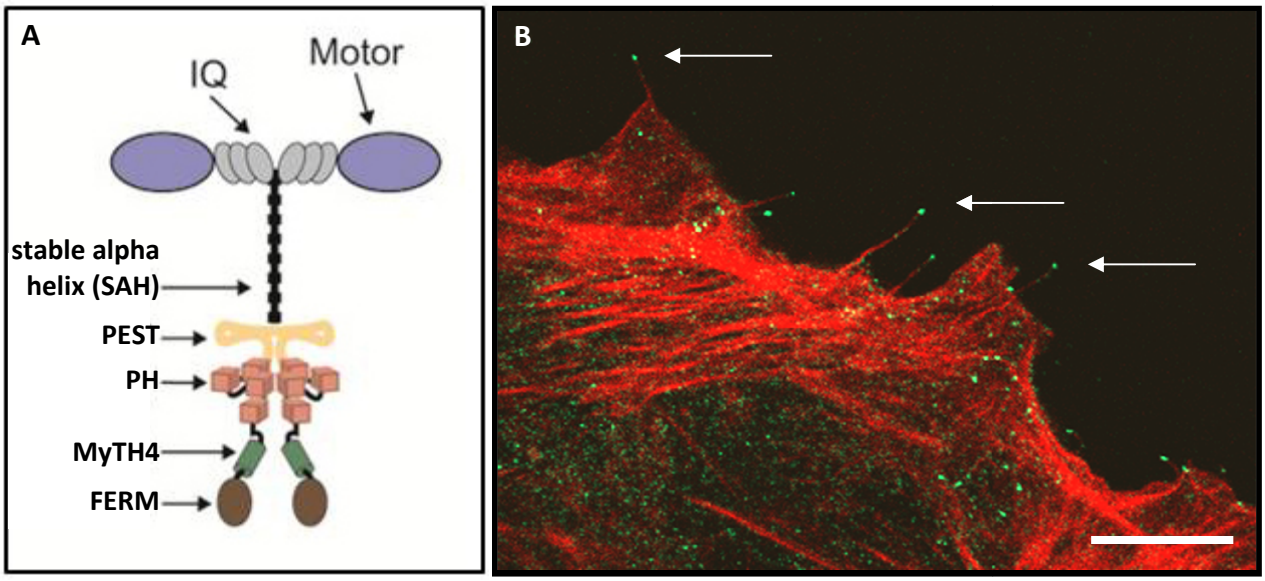

Figure 1.4 Myo10, a molecular motor that localizes to tips of filopodia. (A) Structure of Myo10. (B) In early Caco-2 cells (1-3 days), Myo10 (green) localizes to the tips of filopodia (marked by arrows) stained for F-actin (red). Scale bar = 10 µm.

CHAPTER TWO

MYOSINS IN CELL JUNCTIONS

INTRODUCTION

Myosins are a superfamily of ATP-dependent molecular motors that bind to and move along actin filaments. Myosins serve a growing array of functions within the cell, including force generation, membrane and organelle trafficking, actin organization and cell shape, tethering/anchoring to the actin cytoskeleton, and cell signaling (Hartman et al., 2011; Woolner and Bement, 2009). Conventional class II myosins were first discovered in skeletal muscle where homodimers of myosin-II heavy chains assemble into the thick filaments required for muscle contraction. Importantly, nonmuscle cells also express class II myosins. All other classes of myosins are referred to as unconventional myosins and are found in a variety of tissues and cell types. Myosins are known to be expressed in polarized epithelial cells, a metazoan-specific cell type with specialized cell junctions. Yet, only in recent times have we begun to tease apart the functions of different myosin classes and isoforms in polarized epithelial cells. Also, previous studies have tended to focus on class II myosins, even though the number of unconventional myosin genes easily outnumbers that of conventional myosins. However, several recent studies have identified important functional roles for unconventional myosins in cell junctions in polarized epithelia. Here, we review the functions of myosins at epithelial cell junctions with particular emphasis on unconventional myosins.

Myosins consist of a highly conserved N-terminal head or motor domain that contains binding sites for F-actin and ATP. The motor domain is followed by the neck domain with IQ motifs that can bind calmodulin or calmodulin-like light chains (Cheney and Mooseker, 1992). In the C-terminal tail domain, the structural motifs vary greatly between myosin classes, but are relatively conserved within a myosin class (Mermall et al., 1998). In the human genome, there are at 38 different myosin genes (and five named pseudogenes) that can be divided into 12 classes (Berg et al., 2001; Kollmar, 2006). Of the human myosin genes, 24 encode unconventional myosins, while 14 encode conventional myosins. Several unconventional myosins (myosins VIIa, VIIb, X, XVb) contain MyTH4-FERM domains (myosin tail homology 4-protein 4.1, ezrin, radixin, moesin). The MyTH4 and FERM domains are found in tandem and form a structural supramodule (Wu et al., 2011). Functionally, MyTH-FERM myosins are frequently found in actin-based extensions, such as filopodia and stereocilia, and often have roles in cell adhesion.

In vertebrate epithelial cells that line organs such as the gut and kidney, polarity is defined by the apical, lumen-facing domain and underlying basolateral domain. At the intersection of these two domains, the apical junctional complex is comprised of two parts: the tight junction and adherens junction (Figure 2.2A). The tight junction is the apical-most network of intramembranous strands that form a selective paracellular barrier between neighboring cells (Van Itallie and Anderson, 2006). The adherens junction contains a cadherin-catenin complex that mediates cell-cell adhesion (Nelson, 2008). Cadherins are calcium-dependent transmembrane receptors, and catenins are submembranous scaffolding proteins. The apical junctional complex is coupled to the underlying actin

cytoskeleton with a dense circumferential actin belt adjacent to the adherens junction (Hirokawa et al., 1983; Hirokawa and Tilney, 1982) and a looser network of actin filaments associated with the tight junction (Madara, 1987). Notably, nonmuscle myosin-II is well-known component of the circumferential actin belt (Drenckhahn and Dermietzel, 1988; Ivanov et al., 2005).

The apical junctional complex is essential to maintain the barrier function and integrity of the epithelial cell sheet. Yet, the apical junctional complex is not static, but rather, it is dynamic and constantly remodeling (Kametani and Takeichi, 2007; Sasaki et al., 2003). In cell culture, junction assembly and disassembly are often modeled using the calcium-switch assay (Cereijido et al., 1978). In this assay, removal of extracellular calcium results in loss of cadherin-mediated cell-cell adhesion and disassembly of cell junctions, while subsequent re-addition of calcium triggers junction assembly (Figure 2.2B). After junction disassembly, apical F-actin organizes into ring-like structures in the now unpolarized cells. Then, during junction assembly, radial actin cables are observed at sites of initial cell-cell contact (Vaezi et al., 2002; Vasioukhin et al., 2000). Using this model, it has been observed that nascent adherens-like junctions precede tight junction formation (Ando-Akatsuka et al., 1999; Ivanov et al., 2005). As epithelial cells mature, junctional proteins and the circumferential actin belt organize at the cell junctions.

Indeed, the actin cytoskeleton is critical for the apical junctional complex, as disruption of actin dynamics affects the structural and functional integrity of cell junctions (Ivanov et al., 2005; Ivanov et al., 2004; Madara et al., 1986). Yet, how does the apical junctional complex physically interact with the actin cytoskeleton? Numerous proteins have

been shown to interact with the tight junction cytoplasmic plaque, some of which are actin-binding proteins (Schneeberger and Lynch, 2004; Shen et al., 2011). Despite this, the identity of the linkages between the adherens junction and actin cytoskeleton remains controversial (Drees et al., 2005; Yamada et al., 2005). As actin-binding proteins that can generate force and movement, myosins are prime candidates to interact with the actin cytoskeleton at the apical junctional complex.

Nonmuscle Myosin-II: Isoforms A & B have differential roles at cell junctions

For nonmuscle myosin-II (abbreviated here as Myo2), there exist three isoforms: A, B and C (gene names: MYH9, 10 and 14) (Golomb et al., 2004; Simons et al., 1991). One or more Myo2 isoforms are ubiquitously expressed throughout mouse development and show broad tissue distribution (Golomb et al., 2004). Myo2A and B (Figure 2.1) differ in their duty ratio, which is the proportion of time the motor spends binding actin during its ATPase cycle. Myo2B has a higher duty ratio than Myo2A, that is, Myo2B remains bound to actin for a greater fraction of its ATPase cycle than Myo2A (Kovacs et al., 2003; Rosenfeld et al., 2003; Wang et al., 2003). The Myo2 light chains can be regulated by phosphorylation, for example, via myosin light chain kinase (MLCK) or Rho kinase (ROCK) (Bresnick, 1999; Redowicz, 2001). Finally, all three Myo2 isoforms can be inhibited by blebbistatin (Kovacs et al., 2004; Limouze et al., 2004). The effects of global inhibition of nonmuscle myosin-II at cell junctions have been reviewed previously (Ivanov, 2008). Blebbistatin treatment has been shown to disrupt junction assembly and disassembly (Ivanov et al., 2005; Ivanov et al., 2004), paracellular permeability of the tight junction (Shen et al., 2006), and recruitment of

epithelial cadherin (E-cadherin) to cell-cell contacts (Shewan et al., 2005). Clearly, Myo2 is critical for junctional processes, but are there distinct roles for different Myo2 isoforms? Here, we focus on isoform-specific functions of nonmuscle Myo2.

Isoform-specific knockout studies indicate roles for both Myo2A and Myo2B in cell adhesion and polarized cell junctions. Myo2A knockout mice are lethal; in the embryo, the visceral endoderm shows loss of polarized columnar morphology, whereas knockout embryoid bodies exhibit cell shedding, suggesting a cell adhesion defect. Interestingly, E-cadherin and β-catenin is reduced at cell-cell contacts in the absence of Myo2A (Conti et al., 2004). Myo2B is enriched in brain, particularly in the neuroepithelial layers. Myo2B mutants, also lethal, develop hydrocephalus and spinal canal obstruction; morphologically, the apical domain of neuroepithelial layers in Myo2B mutants show structural defects and discontinuities (Ma et al., 2007).

In polarized epithelial cells, a subset of both Myo2A and Myo2B localize to the apical junctional complex (Ivanov et al., 2005; Shewan et al., 2005) (Figure 2.3A). Specifically, Myo2A functions in the dynamics of junction assembly and disassembly. In regard to junction assembly, Myo2A knockdown cells show a kinetic delay in junction formation, measured by transepithelial resistance (TER) and localization of tight junction and adherens junction markers. Despite the delay of several hours, apical junctions were eventually able to form (Ivanov et al., 2007). In addition, Myo2A knockdown affects junction disassembly, as F-actin reorganization into actin rings was disrupted and translocation of tight junction protein occludin from cell-cell junctions was affected (Ivanov et al., 2007). Thus, Myo2A is needed for the proper kinetics of junction assembly and disassembly.

Isoform-specific knockdown has also identified differential roles for Myo2A and B in E-cadherin-based cell-cell contacts. Myo2A is needed for proper E-cadherin organization at the adherens junction, as Myo2A siRNA reduces the amount of E-cadherin at cell-cell contacts and decreases cadherin-based homophilic adhesion (Smutny et al., 2010). Interestingly, an E-cadherin blocking antibody decreased Myo2A staining at cell-cell contacts (Shewan et al., 2005). Thus, Myo2A activity is needed for E-cadherin localization to the junctions and vice versa. Furthermore, Myo2A knockdown results in increased and irregular oscillatory movement of E-cadherin at cell-cell contacts (Smutny et al., 2011). In contrast, Myo2B maintains the integrity of E-cadherin at the adherens junction, as Myo2B knockdown decreases actin and its dynamics at cell junctions, and fragments E-cadherin localization as well (Smutny et al., 2010). The high duty ratio of Myo2B may allow the motor to generate tension to support dynamic actin at the cell junctions. As a result, live cell imaging of Myo2B knockdown cells shows significantly less translational movement of actin and E-cadherin (Smutny et al., 2011). Interestingly, double knockdown of Myo2A and B leads to disruption of the tight junction, visualized by zonula occludens-1 (ZO-1) localization (Smutny et al., 2010). One potential link between the actin cytoskeleton and the tight junction complex is cingulin, a submembranous tight junction-associated phosphoprotein that co-purifies with and binds Myo2 (Citi et al., 1989; Cordenonsi et al., 1999).

Together, these studies propose isoform-specific roles for Myo2: Myo2A is required for normal kinetics of junction assembly and organizes E-cadherin at the adherens junction; whereas, Myo2B supports the integrity and dynamics of the circumferential actin belt.

Myo1e at specialized glomerular junctional complexes

Class I myosins are single-headed motors with short tails (Albanesi et al., 1985; Stafford et al., 2005). Class I myosins are a phylogenetically ancient class of myosins found in amoebae as well as fungi, worms, flies and vertebrates (Berg et al., 2001). In some organisms, there exist several members of class I myosins; for example, the slime mold *Dictyostelium discoideum* has at least seven different myosin I proteins (Soldati, 2003), and vertebrates possess eight class I myosins (Gillespie et al., 2001). Many class I myosins bind lipids, including Myo1a, which forms a link between actin and the surrounding plasma membrane in microvilli (Tyska et al., 2005). Myo1e (initially called human myosin-1c or myr3) is a "long-tailed" class I myosin (Berg et al., 2001) with a tail containing a membrane-binding domain and an SH3 domain (Bement et al., 1994b) (Figure 2.1). Myo1e is ubiquitously expressed, highest levels of which are found in kidney, prostate, colon, liver and ovary (Bement et al., 1994a). Notably, Myo1e in kidney is predominantly found in the glomerulus and its podocytes, which are epithelial cells that extend "foot processes" to wrap around glomerular capillaries (Mele et al., 2011).

Myo1e localizes to cell junctions in several cell types. The rat homolog of Myo1e was first shown to localize with β-catenin to the adherens junction in chicken intestine and kidney. In Caco-2 cells, Myo1e is enriched at the apical cell junctions in spreading cells and mature monolayers (Skowron et al., 1998). Also, in cultured monolayers of mouse podocyte cells, Myo1e frequently localizes to cell-cell contacts and may be needed for proper actin organization (Krendel et al., 2009). Renal glomeruli from Myo1e knockout mice show disrupted podocyte foot processes as well as thickened and disorganized glomerular

basement membranes (Krendel et al., 2009; Mele et al., 2011). Disruption in the cytoskeleton of the glomerular intercellular junctional complexes has been shown to impair renal function (Faul et al., 2007). As a class I myosin, Myo1e could function to stabilize the actin cytoskeleton by binding the surrounding glomerular membrane.

In Myo1e knockout studies, Myo1e-deficient mice exhibit podocyte injury and impaired renal function (Krendel et al., 2009). Mutations in human Myo1e are associated with familial focal segmental glomerulosclerosis, an autosomal recessive disease of podocytes (Mele et al., 2011). Thus far, no extrarenal defects have been identified in knockout mice or patients with Myo1e mutations. This may indicate that Myo1e is not needed for proper function of other organs and tissues, or perhaps less apparent functional defects have yet to be uncovered.

Apart from Myo1e, little is known regarding class I myosins and epithelial cell junctions. Do any of the other seven class I myosins localize to or function in cell junctions? With the Myo1a knockout mouse available, are there observable junctional defects? Of note, as investigations into class I myosins move forward, functional redundancy should be considered given the many class I myosins.

Myosin VI at cadherin-based cell-cell contacts

Myosin VI (Myo6) is unique in that it is the only known motor that moves toward the minus end of actin filaments (Wells et al., 1999) (Figure 2.1). In general, the plus ends of actin filaments are oriented toward the plasma membrane (Svitkina et al., 1997), so Myo6 might be expected to transport vesicles inward or push actin outward. Myo6 arose early

during the metazoan radiation and is found in most metazoans (Berg et al., 2001). Myo6 is ubiquitously expressed in mammalian cells (Buss et al., 1998). Myo6 is a processive motor that can dimerize by cargo binding to the tail (Nishikawa et al., 2002; Phichith et al., 2009; Rock et al., 2001), and as high duty ratio motor, Myo6 spends most of its ATPase cycle bound to actin (De La Cruz et al., 2001; Robblee et al., 2004). This also means that a single Myo6 dimer would theoretically be able to transport a vesicle along an actin filament. Myo6 is well-known for its roles in clathrin-mediated endocytosis (Buss et al., 2001b) as well as endocytic trafficking and sorting (Hasson, 2003; Morris et al., 2002). In epithelial cells, Myo6 is needed for the polarized transport of certain cargoes to the basolateral membrane (Au et al., 2007).

Importantly, loss of Myo6 causes deafness in both humans and mice (*Snell's waltzer*) (Avraham et al., 1995; Deol and Green, 1966). In the inner ear hair cells, Myo6 is enriched both in the vesicle-rich pericuticular necklace and in stereocilia, and in the *Snell's waltzer* mouse, the inner ear hair cells improperly develop disorganized and fused stereocilia (Self et al., 1999). Furthermore, loss of function studies in fly also indicate Myo6 is critical for epithelial morphogenesis. *Drosophila* Myo6 (Jaguar) deficiency disrupts border cell migration during oogenesis (Deng et al., 1999; Geisbrecht and Montell, 2002) as well as dorsal closure, a process of epithelial sheet fusion at the dorsal midline in late embryogenesis (Lin et al., 2007; Millo et al., 2004).

Myo6 has been demonstrated to have functional roles in cadherin-based cell-cell contacts and the perijunctional actin cytoskeleton. *In vitro* studies in MCF-7 cells show that Myo6 localizes to mature cell-cell contacts and co-localizes with E-cadherin (Maddugoda et

al., 2007). Immunoprecipitation studies indicate Myo6 interacts with E-cadherin (Maddugoda et al., 2007) and β-catenin/Armadillo (Geisbrecht and Montell, 2002). Myo6 also binds Echinoid (Lin et al., 2007), a cell adhesion molecule that cooperates with *Drosophila* epithelial cadherin (DE-cadherin) (Wei et al., 2005). Interestingly, Myo6 and E-cadherin/β-catenin each appear to stabilize the expression of the other protein. In Myo6-null or mutant *Drosophila* border cells, DE-cadherin and Armadillo (β-catenin) levels are reduced (Geisbrecht and Montell, 2002; Millo et al., 2004). Conversely, *Drosophila* Myo6 protein expression is reduced in cells lacking either DE-cadherin or Armadillo (Geisbrecht and Montell, 2002). Similar results were obtained *in vitro* by Myo6 knockdown (Maddugoda et al., 2007). Thus, Myo6 stabilizes E-cadherin at epithelial cell-cell contacts.

Given its high duty ratio, Myo6 may also stabilize the perijunctional actin cytoskeleton and/or tether membrane proteins, such as E-cadherin or β-catenin, to the perijunctional actin cytoskeleton. Myo6 has been previously reported to stabilize actin filament networks in unpolarized cells (Noguchi et al., 2006), and Myo6 serves a similar membrane anchoring role in stereocilia, which are mechanosensing actin-based protrusions on hair cells (Seiler et al., 2004; Self et al., 1999). In epithelial cells, loss of Myo6 leads to disrupted perijunctional actin (Maddugoda et al., 2007; Millo et al., 2004) as well as loss of tight junction markers at cell-cell contacts (Maddugoda et al., 2007). Maddugoda et al. demonstrate that vinculin, a cytoskeletal protein found in focal adhesions and adherens junctions, is a downstream effector of Myo6. Together, Myo6 and vinculin have been proposed to stabilize perijunctional actin and cadherin-based cell-cell contacts (Figure 2.3B) (Maddugoda et al., 2007). However, the precise mechanism of these interactions has yet to

be determined. Functionally, it has been suggested that Myo6's tethering role could provide the protrusive force needed for cell migration, i.e. in border cells during oogenesis (Geisbrecht and Montell, 2002).

Myosin VIIa interacts with junction-associated proteins at epithelial cell-cell contacts

Myosin VIIa (Myo7a) is a member of the MyTH-FERM family of myosins (Figure 2.1). *Drosophila* Myo7a can form an inactive monomer regulated by head-to-tail folding (Umeki et al., 2009) but appears to function as a processive dimer (Sakai et al., 2011; Yang et al., 2006). Biochemical experiments indicate Myo7a has a high duty ratio (Watanabe et al., 2006). Myo7a is conserved in *Dictyostelium* and in metazoans (Berg et al., 2001). In mammals, Myo7a is predominantly expressed epithelial cells (Sahly et al., 1997) with highest levels in the testis, cochlea and retina, and lower expression in kidney (Hasson et al., 1995). Intriguingly, Myo7a is expressed in microvilli- or stereocilia-rich epithelial cells, and the expression pattern of Myo7a parallels the appearance of epithelial microvilli or cilia during development (Sahly et al., 1997).

Mutations in human Myo7a are responsible for Usher Syndrome 1B (USH1B), a disease of congenital deafness, vestibular dysfunction and pre-pubertal onset of retinitis pigmentosa leading to blindness (Adato et al., 1997; Weil et al., 1995; Weil et al., 1996; Weston et al., 1996). Myo7a encodes the *shaker-1* mouse gene locus (Gibson et al., 1995), and *shaker-1* mouse homozygotes are characterized by deafness and vestibular dysfunction (Lord and Gates, 1929). In cochlear hair cells, Myo7a mutations result in disruption in stereocilia structure and organization (Chen et al., 1996; Self et al., 1998). In stereocilia,

Myo7a binds cadherin-23 (Bahloul et al., 2010), an atypical cadherin (Bolz et al., 2001) at the lateral links between stereocilia, and this interaction has been proposed to physically link together stereocilia (Di Palma et al., 2001) and to apply the tension needed for proper stereocilia organization (Bahloul et al., 2010; Boeda et al., 2002) (Figure 2.3C). Myo7a has also been reported to interact with protocadherin-15 in hair cells of the inner ear (Senften et al., 2006). Finally, mutations in *Drosophila* Myo7a are responsible for *crinkled*, a fly mutant with defects in actin-based bristles and hairs, as well as deafness (Kiehart et al., 2004; Todi et al., 2005). Both *shaker-1* and *crinkled* phenotypes indicate a role for Myo7a in the formation of actin-based structures.

In polarized epithelial cells, endogenous Myo7a (Sousa et al., 2004) and the GFP-Myo7a tail (Kussel-Andermann et al., 2000; Sousa et al., 2004) localize to cell-cell contacts. In addition, Myo7a in the testis is found in a dynamic adhesive structure called the ectoplasmic specialization (Velichkova et al., 2002). Myo7a has been shown to interact with several junction-associated proteins at epithelial cell-cell contacts. First, the FERM domain of Myo7a interacts with vezatin, a transmembrane protein at the adherens junction (Kussel-Andermann et al., 2000). Vezatin, also shown to bind E-cadherin and α- and β-catenin, has been proposed to bridge Myo7a to the cadherin-catenin complex at the adherens junction. Functionally, Myo7a and vezatin are needed for the bacterial entry of *Listeria monocytogenes* into epithelial cells (Sousa et al., 2004). The MyTH-FERM domain of Myo7a also mediates the interaction with Shroom2, a tight junction-associated protein (Etournay et al., 2007). Thus, Shroom2 may link Myo7a and the actin cytoskeleton to the tight junction (Etournay et al., 2007). Finally, Myo7a binds the actin-associated protein, Keap1, at the

specialized adhesion junctions in testis (Velichkova et al., 2002). It should be noted that the localizations of vezatin, Shroom2 and Keap1 are Myo7a-independent, as the localization of each Myo7a-binding protein in *shaker-1* mutants is unchanged (Etournay et al., 2007; Kussel-Andermann et al., 2000; Velichkova et al., 2002). Thus, Myo7a may link the apical junctional complex to perijunctional actin via its interactions with junction-associated proteins in epithelial cells. Loss of Myo7a results in functional defects in lateral contacts between stereocilia. Does Myo7a knockdown lead to similar defects in cell-cell contacts of polarized epithelial cells?

Myosin-IXA: a Rho GAP at cell-cell junctions regulates collective epithelial cell migration

Class IX myosins are metazoan-specific motor proteins (Berg et al., 2001) (Figure 2.1). Unique among myosins, class IX myosins are Rho GTPase activating proteins (GAPs) that negatively regulate Rho GTPases (Reinhard et al., 1995). *In vitro*, the purified RhoGAP domain of Myo9a can inactivate RhoA and RhoB, with marginal activity on Cdc42 and none on Rac1 (Chieregatti et al., 1998). Rho GTPases have functional roles in cell morphogenesis, cell migration and proliferation, and actin organization (Jaffe and Hall, 2005; Ridley, 1996). Importantly, Rho GTPases and their downstream effectors are involved in epithelial junction assembly (Braga and Yap, 2005; Terry et al., 2011). Yet, until recently, little was known about the RhoGAP, Myosin-IXA (Myo9a, formerly known as myr 7) or its functions.

Myo9a is expressed at cell junctions both *in vivo* and *in vitro* (Abouhamed et al., 2009), and FRET studies indicate Myo9a negatively regulates Rho GTPase activity (RhoA) at cell-cell contacts (Omelchenko and Hall, 2012). In cultured human bronchial epithelial cells

(16HBE), Myo9a localizes to nascent cell-cell contacts and co-localizes with F-actin and ZO-1 (Omelchenko and Hall, 2012). Similarly, Myo9a is expressed in Caco-2 cells along cell-cell junctions as well as in the cytosol (Abouhamed et al., 2009). Myo9a is ubiquitously expressed during development (Gorman et al., 1999). In adult tissues, Myo9a is particularly abundant in the brain and testis with lower levels of expression in the adrenal gland, kidney, lung and spleen (Chieregatti et al., 1998). In the brain, Myo9a is highly expressed in multiciliated ependymal epithelial cells (Abouhamed et al., 2009). In knockout studies, Myo9a-deficient mice develop severe hydrocephalus along with stenosis and dilation of the ventricular system. Loss of Myo9a results in a distorted ependymal layer by immunostaining for E-cadherin and β-catenin as well as loss of occludin localization to the tight junction (Abouhamed et al., 2009), leading to the hypothesis that Myo9a functions in the formation of epithelial cell junctions.

A recent study by Omelchenko and Hall highlights the role of Myo9a in collective cell migration using its RhoGAP activity at cell-cell junctions (Omelchenko and Hall, 2012) (Figure 2.3D). Similar to the knockout mouse phenotype, Myo9a siRNA knockdown shows loss of ZO-1 and irregular E-cadherin staining at cell-cell contacts, in addition to fewer radial actin bundles observed at cell-cell contacts. Importantly, Myo9a knockdown leads to impaired wound healing and a dramatic cell scattering phenotype as initial cell-cell contact expansion and stabilization are disrupted (Omelchenko and Hall, 2012). However, knockdown studies in Caco-2 cells indicate that cell junctions eventually assemble and have normal apico-basal polarity (Abouhamed et al., 2009). These results suggest Myo9a is needed to form adhesive cell-cell contacts by regulating the expansion and stabilization of

cell-cell contacts. In future experiments, it would be interesting to test whether Myo9a functions in cell junctions in mature epithelial monolayers.

Myosin-X: a MyTH-FERM myosin at the basolateral domain of polarized epithelial cells

Myosin-X (Myo10) is a MyTH-FERM myosin best known for localizing to filopodial tips. It appears to have arisen just prior to the evolution of the metazoans but has been lost in the lineages leading to flies and worms (Berg et al., 2001). The tail of Myo10 has several unique subdomains: three pleckstrin homology (PH) domains bind inositol phospholipids with high affinity for phosphatidylinositol (3,4,5)-triphosphate (PIP3) (Plantard et al., 2010; Tacon et al., 2004; Umeki et al., 2011); and a MyTH-FERM domain that can bind microtubules (Weber et al., 2004) and β-integrins (Zhang et al., 2004) (Figure 2.1). Myo10 is ubiquitously expressed with high levels of expression in epithelial tissues such as kidney (Berg et al., 2000). Notably, Myo10's IQ motifs can bind either calmodulin or calmodulin-like protein (CLP), which is an epithelia-specific light chain (Rogers and Strehler, 2001).

In unpolarized cells, Myo10 localizes to tips of filopodia and is required for the formation of filopodia (Bohil et al., 2006). Myo10 localizes to the cell cortex in *Xenopus* embryos (Woolner et al., 2008), and in polarized MDCK cells, Myo10 localizes to the lateral membrane during junction assembly (Liu et al., 2012). Correspondingly, Myo10 is found at the basolateral domain in kidney (Liu et al., 2012) and biochemically fractionates with the basolateral fraction (Yonezawa et al., 2003). In epithelial cells, since inositol phospholipids are segregated in a polarized fashion such that PIP2 is found at the apical domain and PIP3 is exclusively basolateral (Martin-Belmonte et al., 2007), it is likely that Myo10 is targeted to

the basolateral domain by PH domain binding to PIP3. Consistent with this, the PH domains of Myo10 localize to the basolateral membrane (Lu et al., 2011).

Our recent work reveals that Myo10 has important roles in junction assembly and epithelial morphogenesis (Liu et al., 2012). Myo10 knockdown results in a delay in junction assembly as measured by a delay in peak transepithelial resistance (TER) measurements and a delay in the localization of tight junction and adherens junction markers to cell-cell contacts. This delay in junction assembly is similar to the kinetic delays observed with knockdown of critical junction proteins ZO-1 and E-cadherin (Capaldo and Macara, 2007; McNeil et al., 2006). In addition, Myo10 knockdown monolayers show defects in paracellular permeability. In three-dimensional culture, epithelial cells normally form cysts with a single lumen, but Myo10 knockdown cells form cysts with multiple lumens. Importantly, apico-basal polarity is unaffected, so it is unlikely that defects are due to disruption of epithelial cell polarity. Although Myo10 has been reported to interact with VE-cadherin and to undergo co-transport with it in filopodia (Almagro et al., 2010), but no interaction between Myo10 and E-cadherin has been detected thus far (Liu et al., 2012).

In junction assembly, filopodia or radial actin cables are theorized to form initial cell-cell contacts (Vasioukhin et al., 2000). Interestingly, GFP-Myo10 shows localization to the tips of dynamic filopodia-like structures at the basal surface during junction assembly (Liu et al., 2012). Thus, Myo10 is likely to function in the formation of filopodial cell-cell contacts during early junction assembly (Figure 2.3E). Also, since Myo10 is needed for normal spindle positioning and orientation (Kwon et al., 2008; Liu et al., 2012; Toyoshima and Nishida, 2007; Weber et al., 2004; Woolner et al., 2008), and spindle misorientation can result in

multi-lumen cysts in three-dimensional culture (Jaffe et al., 2008; Rodriguez-Fraticelli et al., 2010; Zheng et al., 2010), Myo10 knockdown may affect lumen formation in cysts via its function in spindle orientation. Although Myo10 is reported to localize to the spindle poles in Xenopus, future studies are needed to determine the precise interactions between Myo10 and the mammalian mitotic spindle.

Myosin XVa in stereocilia and *Drosophila* Sisyphus in dorsal closure

Myosin XVa (Myo15a) is a member of the MyTH-FERM family of myosins, and exists as two alternatively spliced isoforms with or without a large N-terminal extension (Belyantseva et al., 2003; Liang et al., 1999) (Figure 2.1). Mammalian Myo15a has limited expression and is enriched in a subset of inner ear neurosensory cells (Lloyd et al., 2001).

Human mutations in Myo15a are responsible for human non-syndromic autosomal recessive deafness (DFNB3) (Friedman et al., 1995; Liburd et al., 2001; Nal et al., 2007; Shearer et al., 2009; Wang et al., 1998). In mouse, Myo15a mutations (*shaker-2*) result in deafness and vestibular dysfunction (Probst et al., 1998; Wakabayashi et al., 1998; Wang et al., 1998). Myo15a localizes to the tips of stereocilia in the inner ear (Belyantseva et al., 2003), and *shaker-2* mice have shorter and disorganized stereocilia that are defective in forming their characteristic staircase structure (Probst et al., 1998). Therefore, Myo15a is necessary for the graded elongation of stereocilia. In stereocilia, Myo15a interacts with whirlin (Belyantseva et al., 2005), a scaffolding protein associated with Usher syndrome type 2 (Ebermann et al., 2007), and with Eps8, an actin capping protein, to form a stereocilia tip complex (Manor et al., 2011).

Initial investigations of Myo15a in epithelial cells have been carried out in Sisyphus, the *Drosophila* homolog of Myo15 (Liu et al., 2008). Liu et al. show that Sisyphus is required for epithelial morphogenesis and likely functions in cell adhesion. As epithelial sheets close during dorsal closure, Sisyphus accumulates in contact-making filopodia and newly formed junctions. Sisyphus-deficient mutants show defects in epithelial alignment, and delay and/or failure in fusion of epithelial sheets. Sisyphus was reported to co-localize with and bind DE-cadherin, and Sisyphus-deficient embryos show reduced DE-cadherin at the dorsal side of leading edge cells during dorsal closure (Liu et al., 2008).

It appears that Myo15a has varying roles in different tissue types. In the mammalian inner ear, Myo15a functions in stereocilia length regulation and organization. *Drosophila* Myo15 is reported to interact with DE-cadherin and is critical for epithelial morphogenesis, particularly epithelial sheet alignment and adhesion during dorsal closure.

Dachs: a *Drosophila* unconventional myosin is planar-polarized at apical junctions

Dachs is a unique class of unconventional myosin in *Drosophila* (Bridges and Morgan, 1919; Mao et al., 2006; Tzolovsky et al., 2002) that lacks a clear mammalian homolog (Mao et al., 2006) (Figure 2.1). Recent investigations reveal that Dachs is required for proper orientation of cell division and tissue growth (Mao et al., 2011). Dachs has an N-terminal extension preceding the head and neck. The structure of the tail is unknown and shows no sequence similarity to other proteins. Dachs mRNA is broadly expressed throughout embryonic and wing disc development (Mao et al., 2006). In the wing disc epithelium, Dachs

is planar polarized along the proximal-distal axis, localizing to the distal side near the adherens junction (Mao et al., 2006; Rogulja et al., 2008).

Loss of Dachs results in tissue undergrowth, shortened wings and legs, and often fused tarsal segments (Mao et al., 2006; Waddington, 1940). In *dachs* mutants, tissue undergrowth specifically involves disrupted wing disc elongation along the proximal-distal axis, as *dachs* mutant wing discs are rounded and shortened in the proximal-distal axis (Mao et al., 2011). Importantly, *dachs* mutants show mitotic spindle misorientation (Mao et al., 2011) (Figure 2.3F). Apical junction proteins have been previously reported to affect mitotic spindle orientation (Hao et al., 2010). Interestingly, *dachs* mutants have dilated apical cell surfaces, which suggests that the Dachs myosin exerts a polarized contractile force to constrict the apical junctions and to orient the mitotic spindle along the proximal-distal axis (Mao et al., 2011).

Dachs has been identified as a downstream component of the Fat signaling pathway (Mao et al., 2006). Fat is a large protocadherin (Mahoney et al., 1991), and the planar polarized distribution of Dachs is disrupted in the absence of Fat or other Fat signaling regulators (Rogulja et al., 2008). Functionally, the planar polarization of Dachs generates polarized cell tension that orients the mitotic spindle and resultant cell division to produce net elongation and tissue growth along the proximal-distal axis. As an unconventional myosin only recently discovered, it would be useful to determine the structural and biochemical properties of Dachs.

CONCLUSIONS

In addition to nonmuscle myosin-II, several unconventional myosins have been identified to have important roles at epithelial cell junctions, many of which are members of the MyTH-FERM family of myosins. As knowledge of the roles of unconventional myosins in cell junctions continues to grow, several themes begin to emerge. Unconventional myosins and nonmuscle myosin-II can function at cell junctions by affecting cell adhesion, tethering of junctional proteins, actin organization, and mitotic spindle orientation. Another obvious function for myosin motors is cargo transport. Are there unconventional myosins that transport cargoes to cell junctions in polarized epithelial cells? At present, there are numerous unconventional myosins with yet unknown functions in polarized epithelia and cell junctions. It is clear that the importance of myosins at cell junctions spans well-beyond conventional myosin-II, and indeed, unconventional myosins offer a great deal that remains to be explored in cell junctions.

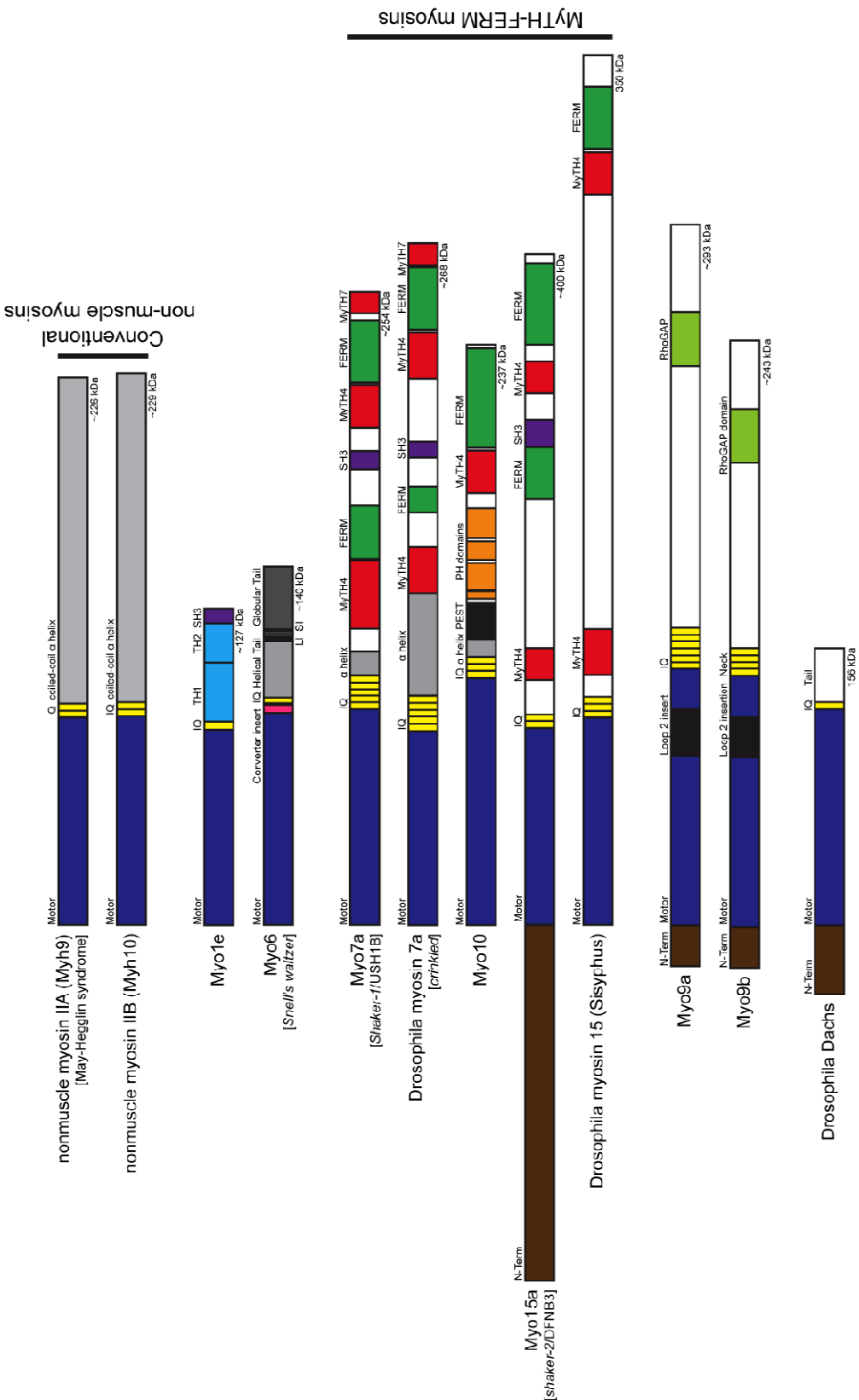

Figure 2.1 Conventional and unconventional myosins with roles in cell junctions of vertebrates and fly. Several MyTH-FERM myosins have identified roles in cell junctions.

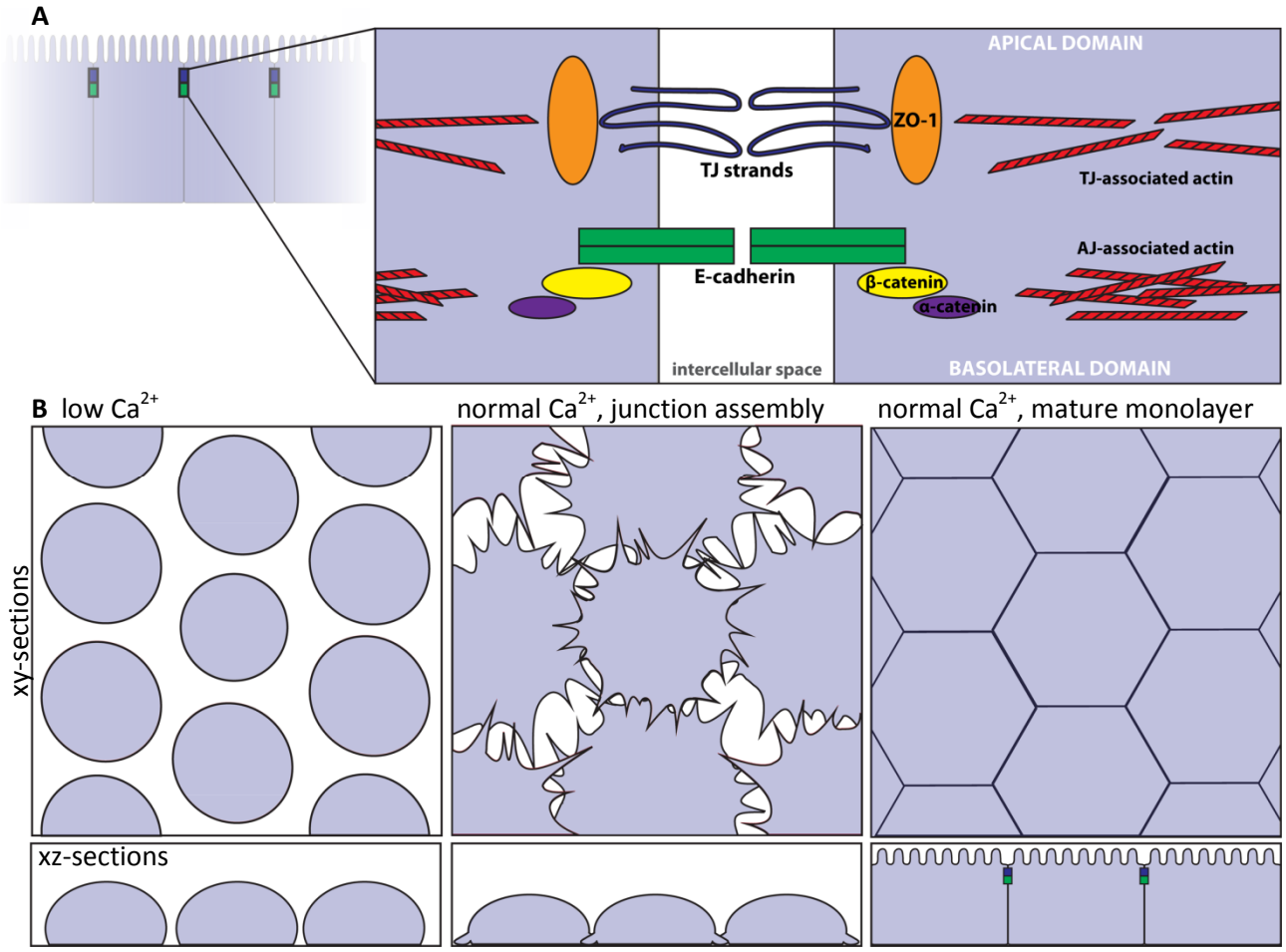

Figure 2.2 The apical junctional complex and calcium switch model of junction assembly. (A) The tight junction and adherens junction, and their associated actin cytoskeleton, comprise the apical junctional complex. The tight junction strands form a semi-permeable barrier, and ZO-1 functions as a tight junction scaffolding protein. At the adherens junction, the cadherin-catenin complex contributes to cell adhesion. The apical junctional complex separates the apical and basolateral domains. (B) In the calcium-switch model, junctions are disassembled by removing calcium (left, low Ca^{2+}). Upon calcium re-addition (center), the junctions begin to assemble, and radial actin cables are observed at early cell-cell contacts. Cells are fully polarized in a mature monolayer (right). The red lines indicate the cross-section slice.

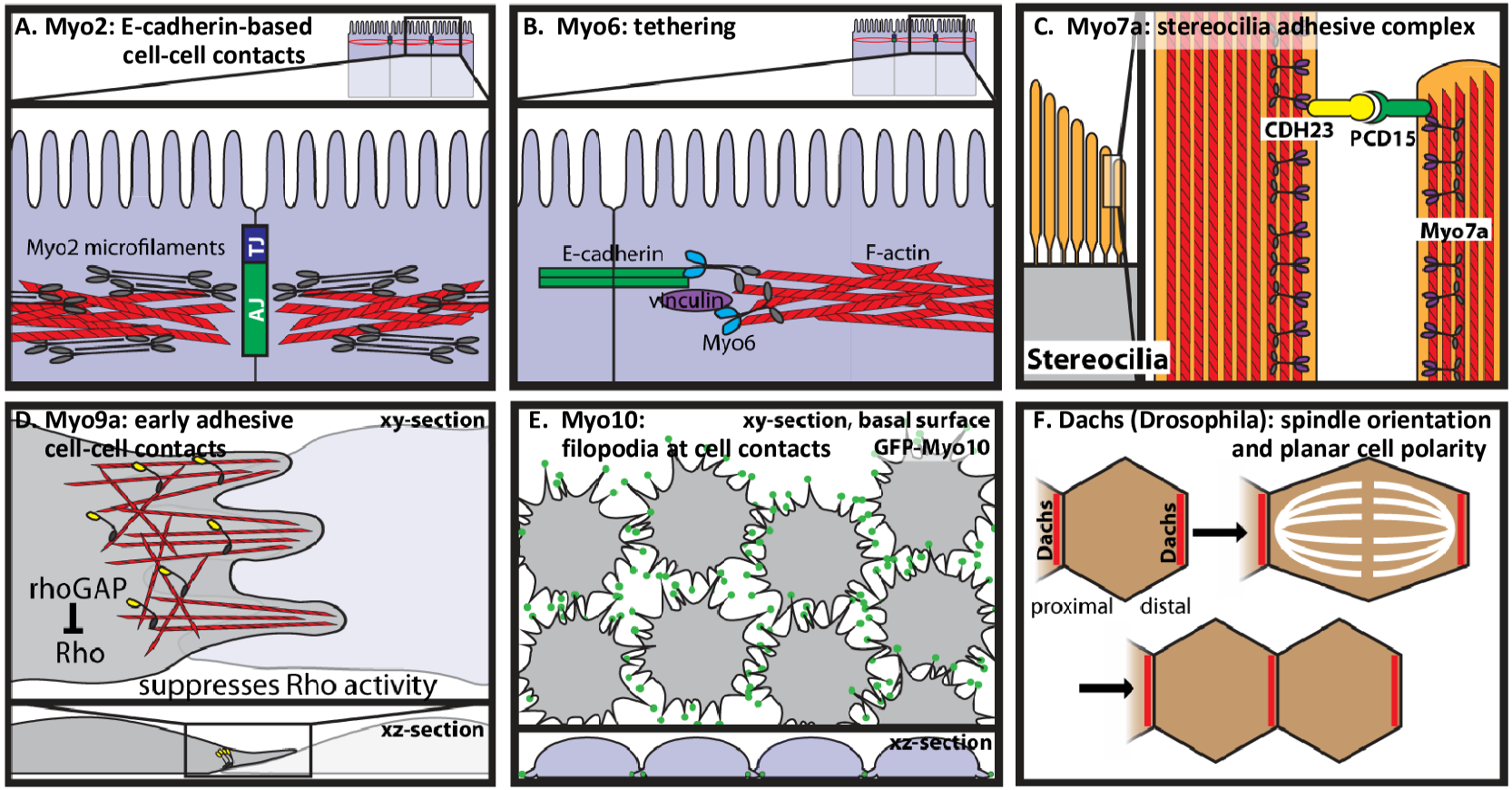
A. Myo2: E-cadherin-based cell-cell contacts
Myo2 microfilaments
TJ
AJ
B. Myo6: tethering
E-cadherin
F-actin
vinculin
Myo6
C. Myo7a: stereocilia adhesive complex
CDH23
PCD15
Myo7a
Stereocilia
D. Myo9a: early adhesive cell-cell contacts
xy-section
rhoGAP
Rho
suppresses Rho activity
xz-section
E. Myo10: filopodia at cell contacts
xy-section, basal surface
GFP-Myo10
xz-section
F. Dachs (Drosophila): spindle orientation and planar cell polarity
Dachs
Dachs
proximal
distal

Figure 2.3 Functional roles of myosins in cell junctions and cell-cell contacts. (A) Myo2 (isoforms A and B) localizes to the adherens junction-associated circumferential actin belt, and Myo2 knockdown disrupts E-cadherin-based cell-cell contacts. (B) Myo6 and vinculin have been suggested to tether E-cadherin to the perijunctional actin cytoskeleton. (C) In stereocilia, Myo7a binds cadherin-23 and protocadherin-15 in a stereocilia adhesive tip complex. (D) Myo9a is a RhoGAP that localizes to cell-cell contacts and suppresses Rho activity. Myo9a knockdown shows defects in formation and stabilization of early cell-cell contacts, resulting in a cell scattering phenotype. (E) Myo10 localizes to the tips of filopodia at nascent cell-cell contacts during junction assembly, and Myo10 knockdown delays junction assembly. (F) Dachs has a planar polarized distribution in Drosophila wing disc epithelia. Loss of Dachs disrupts orientation of the mitotic spindle and cell division along the proximal-distal axis.

CHAPTER THREE

MYOSIN-X FUNCTIONS IN POLARIZED EPITHELIAL CELLS

INTRODUCTION

Myosin-X (Myo10) is an unconventional myosin that localizes to the tips of filopodia and has critical functions in filopodia. Although Myo10 has been studied primarily in non-polarized, fibroblast-like cells, Myo10 is expressed *in vivo* in many epithelia-rich tissues such as kidney. Here, we investigate the localization and functions of Myo10 in polarized epithelial cells, using MDCK (Madin-Darby Canine Kidney II) cells as a model system. Calcium-switch experiments demonstrate that, during junction assembly, GFP-Myo10 localizes to lateral membrane cell-cell contacts and to filopodia-like structures imaged by TIRF on the basal surface. Knockdown of Myo10 leads to delayed recruitment of E-cadherin and ZO-1 to junctions, as well as a delay in tight junction barrier formation as indicated by a delay in the development of peak transepithelial electrical resistance (TER). Although Myo10 knockdown cells eventually mature into monolayers with normal TER, these monolayers do exhibit increased paracellular permeability to fluorescent dextrans. Importantly, knockdown of Myo10 leads to mitotic spindle misorientation, and in 3D culture, Myo10 knockdown cysts exhibit defects in lumen formation. Together, these results reveal that Myo10 functions in polarized epithelial cells in junction formation, regulation of paracellular permeability, and epithelial morphogenesis.

Myosin-X (Myo10) is an unconventional myosin that is broadly expressed in vertebrate tissues (Berg et al., 2000; Kerber and Cheney, 2011). Myo10 has key functions in filopodia and experiments with fibroblast-like cells have revealed that Myo10 localizes to the tips of filopodia and undergoes intrafilopodial motility (Berg and Cheney, 2002; Kerber et al., 2009; Watanabe et al., 2010). Importantly, overexpression of Myo10 induces filopodia, while knockdown of Myo10 inhibits the formation of filopodia (Berg and Cheney, 2002; Bohil et al., 2006). Knockdown of Myo10 also inhibits the formation of invadopodia (Schoumacher et al., 2010), actin-based extensions involved in the spread of cancer cells. Although mRNA and blotting studies indicate that Myo10 is expressed at highest levels in epithelia-rich tissues such as kidney (Berg et al., 2000), very little is known about the localization and functions of Myo10 in polarized epithelial cells.

Myo10 is a member of the MyTH4-FERM family of myosins, a phylogenetically ancient group of actin-based motor proteins that have key functions in membrane-cytoskeleton interactions (Breshears et al., 2010; Sousa and Cheney, 2005). The ~237 kDa Myo10 heavy chain can be divided into three regions, a myosin head with motor activity (Kovacs et al., 2005; Nagy et al., 2008; Sun et al., 2010), a neck consisting of three IQ motifs that bind calmodulin or calmodulin-like light chains, and a large tail. The Myo10 tail includes three pleckstrin homology (PH) domains, one of which can bind to phosphatidylinositol-3,4,5-trisphosphate (PIP_3) (Lu et al., 2011; Mashanov et al., 2004; Plantard et al., 2010). Binding to PIP_3 targets Myo10 to phagosomes (Cox et al., 2002) and has recently been reported to facilitate targeting to filopodia (Lu et al., 2011; Plantard et al., 2010; Umeki et al., 2011). The structure of the MyTH4-FERM (Myosin Tail Homology 4 domain and band

4.1/ezrin/radixin/moesin domain) region was recently solved (Wei et al., 2011). This region of Myo10 can bind directly to microtubules (Weber et al., 2004) and Myo10 is required for normal spindle positioning and orientation (Kwon et al., 2008; Toyoshima and Nishida, 2007; Weber et al., 2004; Woolner et al., 2008). The FERM domain of Myo10 can bind the cytoplasmic domains of β1, β3 and β5 integrins (Zhang et al., 2004), important transmembrane receptors for extracellular matrix components. It should also be noted that the neck domain of Myo10 binds to calmodulin-like protein (CLP), an epithelial specific calcium-binding protein that can function as a Myo10 light chain (Bennett et al., 2007).

Epithelial cells have critical functions in normal physiology and disease, and epithelial morphogenesis is required for the proper development of tissues and organs. In tissues such as kidney, the epithelium of a tubule is organized into a single layer of polarized cells. The polarity of the epithelial cell is defined by the apical and basolateral domains, with the apical domain facing the lumen, and the basolateral domain contacting the extracellular matrix. The two domains are separated by the apical junctional complex (AJC), the major components of which are the adherens junction and the tight junction. The adherens junction promotes cell-cell adhesion and coordinates changes in cell shape during morphogenesis of tissues and organs (Perez-Moreno et al., 2003). A key component of the adherens junction is the cadherins, which are calcium-dependent, homophilic cell adhesion receptors located in the basolateral domain. Cadherins at the adherens junction are linked to actin filaments by scaffolding proteins such as the catenins (Harris and Tepass, 2010). The tight junction (also known as the zonula occludens) is located immediately above the adherens junction and provides a paracellular barrier to the movement of ions and solutes

between cells. The first protein to be identified at the tight junction was Zonula Occludens-1 (ZO-1) (Stevenson et al., 1986), a cytoplasmic scaffolding protein that has important functions in tight junctions. In addition, over 40 proteins are now known to associate with the tight junction (Schneeberger and Lynch, 2004; Shen et al., 2011) including the claudins, the transmembrane proteins that are major elements of the tight junction strands that form the paracellular barrier (Van Itallie and Anderson, 2006).

It is now theorized that the paracellular barrier includes at least two pathways (Anderson and Van Itallie, 2009), and different methods are used to measure the integrity of the tight junction barrier and to distinguish between these pathways. Small pores in the tight junction allow some charged ions to pass, and the transepithelial electrical resistance (TER) of an epithelial monolayer provides an instantaneous measurement of this paracellular barrier to ion movement (Anderson and Van Itallie, 2009). The second pathway, termed the 'leak' pathway, allows for the passage of larger solutes, and this permeability can be measured as the cumulative paracellular movement (flux) of a solute, such as dextran, over time. Although changes in electrical resistance and solute flux often coincide, it is now apparent that the two pathways can be independently regulated (Anderson and Van Itallie, 2009; Balda et al., 1996; Van Itallie et al., 2009). Since the pores in tight junctions are too small to allow for passage of large solutes, permeability to larger solutes is thought to be due to a different mechanism, such as relatively slow rearrangements of the tight junction strands (Anderson and Van Itallie, 2009; Shen et al., 2011).

The actin cytoskeleton serves as an important structural scaffold for the formation and function of the apical junctional complex (Hirokawa et al., 1983; Hirokawa and Tilney,

1982; Zhang et al., 2005). Ultrastructural studies show that actin filaments associate with both the adherens junction and the tight junction; at the adherens junction, the cadherin-based cell-cell contacts are clearly associated with a circumferential bundle of actin filaments (Hirokawa and Heuser, 1981; Hirokawa et al., 1983; Hirokawa and Tilney, 1982). Importantly, changes to the actin cytoskeleton can regulate paracellular permeability (Hartsock and Nelson, 2008; Madara, 1998); for example, there is evidence that contraction of actin bundles at the zonula adherens may modulate paracellular permeability (Shen et al., 2006).

While conventional myosin-II has been shown to have important roles in junction assembly, permeability, and epithelial morphogenesis (Ivanov et al., 2007; Ivanov et al., 2008; Ivanov et al., 2004; Shewan et al., 2005; Smutny et al., 2010), growing evidence indicates unconventional myosins also have critical functions in these processes. Mutations in Myo5b cause microvillar inclusion disease (Muller et al., 2008) and Myo5b has recently been implicated in apical membrane trafficking and lumen formation during epithelial morphogenesis (Roland et al., 2011). Myo6 has been shown to regulate polarized trafficking (Au et al., 2007) as well as E-cadherin adhesion at epithelial cell-cell contacts (Maddugoda et al., 2007; Mangold et al., 2011). Mutations in Myo7a and Myo15a, two MyTH4-FERM myosins distantly related to Myo10, lead to defects in the stereocilia on the apical surfaces of the inner ear hair cells and cause human deafness (Friedman et al., 1995; Liu et al., 1997). Myo9a, an unconventional myosin that acts as a Rho-GAP, is reported to localize to cell junctions and loss of Myo9a leads to defects in epithelial differentiation and to hydrocephalus (Abouhamed et al., 2009). Finally, recent work with Dachs, an

unconventional myosin in fly, indicates that that this myosin generates tension in cell-cell junctions and is involved in spindle orientation (Mao et al., 2011).

Although Myo10's functions in the filopodia of non-polarized cells have been the subject of intensive study, its localization and functions in polarized epithelial cells remain largely unknown. Here, we show Myo10, an unconventional myosin that is broadly expressed in epithelial tissues, has important functions in tight junction biogenesis, the maintenance of paracellular permeability, and epithelial morphogenesis.

MATERIALS AND METHODS

Cell culture and Plasmids

MDCK II tet-off cells (Clontech, Mountain View, CA), referred to as "MDCK", were grown in complete media: DMEM high glucose (Gibco/Invitrogen, Carlsbad, CA) with 10% fetal bovine serum (Gibco) and 100 units/ml penicillin-streptomycin (Sigma, St. Louis, MO). MDCK cells were maintained at 37°C and 5% CO_2 and were passaged every five days.

Plasmids: Canine Myo10 shRNA constructs were generated by cloning Myo10 shRNA (target sequences: ggagaagaacagagataca (sh#2); and ggagatgcatcactggata (sh#5)) into the BglII/HindIII sites of the pSuper vector (Oligoengine, Seattle, WA). The non-silencing (NS) shRNA construct was generated by cloning a non-specific shRNA (gatcgacttacgacgttat) into the pSuper vector. To generate Myo10 knockdown or NS shRNA expressing cell lines, MDCK cells were plated at $150x10^4$ cells per 10 cm dish. After overnight incubation, 2 µg Myo10 shRNA (pool of Myo10 shRNAs #2 & #4) and 0.2 ug pBLAST49 with blasticidin resistance (InvivoGen, San Diego, CA) were co-transfected using 41 µl lipofectamine 2000 (Invitrogen,

Carlsbad, CA). Cells were incubated for three days and plated at different dilutions into 15 cm dishes. Clonal cell lines were selected by antibiotic resistance using complete media with 10 µg/ml blasticidin (InvivoGen). Myo10 shRNAs #16, 38 and 44 are clones of pooled Myo10 shRNAs as described above. All results were confirmed using two independent Myo10 shRNAs, sh#2 (clone 8) and sh#5 (clones 16, 35).

Since the antibodies to human Myo10 exhibited high background in immunofluorescence experiments with MDCK cells, we generated MDCK cells stably expressing a GFP-Myo10 plasmid. The GFP-Myo10 plasmid (BD71) contains an EGFP-1xFLAG tag at the N-terminus of full-length bovine Myo10 (aa 1-2052) and a Spe1 site immediately 5' to the Myo10 stop codon. The GFP-Myo10 is expressed by a pSNAPtag(m) (New England Biolabs) vector that was modified by deleting the SNAP tag while retaining the vector's IRES for expression of neomycin resistance in mammalian cells. MDCK II cells were transfected with the BD71 GFP-Myo10 by Nucleofection using conditions optimized for MDCK II cells (Lonza, Basel, Switzerland). Clonal stable cell lines (#3) were selected using 0.9 mg/ml G418 (Sigma). Expression of GFP-Myo10 was confirmed by immunoblot.

To demonstrate that the knockdown effects were specific, stable knockdown cells were stably rescued by co-transfection with 2 µg GFP-Myo10 (BD71) and 0.1 µg pSVZeo (Invitrogen) by Amaxa nucleofection Kit L using conditions optimized for MDCK II cells. Clonal cell lines (#7) were selected using 1 mg/ml zeocin (InvivoGen). Expression of GFP-Myo10 was confirmed by immunoblot.

Immunofluorescence Microscopy and Immunoblotting

Antibodies: rabbit anti-human Myo10 (Sigma, HPA024223; SDIX, 2243.00.02), mouse anti-human ZO-1 (Invitrogen, 33-9100), mouse anti-human E-cadherin (Sigma, U3254), mouse monoclonal gp135 (Ojakian, SUNY Downstate), rabbit anti-actin (Sigma, A2066), goat anti-human aquaporin-2 (Santa Cruz, Santa Cruz, CA), monoclonal rat aquaporin-1 (Thermo Fisher Scientific, Waltham, MA), mouse monoclonal γ-tubulin (Sigma, T6557), rabbit anti-mouse Par3 (Millipore, 07-330), mouse anti-human aPKCλ (BD Biosciences, 610207), rabbit anti-GFP (Invitrogen, A6455).

Cells were prepared for immunofluorescence by fixation in 4% paraformaldehyde (Electron Microscopy Sciences, Hatfield, PA) in PBS for 30 minutes at room temperature, permeabilization for 10 minutes in 0.5% Triton-X (Sigma) in PBS, blocking for one hour in 5% heat-inactivated goat serum (Sigma), incubation in primary antibody (Myo10 Sigma, E-cadherin, ZO-1, gp135; 0.5-1.0 μg/ml in 5% goat serum + 0.05% NaN_3) overnight at 4°C and secondary antibody (1.0 μg/ml in goat serum) for two hours at room temperature. Alexa Fluor 568 phalloidin (13 nM) (Invitrogen Molecular Probes) and DAPI (200 nM) (Sigma, D9542) were added with secondary antibody in 5% goat serum. Alexa Fluor 488 goat anti-rabbit or anti-mouse, and Alexa Fluor 568 goat anti-mouse IgG (Invitrogen Molecular Probes) were used as secondary antibodies (1.0 μg/ml).

Immunofluorescence samples were imaged on an Olympus FLUOVIEW FV1000 confocal, inverted microscope (Center Valley, PA) using a PlanApo 60X Oil (1.42 NA) objective. The confocal is equipped with diode lasers for 405nm, 559nm and 635nm and an

Argon laser for 488nm. For z-stacks, 640 x 640 pixel, 0.44-0.5 µm slices were collected at 4.0 µs/pixel sampling speed in sequential line mode and using Kalman integration.

Samples were prepared for immunoblot by lysing in SDS sample buffer with protease inhibitor cocktail, EDTA-free (Roche, Indianapolis, IN). Samples were either used immediately or flash frozen in liquid nitrogen and stored at -80°C. Samples were loaded onto 4-12% Bis-Tris gels (Invitrogen). Following gel electrophoresis, protein was transferred onto nitrocellulose (Fisher Scientific). The membrane was blocked in 5% milk in TBST (50 mM Tris, 150 mM NaCl, 0.05% Tween 20, pH 7.5) for 30 minutes followed by primary antibody (Myo10 Sigma, Actin; 0.8-1.0 µg/ml) in TBST overnight at 4°C. For chemiluminescence, HRP donkey anti-rabbit or donkey anti-mouse secondary antibodies (Jackson ImmunoResearch Laboratories, West Grove, PA) were used at 1:10,000 and incubated for 50 minutes in TBST, followed by developing. For LI-COR, membranes were incubated in anti-rabbit IgG IRDye700 (Rockland Immunochemicals Inc., Gilbertsville, PA) at 1:10,000 in TBST and incubated for 45 minutes. Blots were imaged using the Odyssey Infrared Imaging System (LI-COR Biosciences, Lincoln, NE) and analyzed by measuring integrated intensities in the Odyssey applications software version 3.0 (LI-COR Biosciences).

Immunohistochemistry

Protocols were approved by IACUC at UNC-Chapel Hill. 5 µm parrafin-embedded kidney sections from C57BL/6 mice were a gift from Dr. Carie Facemire (UNC-Chapel Hill). Sections were incubated for two hours at 60°C. Samples were washed twice with xylene, then through a graded series of ethanol to distilled water washes: 6 minutes in 100%

ethanol, 5 minutes in 95% ethanol, 3 minutes in 70% ethanol, and 1 minute in distilled water. Antigen retrieval was performed by decloaking in citrate buffer solution, pH 6 (Dako, S1699, Carpinteria, CA) in a decloaking chamber (Biocare Medical, Concord, CA) heated at 120°C for 30 s, 90°C for 10 s and room temperature for 20 minutes. Sections were blocked in 5% heat-inactivated goat serum for one hour. Samples were incubated in 5-10 µg/ml primary antibody (Myo10 Sigma, AQP1, AQP2) in 5% goat serum overnight at 4°C, followed by rinses in PBS and incubation in secondary antibody at 1 µg/ml in 5% goat serum for 2 hours at room temperature.

Barrier assays: Calcium-switch, TER, and Paracellular flux

For calcium-switch assays, MDCK cells were plated in quadruplicate at $7.5x10^4$ cells/well on 10-mm Transwell-Clear filters with 0.4 µm pore size (Corning, Corning, NY) in 0.5 ml complete media. MDCK cells were grown for at least five days until confluent. Cells were then incubated overnight at 37°C in low calcium media: SMEM (Gibco) with 5% calcium-depleted fetal bovine serum, 100 units/ml pen-strep and 5 µM $CaCl_2$ to disrupt junctions as previously described (Gumbiner and Simons, 1986). After overnight incubation, low calcium media was replaced with complete normal calcium media. For time-course experiments, samples were fixed in 4% paraformaldehyde at 0, 0.5, 2, 2.5, 4.5, 5.5 and 24 hours for immunofluorescence microscopy. For transepithelial electrical resistance assays, TER measurements of transwell filters were taken at regular time intervals using an EndOhm-12 chamber and an EVOM epithelial volt-ohm-meter (WPI, Sarasota, FL). Paracellular flux of uncharged macromolecules was measured using 3.0 kD fluorescein-

conjugated dextran (Invitrogen) on 6-7 day monolayers (Van Itallie et al., 2009). Transwell filters were preincubated for 30 minutes with Hanks' buffered salt solution (-$CaCl_2$, $MgCl_2$, $MgSO_4$) (Gibco) supplemented with 1.8 $CaCl_2$. 0.3 mg/ml FITC-dextran was added to the apical compartment; after two hour incubation, samples were taken from the basolateral compartment. FITC-dextran concentrations were measured in replicate using the Synergy HT plate reader with Gen5 Data Analysis Software (BioTek, Winooski, VT). Sample concentrations were determined by plotting against a standard curve of known FITC-dextran concentrations using linear regression in Microsoft Excel.

Spindle angle and length measurements

MDCK cells were grown to confluence on glass coverslips. MDCK monolayers were fixed in 4% paraformaldehyde for 30 minutes, permeabilized with 0.5% Triton-X for 10 minutes, and blocked with 5% heat-inactivated goat serum. Cells were stained with DAPI (1:500) and anti-γ-tubulin (1:1000). Metaphase cells were identified by DAPI staining of condensed chromosomes located at the metaphase plate. Centrosomes were identified by γ-tubulin. Z-stacks (0.5 µm slice thickness) were collected by laser scanning confocal microscopy (UNC-Olympus Imaging Center). Z-stacks were imported into ImageJ, and for each centromere, the z-position was determined by measuring the plane of maximum fluorescence using the 'plot z-axis profile' function. The z-distance between two centromeres within a cell was calculated by the difference between z-positions. Then, maximum xy-projections were generated from γ-tubulin z-stacks. The projected xy-distance between two centromeres within a cell was measured, and given the z-distance (z) and

projected xy-distance (xy), the spindle angle (α^o) was calculated by the equation, $\alpha^o=\tan^{-1}(z/xy)$. Spindle angle is defined by 0^o being horizontal or parallel to the coverslip. Spindle length was calculated by the Pythagorean theorem, spindle length = $\sqrt{(z^2+(xy)^2)}$. 50 metaphase cells were measured per condition. Statistical analysis was performed in GraphPad Prism 5.

3D cysts

MDCK cells were grown in 3D culture using a protocol modified from Jaffe *et al.* (2008). Trypsinized MDCK cells were resuspended at $0.5x10^4$ cells/well in 40% Matrigel phenol-free (BD Biosciences, San Jose, CA), 1 mg/ml rat tail collagen I (Sigma) and 20 mM Hepes pH 7.5, and plated on 10-mm transwell filters. The gels were allowed to set for 30 minutes at 37°C before adding complete media. 3D cysts were grown for six days, then fixed in 4% paraformaldehyde as described above. For each experiment, random fields of view were imaged and cysts were counted as having single or multiple lumens from these images. One hundred cysts were counted for each experiment per condition.

Statistical analysis

For steady state TER and paracellular flux measurements, statistical analysis was determined using a two-tailed Student's *t* test with significance defined by p-value < 0.01. For 3D cysts, the average numbers of single lumens were compared between groups using one-way ANOVA. If significant, post hoc comparisons using Tukey's method were

performed. All statistical analyses were performed in GraphPad Prism 5. All error bars denote standard error of the mean.

RESULTS

Myo10 Localizes to the Basolateral Domain in Kidney Tubules

To investigate the functions of Myo10 in polarized epithelial cells, we first asked where Myo10 localizes in kidney cells *in vivo*. Kidney is one of the tissues that expresses the highest levels of Myo10, although it should be noted that Myo10 is a low abundance protein and that even in the kidney, it is estimated to constitute only ~0.0005% of total protein (Berg et al., 2000). Immunofluorescence of kidney sections from adult mouse showed that anti-Myo10 labels a subset of tubules (Figure 1). To identify the types of tubules that express Myo10, sections were double-labeled with antibodies to aquaporin-2 (AQP2), an apical integral membrane protein that is selectively expressed in connecting tubules and collecting ducts (Nielsen et al., 2002). Since all AQP2-positive tubules were also labeled by Myo10 (Figure 1A), this indicated that Myo10 is expressed both in connecting tubules, an element of the distal nephron, and in the subsequent collecting ducts. Strikingly, although AQP2 showed its expected apical localization, Myo10 was largely basolateral (Figure 1B). The basal Myo10 staining often appears to extend into the cytoplasm, potentially due to the numerous infoldings of the basal plasma membrane present in renal tubules (Windhager, 1992). Also, anti-Myo10 did stain renal vasculature (data not shown), consistent with previously reported expression in endothelial cells (Pi et al., 2007). Since some Myo10 positive tubules were not labeled by AQP2, we also performed double-label

experiments with aquaporin-1 to determine if Myo10 is expressed in proximal tubules (Nielsen et al., 2002). No colocalization of Myo10 and aquaporin-1 was detected (Figure 1C), indicating that little or no Myo10 is expressed in proximal tubules, a region with an extensive brush border and numerous apical microvilli (Booth and Kenny, 1976). Relatively little Myo10 staining was detected in glomeruli (Figure 1C, asterisk). These experiments demonstrate that Myo10 is expressed in connecting tubules and collecting ducts, and that Myo10 exhibits a largely basolateral localization in these polarized epithelial cells.

Myo10 Localizes to Lateral Membranes during Polarized Junction Assembly

Based on our observations in mouse kidney, we used Madin-Darby Canine Kidney (MDCK) II cells as a model system to determine the functions of Myo10 in polarized epithelial cells. Immunoblotting showed that Myo10 is expressed in MDCK cells (Figure 2A). Since trial immunofluorescence experiments with antibodies to human Myo10 yielded high background in MDCK cells (data not shown), for localization studies, we generated MDCK lines that stably express GFP-Myo10 at levels comparable to endogenous Myo10 (Figure 2A). In subconfluent, spreading MDCK cells, GFP-Myo10 localized to the tips of filopodia (Figure 2B), as expected from results in other cell types (Berg and Cheney, 2002).

Next, we examined the subcellular distribution of GFP-Myo10 in MDCK cells during junction formation. Junction assembly was induced using the calcium-switch assay (Cereijido et al., 1978). In this assay, monolayers of MDCK cells are exposed overnight to low calcium, which disrupts cadherin-dependent cell-cell adhesion, leading to a loss of cell-cell junctions and cell polarity. Re-addition of calcium triggers cell-cell adhesion, and over

several hours, the adherens junctions and tight junctions re-assemble. In many types of epithelial cells, E-cadherin exhibits initial localization to cell-cell contacts that matures into a narrow band at the adherens junction (Adams et al., 1996; Boller et al., 1985); however, in MDCK cells, E-cadherin remains localized throughout the lateral membrane (Gumbiner and Simons, 1987). As junctions re-assemble, TER transiently increases to high levels, and then declines over 1-2 days towards the much lower "steady state" TER of mature monolayers (Gonzalez-Mariscal et al., 1985). After overnight incubation in low calcium media, MDCK cells had a rounded and unpolarized morphology; GFP-Myo10 localization was diffuse within these cells (Figure 2C). We also found that GFP-Myo10 showed variable levels of expression from cell to cell. Upon re-addition of calcium to trigger junction assembly, GFP-Myo10 showed clear but transient labeling at the lateral membrane of cell-cell contacts, most notably at 2-6 hours. The transient localization of GFP-Myo10 to lateral membranes could also be seen in xz-projections (Supplemental Figure S1). By 24 hours, the lateral staining of GFP-Myo10 largely disappears (Figure 2G).

Since GFP-Myo10 localized to the lateral membrane during junction assembly, we examined the subcellular distribution of GFP-Myo10 relative to the adherens junction protein E-cadherin. As expected, after incubation in low calcium, E-cadherin showed a diffuse localization in the cytoplasm. Following re-addition of calcium, E-cadherin rapidly redistributed to cell-cell contacts and formed adherens junctions. GFP-Myo10 co-localized with E-cadherin at the lateral membrane at 2 and 4.5 hours after calcium re-addition (Figure 2; E" and F"). E-cadherin localization to the lateral membrane, however, preceded that of

GFP-Myo10; E-cadherin was detected at the lateral membrane at 0.5 hours (Figure 2; D and D').

Like E-cadherin, ZO-1 localization was disrupted after incubation in low calcium and was apparent at cell-cell contacts prior to Myo10 (Supplemental Figure S2; B and B'). Although both ZO-1 and Myo10 were present in lateral membranes, the distribution of ZO-1 was more focused at the apical junctional complex. In fact, little if any Myo10 was detected in xy-sections at the level of ZO-1 and the apical junction complex (Supplemental Figure S2; A-E). Thus, although GFP-Myo10 co-localizes with E-cadherin at the lateral membrane during junction assembly, Myo10 is not enriched at the apical junctional complex in MDCK cells. Furthermore, GFP-Myo10 was not detected at the lateral membrane during the initial recruitment of E-cadherin (or ZO-1) to cell junctions.

To investigate the dynamics of Myo10 during junction assembly, we imaged GFP-Myo10 during calcium-switch (Movie 1). TIRF microscopy of the basal surface revealed numerous puncta of GFP-Myo10, many of which localize to the tips of highly dynamic, filopodia-like projections. GFP-Myo10 was present at filopodia-like projections throughout junction assembly, even prior to localization of GFP-Myo10 to lateral membranes.

Myo10 Knockdown Delays the Assembly of E-cadherin and ZO-1 to Cell-Cell Contacts

Given the localization of Myo10 during junction assembly, we tested whether Myo10 has functional roles in junction formation in polarized epithelial cells. Since Myo10 has previously been efficiently knocked down in other cell lines using RNAi approaches (Bohil et al., 2006; Pi et al., 2007; Zhang et al., 2004), we established stable Myo10

knockdown lines in MDCK cells using shRNA constructs. Knockdown of full-length Myo10 was confirmed by immunoblot (Figure 5A), and Myo10 was depleted by ~70-80%. We then employed the calcium-switch assay to examine the process of junction assembly in Myo10 knockdown cells. Importantly, Myo10 knockdown cells showed a delay in the recruitment of both E-cadherin and ZO-1 to cell-cell contacts (Figure 3). Most notably, at 2.5 hours, E-cadherin and ZO-1 staining was discontinuous or punctate in Myo10 knockdown cells (Figure 3; G and G'), whereas E-cadherin and ZO-1 were organized in a continuous, linear pattern in control MDCK cells (Figure 3; C and C'). Assembly of ZO-1 into continuous, linear contacts was quantified using ImageJ (Arganda-Carreras et al., 2010). Consistent with immunofluorescence studies, Myo10 knockdown cells showed reduced continuous ZO-1 length at all time points until 4.5 hours (Supplemental Figure S3). E-cadherin was properly restricted to the lateral membrane and ZO-1 to the apical junction; therefore, knockdown of Myo10 does not appear to affect overall cell polarity. We stained for other additional polarity markers, ezrin and gp135, and their localization was also unchanged in five day old MDCK monolayers with Myo10 knockdown (Figure 4). Also, the localization of polarity protein markers, Par3 and aPKC, in MDCK monolayers grown for five days were unaffected by Myo10 knockdown (Supplemental Figure S4). These and subsequent studies were confirmed with two independent shRNAs (Supplemental Figure S5).

Loss of Myo10 Leads to a Delay in Tight Junction Barrier Formation as Assayed by TER

The delay in localization of E-cadherin and ZO-1 to cell-cell contacts suggested that loss of Myo10 might result in a delay in reestablishing tight junction barrier function. We

thus tested if loss of Myo10 leads to defects in the formation of the epithelial barrier by measuring transepithelial electrical resistance (TER) during junction assembly. As expected for control MDCK cells, TER was low in the absence of calcium; upon re-addition of calcium, TER increased substantially and peaked between 6-8 hours. Myo10 knockdown cells, however, showed a marked delay in attaining peak TER (Figure 5B). This ~4 hour delay to peak TER indicates a defect in the kinetics of tight junction formation, a phenomenon that has also been observed in MDCK cells in which critical tight junction and adherens junction proteins, such as ZO-1 and E-cadherin, have been depleted (Capaldo and Macara, 2007; McNeil et al., 2006).

Although Myo10 knockdown led to a delay in the development of peak TER, by ~28 hours, the TER of both knockdown and control cells declined to typical steady state levels, ~60 $\Omega \cdot cm^2$ (Figure 5B). Knockdown and control cells were also indistinguishable when the TER was assayed after five days in culture (Figure 5C). This demonstrates that although Myo10 is required for normal kinetics of junction assembly, it is not necessary for maintenance of TER once junctions have formed. Consistent with the latter point, knockdown of Myo10 in Caco-2 cells (a model for intestinal epithelial cells), also had no effect on the steady state TER (Supplemental Figure S6; A and B).

Loss of Myo10 Increases Paracellular Permeability to Uncharged Solutes

A key feature of epithelial barrier function is the 'leak' pathway, which represents the paracellular permeability to large solutes (Anderson and Van Itallie, 2009). The leak pathway can be regulated independently of permeability to small ions that is assayed by

TER (Balda et al., 1996) and is most frequently analyzed by measuring the movement of uncharged dextran conjugates across the monolayer. Importantly, paracellular permeability to 3.0 kD dextran more than doubled in Myo10 knockdown cells (Figure 5D). This demonstrates that, although Myo10 is not required to maintain the permeability barrier to small ions, Myo10 is required to establish or maintain the permeability barrier to large solutes. Myo10's role in regulating permeability is not limited to MDCK cells, since knockdown of Myo10 in Caco-2 cells led to similar results (Supplemental Figure S6; C and D).

Myo10 is Required for Proper Mitotic Spindle Orientation

Myo10 can bind to microtubules through its MyTH-FERM domain (Weber et al., 2004), and Myo10 has been shown to be important for spindle formation and length in Xenopus (Woolner et al., 2008) and proper spindle orientation in fibroblast-like cells (Toyoshima and Nishida, 2007). Yet, whether Myo10 is required for spindle orientation in polarized epithelial cells is largely unknown. To investigate role of Myo10 in the spindles of MDCK cells, we fixed mature monolayers and stained for DAPI to identify dividing metaphase cells. By co-staining for γ-tubulin to identify centromeres, we measured the spindle angle and spindle length, and found that Myo10 knockdown cells showed increased average spindle angle (0^{o}=horizontal) and a wider distribution of spindle angles when compared with control cells (Figure 6; A and B). This defect in spindle orientation is similar to those reported for key proteins required for spindle orientation such as Cdc42 (Jaffe et

al., 2008) and cadherins (den Elzen et al., 2009). No difference in average spindle length was detected with Myo10 knockdown (Figure 6C).

Myo10 is Required for Normal Lumen Formation in MDCK Cysts

Our experiments on two-dimensional MDCK monolayers demonstrated that Myo10 has a role in the formation of adherens and tight junctions as well as in spindle orientation. Since cell junctions and the spindle have been shown to have important roles in epithelial morphogenesis (Krasnow and Nelson, 2002), we tested whether Myo10 is required for morphogenesis of epithelial cysts. We seeded cells at low density in a collagen-matrigel matrix and allowed each cell to grow into a cyst for six days before staining with various markers. While the majority (~80%) of control MDCK cells were able to form a single lumen, only ~20-40% of Myo10 knockdown cells formed single lumens and instead showed a striking multi-lumen phenotype (Figure 7; A and B). Although there was a clear defect in lumen formation, Myo10 knockdown cysts did not appear to have defects in the polarized localization of the junctional marker ZO-1, the apical marker gp135, or the basolateral marker E-cadherin (Figure 7; B and D). Similar to what was observed in 2D culture, normal apico-basal polarity was also confirmed by additional markers including ezrin at the apical domain and Na,K-ATPase at the basolateral domain (Supplemental Figure S7). Thus, Myo10 does not appear to be necessary for establishment of apico-basal polarity, but is required for epithelial morphogenesis to form normal cysts with single lumens.

GFP-Myo10 Rescues Defects in Cyst Formation

To confirm that the effect of Myo10 shRNA was specific, we generated Myo10 knockdown lines that stably express bovine GFP-Myo10 and asked whether expression of the transgene rescued the multiple lumen phenotype. Immunoblotting confirmed the knockdown of endogenous Myo10 and the expression of GFP-Myo10 (Figure 8A). In addition, confocal imaging of rescue cells plated at low density showed GFP-Myo10 labeling at the tips of filopodia (Figure 8B). Rescue cells were plated in collagen-matrigel to assay the efficacy of cyst formation in 3D culture. Although the number of single lumens in control cells was somewhat lower in this series of experiments (~70-75%), GFP-Myo10 expression partially rescued the multi-lumen phenotype of Myo10 knockdown cells (Figure 8E); ~60% of GFP-Myo10 rescue cysts had single lumens compared to ~35% of Myo10 knockdown cysts. The partial rescue is probably attributable to the heterogeneous expression of GFP-Myo10 in the rescue cells, especially given that some cells exhibited little to no expression of GFP-Myo10, much like the stable GFP-Myo10 cells shown in Figure 2. Apico-basal polarity also remained intact in GFP-Myo10 rescue cysts (data not shown). To further confirm the specificity of the Myo10 knockdown, we generated additional knockdown lines that stably express different shRNAs to Myo10 and confirmed all the phenotypes in junction assembly, paracellular permeability, and cyst formation (Supplemental Figure S5).

DISCUSSION

Although Myo10 is broadly expressed in epithelial tissues, its functions in polarized epithelial cells have remained largely unknown. Here we show that Myo10 has important

and unexpected functions in epithelial cells, including junction formation, maintenance of the permeability barrier to large solutes, and epithelial morphogenesis.

Myo10 Localizes to the Basolateral Domain in Polarized Epithelial Cells

While previous work with non-polarized cells has shown that Myo10 localizes to protrusive structures such as the tips of filopodia (Berg et al., 2000; Tokuo et al., 2007), the *in vivo* localization data here from the kidney connecting tubules and collecting ducts show that Myo10 exhibits a largely basolateral distribution in polarized epithelial cells. Given that Myo10 localizes to dorsal filopodia in non-polarized cells, it is somewhat surprising that Myo10 was not detected in proximal tubules, which have numerous apical microvilli, and that GFP-Myo10 was not detected in the apical microvilli of MDCK cells. This demonstrates that Myo10 is not targeted to the tips of all actin-based bundles and suggests that there are important differences between the dorsal filopodia of non-polarized cells and the apical microvilli of polarized epithelial cells. Our results showing a basolateral localization of Myo10 are consistent with biochemical fractionation experiments that identified Myo10 in basolateral rather than apical fractions from kidney (Yonezawa et al., 2003). They are also consistent with proteomics data showing that Myo10 was not among the 14 myosins detected in the intestinal brush border (McConnell et al., 2011). Although the precise mechanisms underlying the basolateral localization of Myo10 remain unknown, the Myo10 tail domain binds to PIP_3 and to β-integrins, (Mashanov et al., 2004; Wei et al., 2011; Zhang et al., 2004), both of which localize basolaterally in MDCK cells (Martin-Belmonte et al., 2007; Schoenenberger et al., 1994).

Loss of Myo10 Delays Junction Formation

Using MDCK cells and the calcium-switch model, we found that at early stages of junction assembly GFP-Myo10 was diffusely distributed within the cell, and as cell-cell contacts formed, it localized to the lateral membrane. More importantly, Myo10 knockdown cells showed a delay in junction formation as indicated by, (1) delays in the localization of E-cadherin and ZO-1, (2) delay in barrier function as indicated by the ~4 hour delay to reach peak TER. The delay in junction formation was temporary, and by ~28 hours, knockdown cells exhibited normal TER. Knockdown of Myo10 thus leads to defects remarkably similar to those resulting from loss of key junction components such as E-cadherin and ZO-1, both of which lead to similar delays in junction formation and TER without affecting steady state TER (Capaldo and Macara, 2007) (McNeil et al., 2006; Umeda et al., 2004).

Loss of Myo10 could delay junction formation by several mechanisms. In keratinocytes, nascent junctions have been hypothesized to form by filopodial contacts between adjacent cells (Vasioukhin et al., 2000). Since we observed Myo10 at the tips of filopodia in unpolarized MDCK cells, Myo10 is well-positioned to facilitate the formation of initial cell-cell contacts. Furthermore, TIRF microscopy revealed that GFP-Myo10 localizes to the tips of filopodia-like structures at the basal surface of MDCK monolayers; these basolateral puncta of GFP-Myo10 were very dynamic (Movie 1). This data illustrating GFP-Myo10 at the tips of filopodia-like structures suggests a mechanism whereby Myo10 functions in junction formation by affecting filopodial cell-cell contacts. A similar role has recently been suggested for Myo10 in endothelial cells, where Myo10 transiently co-

localized with VE-cadherin at the tips of filopodia during the initial stages of cell-cell contact (Almagro et al., 2010). This suggested that knockdown of Myo10 might impair junction formation, although this was not tested. Here, we directly show that knockdown of Myo10 leads to a delay in junction formation. Since it is reasonable to suspect that the role of Myo10 in junction formation could be due to an interaction with E-cadherin, we performed series of preliminary immunoprecipitation experiments, both during calcium-switch and in mature monolayers, but did not detect an interaction between Myo10 and E-cadherin (data not shown).

As an actin-based motor, Myo10 could potentially transport or localize proteins involved in junction formation. Although E-cadherin was detected at lateral membranes prior to GFP-Myo10, E-cadherin localization to the lateral membrane was delayed in Myo10 knockdown cells. This suggests that loss of Myo10 leads to delays at an earlier step, such as formation of initial contacts, or that amounts of Myo10 too low for us to detect are sufficient to localize E-cadherin to lateral membranes. The normal apico-basal polarity observed in Myo10 knockdown cells suggests that Myo10 is not essential for pathways required for polarized membrane trafficking.

It is also possible Myo10 is required to properly regulate actin dynamics at cell junctions. Interestingly, we observed differences in actin morphology with Myo10 knockdown, most notably in calcium-depleted cells. While in control cells F-actin formed apical ring-like structures (Figure 3A", arrows) as previously described (Ivanov et al., 2004), Myo10 knockdown cells showed fewer apical F-actin rings and more F-actin "condensations" within the cells (Figure 3E", arrowheads). Upon calcium re-addition, actin

condensations could be observed at early stages (0.5-2 hrs), but by 5.5 hrs and in mature monolayers, the Myo10 knockdown cells exhibit apparently normal actin organization. Although the nature of the actin condensations is not clear, similar actin structures have been reported in cells knocked down for ZO-1 (McNeil et al., 2006). It is thus possible that Myo10 knockdown delays junction assembly by perturbing actin organization, especially given that myosin-II and Myo6 are involved in the assembly of junctions and associated actin structures (Ivanov, 2008; Ivanov et al., 2007; Mangold et al., 2011; Smutny et al., 2010).

Loss of Myo10 Results in Increased Paracellular Permeability

Myo10 knockdown monolayers showed increased movement of dextran solute through the paracellular pathway over a period of two hours. This finding indicates that Myo10 is required for maintenance of the paracellular barrier. Although the mechanisms underlying the paracellular 'leak' pathway are unclear, the actin cytoskeleton is integral for retaining the paracellular barrier (Shen et al., 2011). It is thus possible that Myo10 is required for cytoskeletal organization or dynamics that are necessary to maintain normal paracellular flux. Although Myo10 was not enriched at the tight junction, other proteins that localize outside of the tight junction, such as E-cadherin, have been shown to affect paracellular permeability in MDCK cells (Capaldo and Macara, 2007).

Loss of Myo10 increases paracellular permeability, but at the same time, it does not affect steady state TER. How can this be reconciled? Transepithelial electrical resistance and paracellular permeability are not necessarily coupled. This has been shown in several cases

(Balda et al., 1996; Bruewer et al., 2004; McCarthy et al., 2000), most recently in ZO-1 knockdown in MDCK cells, where steady state TER is unchanged and paracellular flux is increased (Fanning et al., 2012; Van Itallie et al., 2009). It has been theorized that the highly dynamic tight junction fibrils act akin to a series of gates (Claude, 1978), where the opening and closing of tight junction fibrils allow solute particles to progress through the paracellular pathway over time. Thus, while TER is an instantaneous, static reading of the epithelial barrier to small ions, paracellular flux is a time-dependent, dynamic measurement of the barrier to larger solutes.

Myo10 is Needed for Normal Lumen Formation in Epithelial Morphogenesis

In three-dimensional culture, Myo10 knockdown leads to a dramatic increase in the number of cysts with multiple lumens. Defects in several different pathways can result in a multiple lumen phenotype, including establishment of apico-basal polarity (Schluter et al., 2009; Shin et al., 2005) or mitotic spindle orientation (Jaffe et al., 2008). Apico-basal polarity is established in part by polarity proteins, and the loss of polarity proteins such as Crumbs3 gives rise to multiple lumens or an absence of lumens in 3D cysts (Schluter et al., 2009; Shin et al., 2005). Disruption of the normally basolateral PIP_3 localization in MDCK cells also results in cysts with multiple lumens (Martin-Belmonte et al., 2007). Since Myo10 binds PIP_3 (Lu et al., 2011; Plantard et al., 2010; Umeki et al., 2011), it may act downstream of PIP_3 in cyst morphogenesis.

Myo10 could also act via its involvement in spindle orientation, since spindle misorientation can lead to multi-lumen cysts, as demonstrated with Cdc42 knockdown

(Jaffe et al., 2008) as well as Tuba and Par3 knockdown (Hao et al., 2010; Qin et al., 2010). Consistent with this, we show that Myo10 knockdown leads to defects in spindle orientation in MDCK monolayers (Figure 6). Although Woolner et al. (2008) report that morpholino-mediated knockdown of Myo10 in Xenopus embryos led to a ~35% increase in spindle length, we did not detect changes in spindle length in Myo10 knockdown MDCK cells. This may reflect differences in species, cell type, or method of knockdown. Whereas Toyoshima and Nishida (2007) showed that Myo10 is required for spindle orientation in unpolarized HeLa cells, a process that depends on integrin-based cell-substrate adhesions, our work reveals that Myo10 is also required for spindle orientation in polarized epithelial cells, where the cues for spindle orientation are thought to be provided, at least in part, by cell-cell contacts.

Together, our results demonstrate important and unexpected roles for Myo10 in polarized epithelial cells. The phenotypes we observe in tight junction formation and epithelial morphogenesis are similar to those observed with critical junctional proteins such as E-cadherin and ZO-1, and indicate that it will be important for future studies to investigate Myo10's precise mechanisms of action and its functions *in vivo*.

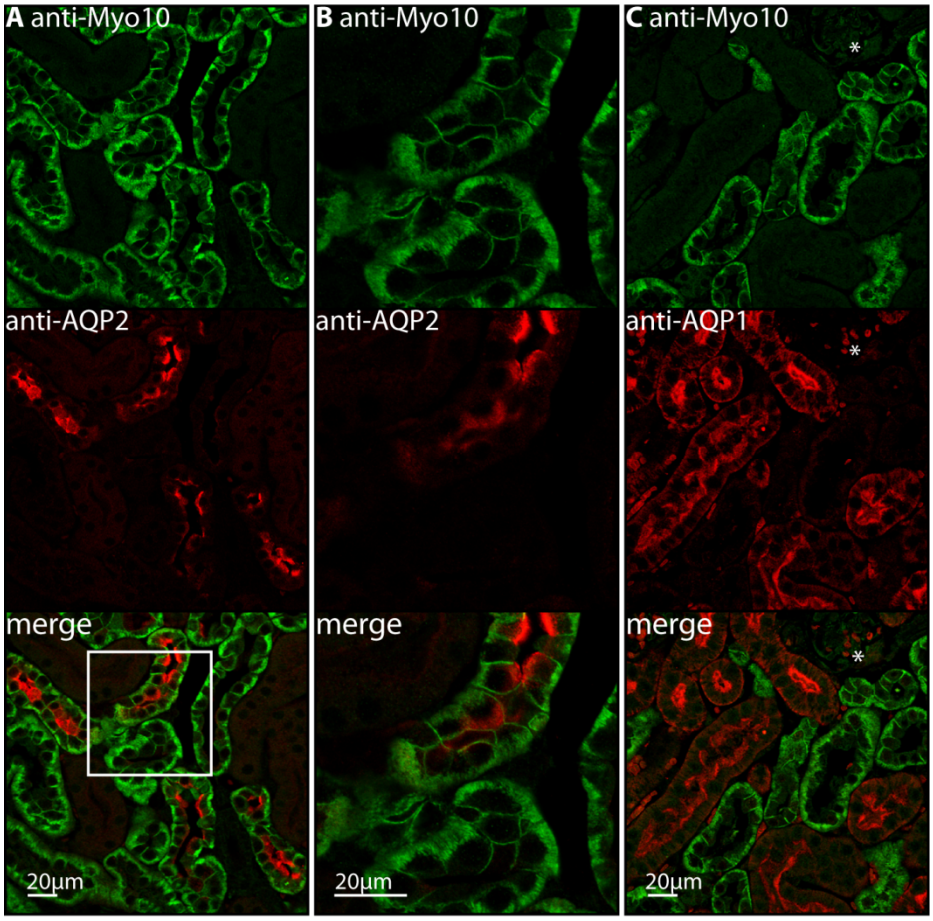

Figure 3.1 Myo10 localizes basolaterally in kidney. (A) Anti-Myo10 antibody labels the basolateral domain in several types of tubules in the renal cortex. These include connecting tubules and collecting ducts, which are labeled by aquaporin-2, an apical protein. (B) A magnified image of the inset box details Myo10's basolateral localization. (C) Little or no Myo10 signal is detected in proximal tubules (labeled with aquaporin-1, red) or in glomeruli (asterisk).

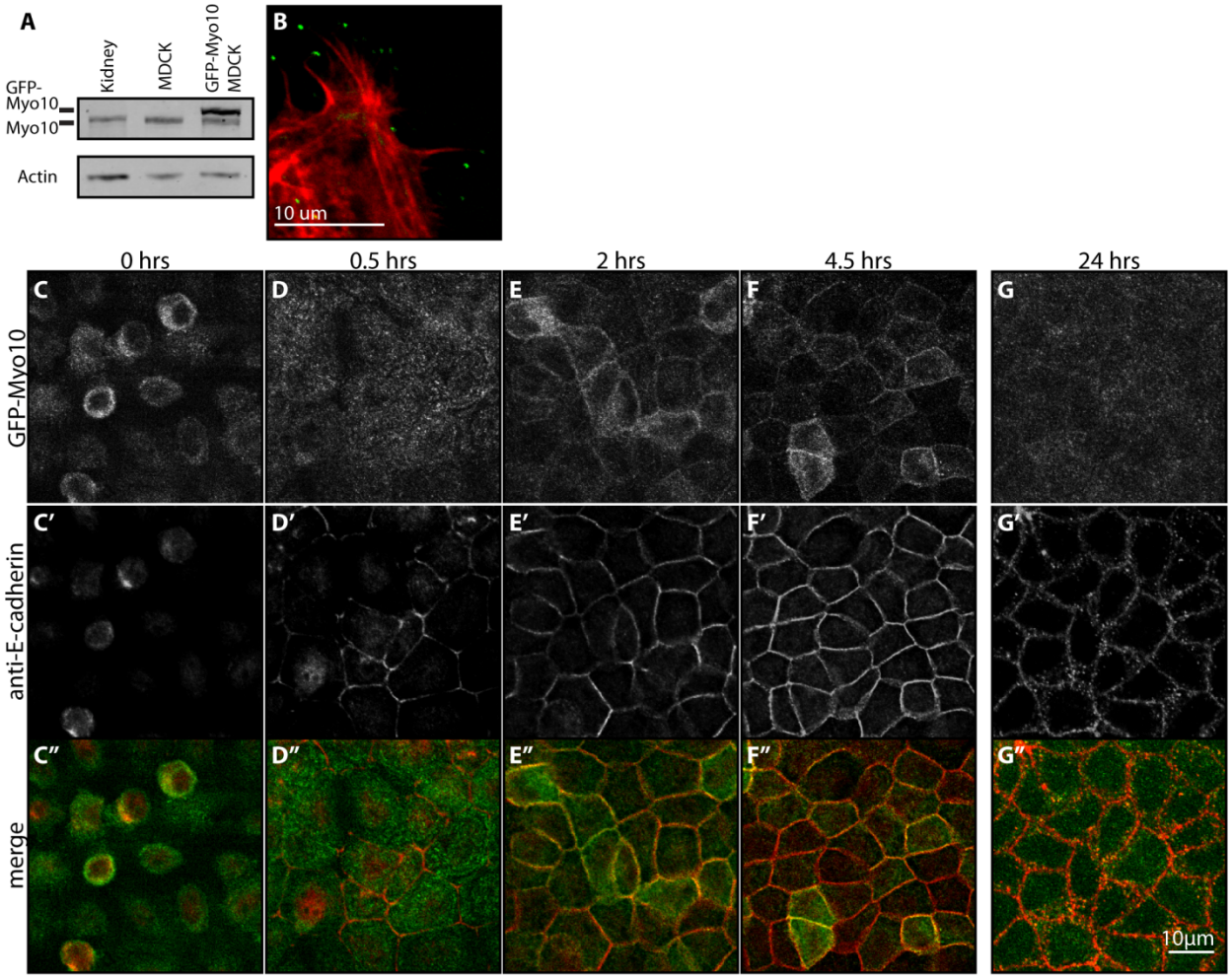

Figure 3.2 GFP-Myo10 localizes to the tips of filopodia in spreading MDCK II cells and to lateral membranes during junction formation. (A) Immunoblot showing expression of Myo10 in mouse kidney, MDCK cells, and MDCK cells stably expressing GFP-Myo10. Actin was used as a loading control. MDCK samples were collected from monolayers after 5 days in culture, and kidney lysates were obtained from adult C57BL/6 mice. (B) GFP-Myo10 (green) localizes to the tips of filopodia in spreading MDCK cells. Cells were fixed one day post-plating and were also stained for F-actin with 568 phalloidin (red). (C-G) GFP-Myo10 transiently localizes to the lateral membrane during junction assembly. After overnight incubation in low calcium to disrupt cell-cell adhesion, cells were rounded and GFP-Myo10 showed a diffuse cortical localization (C). After junction assembly was triggered by re-addition of calcium (D-G), GFP-Myo10 is transiently recruited to the lateral membrane, most strongly between 2-4.5 hours. (C'-G') Localization of E-cadherin during junction assembly. Note that E-cadherin is present at the lateral membrane at 0.5 hours (D'), prior to the recruitment of GFP-Myo10. (C”-G”) Merged images of GFP-Myo10 (green) and E-cadherin (red). GFP-Myo10 co-localizes with E-cadherin at the lateral membranes at 2 and 4.5 hours (E”,F”). Images (G-G”) from a 24 hour time point showing lack of Myo10 staining at lateral membrane in more mature monolayers. Images are single confocal planes taken from mid-section of the cell monolayers.

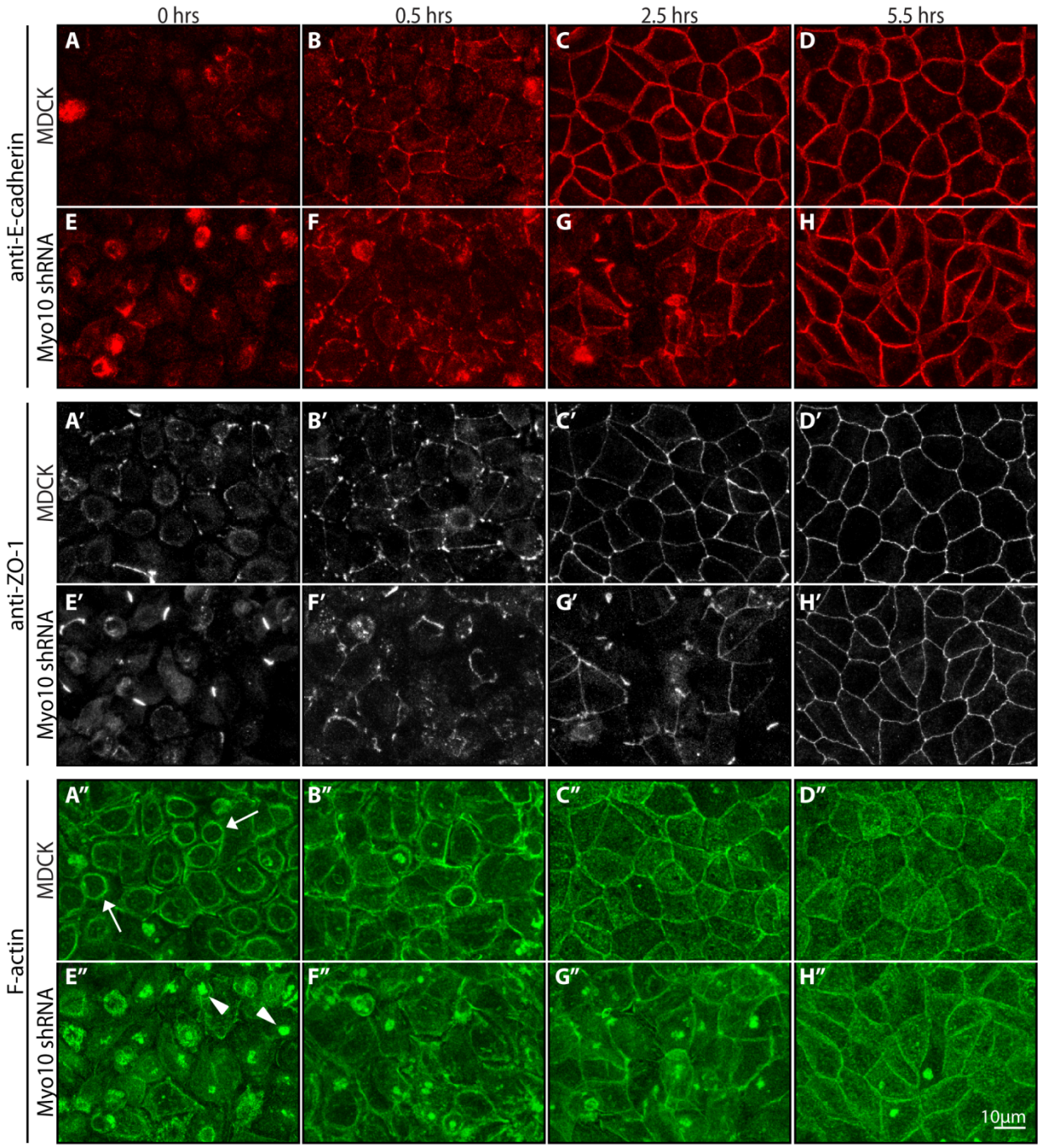

Figure 3.3 Myo10 knockdown delays E-cadherin and ZO-1 localization during junction formation. In calcium-switch experiments, knockdown of Myo10 (sh#44) delays the appearance of E-cadherin (A-H). This is most evident at the 2.5 hour time point, where the cadherin staining in Myo10 knockdown cells shows a more punctate and discontinuous pattern that largely normalizes by 5.5 hrs. Similar delays were observed with ZO-1 (A'-H') and F-actin (A''-H''). In control calcium-depleted MDCK cells, concentric actin "rings" were observed (A", arrows), whereas fewer actin rings and many actin "condensations" were detected in Myo10 knockdown cells at early time points, most notably at t=0 (E", arrowheads). All images are maximum projections of confocal z-stacks with 0.5 µm slice thickness.

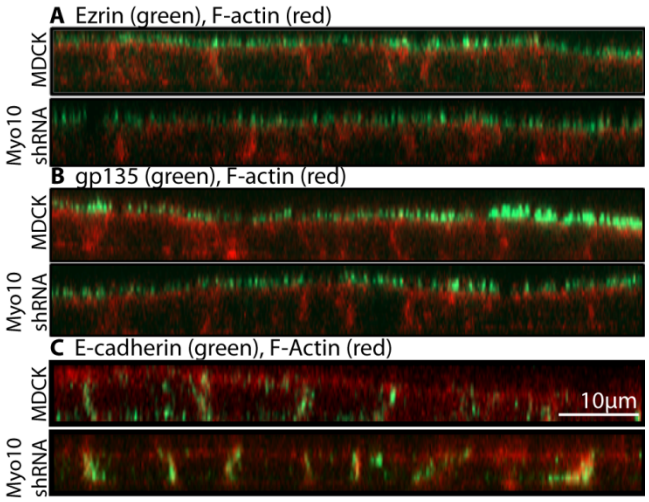

Figure 3.4 Myo10 knockdown does not affect markers of apico-basal polarity in MDCK monolayers. (A,B) Apical markers, ezrin and gp135, localize to the apical microvilli in knockdown (sh#16) and control MDCK cells. (C) E-cadherin localizes to the basolateral membrane in knockdown and control cells. Cells were fixed at 6 days post-plating. Confocal images were acquired on a Zeiss 510 LSM using a 63X Plan-Apochromat 1.4 NA Oil objective. Sections were acquired every 0.5 µm.

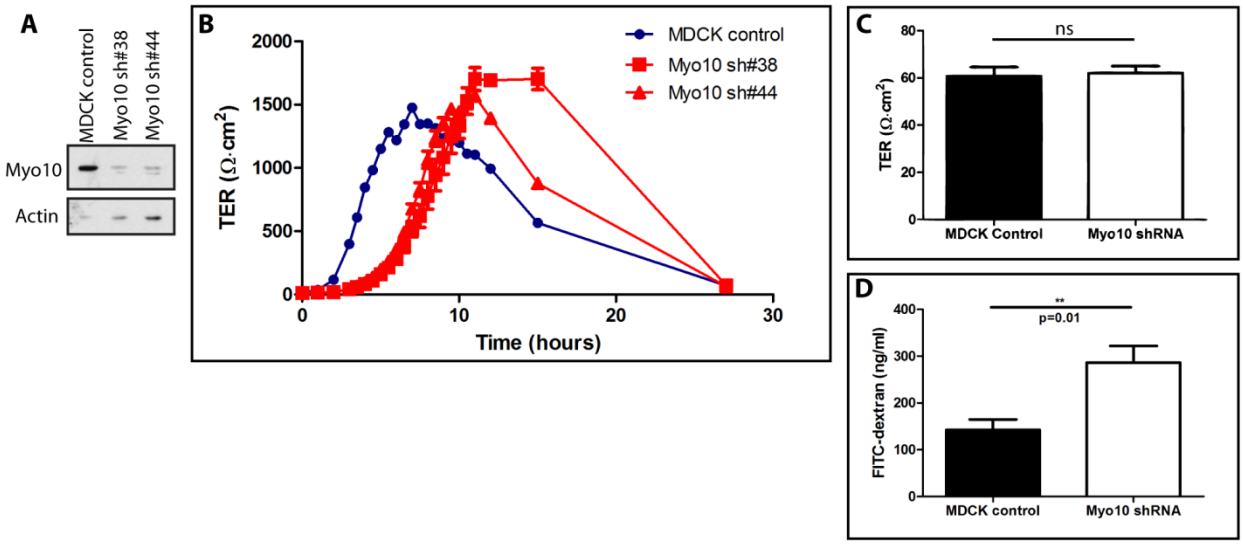

Figure 3.5 Myo10 knockdown delays tight junction formation measured by TER. (A) Immunoblot showing knockdown of Myo10 in stable MDCK lines, sh#38 and #44. Actin was used as a loading control. (B) Myo10 knockdown cells show a ~4 hr delay in the timing of the peak TER during the calcium-switch assay, thus demonstrating a kinetic defect in junction formation. By ~28 hours, the TER in both control and knockdown cells return to normal levels, ~60 $\Omega \cdot cm^2$. (C) Knockdown of Myo10 does not affect TER in mature monolayers (measured after 5 days in culture). (D) Knockdown of Myo10 does increase paracellular permeability to large solutes in mature monolayers. Cells were cultured for 5 days, then flux assays were performed to measure the movement of 3.0 kD FITC-dextran over a two hour time period. Calcium-switch experiments were performed in quadruplicate. Paracellular permeability results were averaged over two experiments. ** denotes significance of p=0.01, ns = not significant.

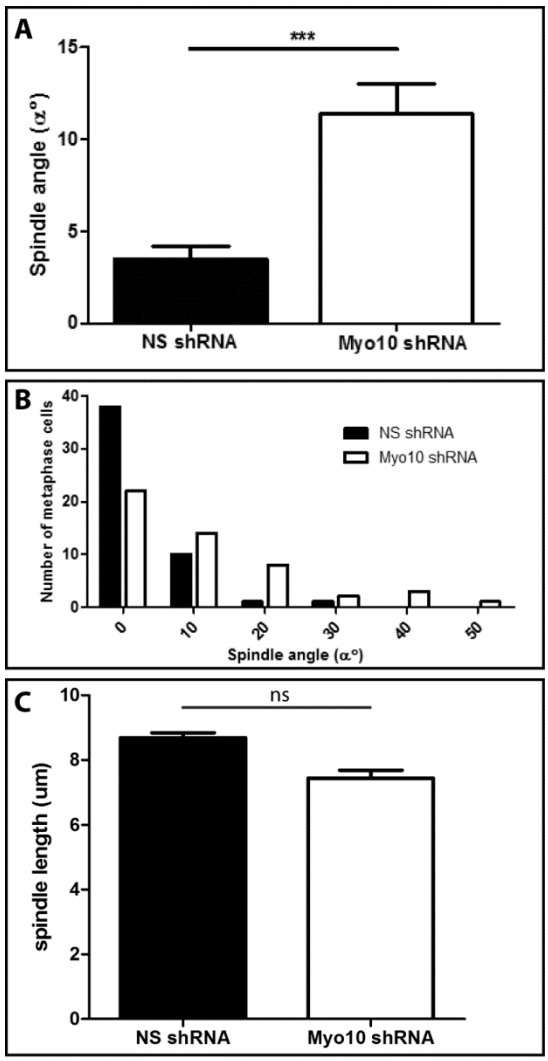

Figure 3.6 Myo10 knockdown cells show a defect in proper spindle orientation but not spindle length in mature MDCK monolayers. (A) Myo10 knockdown cells (sh#2-8) show increased average spindle angle from horizontal (0^o) and a larger distribution of spindle angles (B) (see Supplemental Methods). The histogram in (B) plots the number of metaphase cells with spindle angles binned in 10^o increments. (C) Myo10 knockdown has no significant effect on spindle length in MDCK monolayers. 50 cells/condition were counted. *** denotes significance of $p<0.001$, ns = not significant.

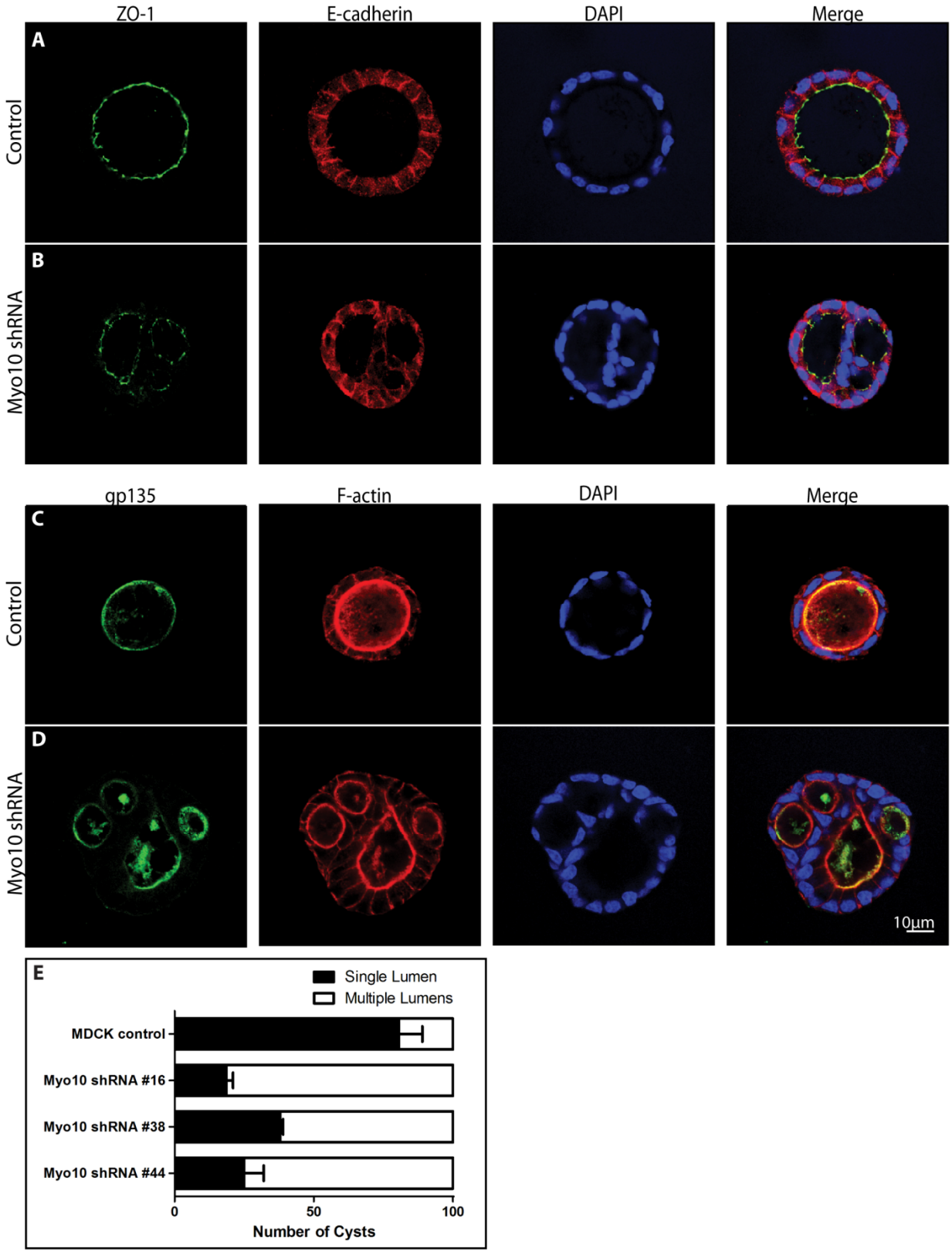
ZO-1
E-cadherin
DAPI
Merge
A
Control
B
Myo10 shRNA
gp135
F-actin
DAPI
Merge
C
Control
D
Myo10 shRNA
10μm
E
Single Lumen
Multiple Lumens
MDCK control
Myo10 shRNA #16
Myo10 shRNA #38
Myo10 shRNA #44
0
50
100
Number of Cysts

Figure 3.7 Myo10 knockdown leads to the formation of cysts with multiple lumens. (A,C) The majority of control MDCK cells grown in three-dimensional collagen-matrigel matrix for six days form cysts with a single lumen whereas the majority of Myo10 knockdown cells (sh#44) form cysts with multiple lumens (B, D). Cysts were stained for the tight junction marker ZO-1, the basolateral marker E-cadherin, and the apical markers gp135 and F-actin, as well as DAPI to stain for nuclei. Myo10 knockdown cells retain apico-basal polarity, as the apical and basolateral markers localize to their proper domains. (E) Bar diagrams showing the number of cysts with single versus multiple lumens, ascertained from 100 randomly selected cysts per condition and averaged over two experiments. While ~80% of control MDCK cells form single lumen cysts, only ~20-40% of Myo10 knockdown cells form single lumen cysts. Statistical significance ($p<0.05$) was achieved between MDCK vs. sh#16, MDCK vs. sh#38, and MDCK vs. sh#44.

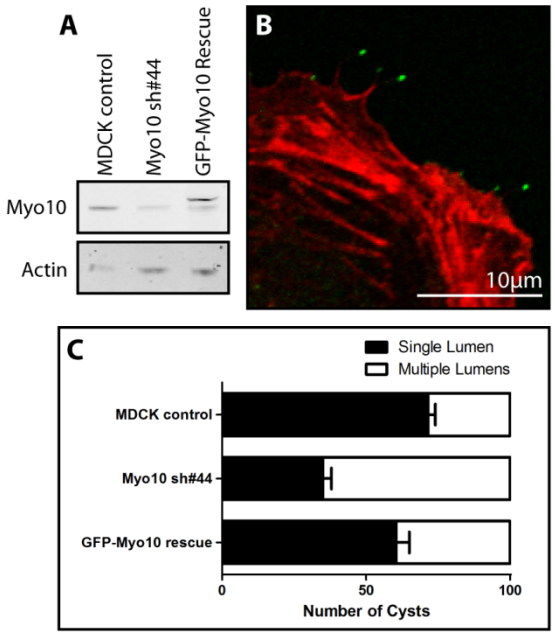

Figure 3.8 Partial rescue of multiple lumen cyst phenotype by expression of GFP-Myo10. (A) Immunoblot showing knockdown and rescue of Myo10 expression in MDCK lines. Anti-actin is shown as a loading control. (B) Fluorescence image of a rescue MDCK cell during spreading shows that GFP-Myo10 (green) localizes to filopodia tips as expected for functional Myo10; F-actin (red) was stained with phalloidin. (C) Myo10 knockdown (sh#44) increased the number of cysts with multiple lumens relative to control cells, and expression of GFP-Myo10 partially rescued this defect. Statistical significance ($p<0.05$) was achieved for MDCK vs. sh#44, and sh#44 vs. GFP-Myo10 rescue.

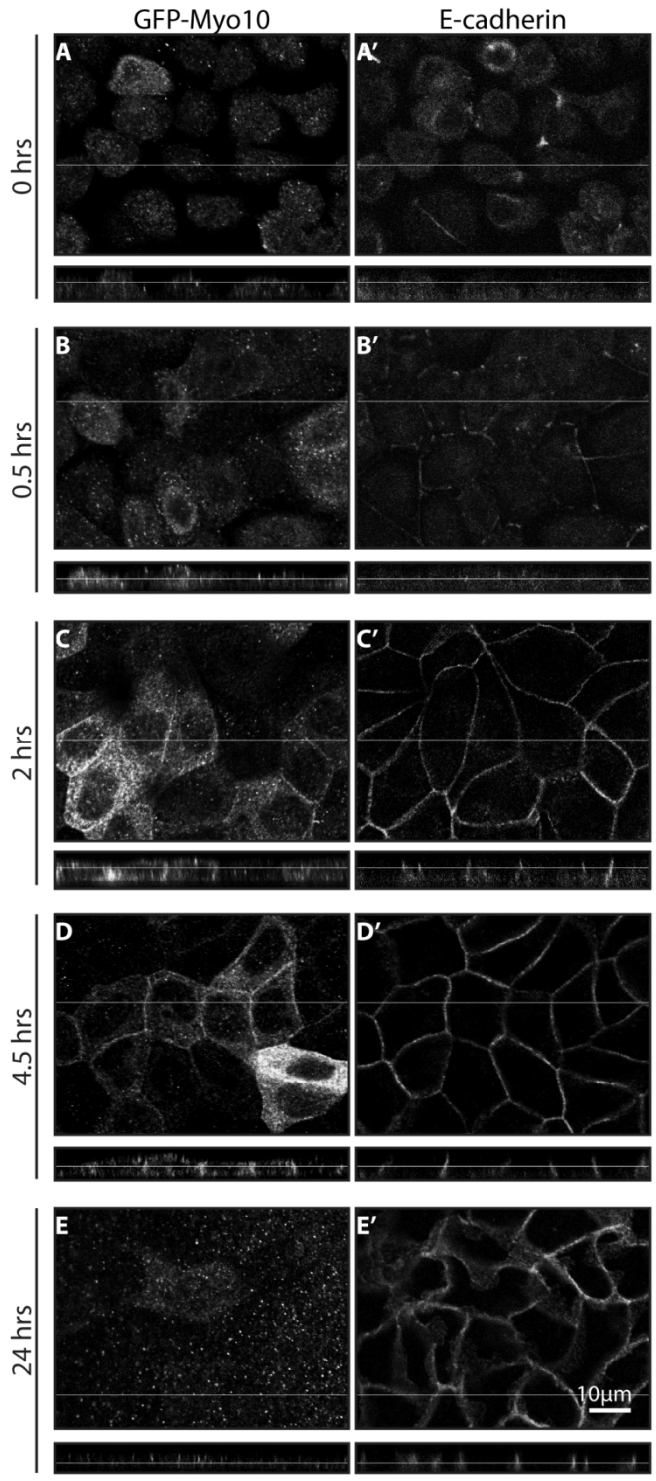

Figure 3.S1 GFP-Myo10 localizes along the lateral membranes in xz-sections during junction assembly. After re-addition of calcium, GFP-Myo10 transiently localizes to the lateral membranes at 2 and 4.5 hours during calcium-switch (B,C). (A-E) MDCK cells expressing GFP-Myo10 were fixed and stained with an antibody against GFP. (A'-E') Localization of E-cadherin during junction assembly. Lines in xy-sections denote the plane of xz-cross sections. Lines in xz-sections denote the plane of xy-planes.

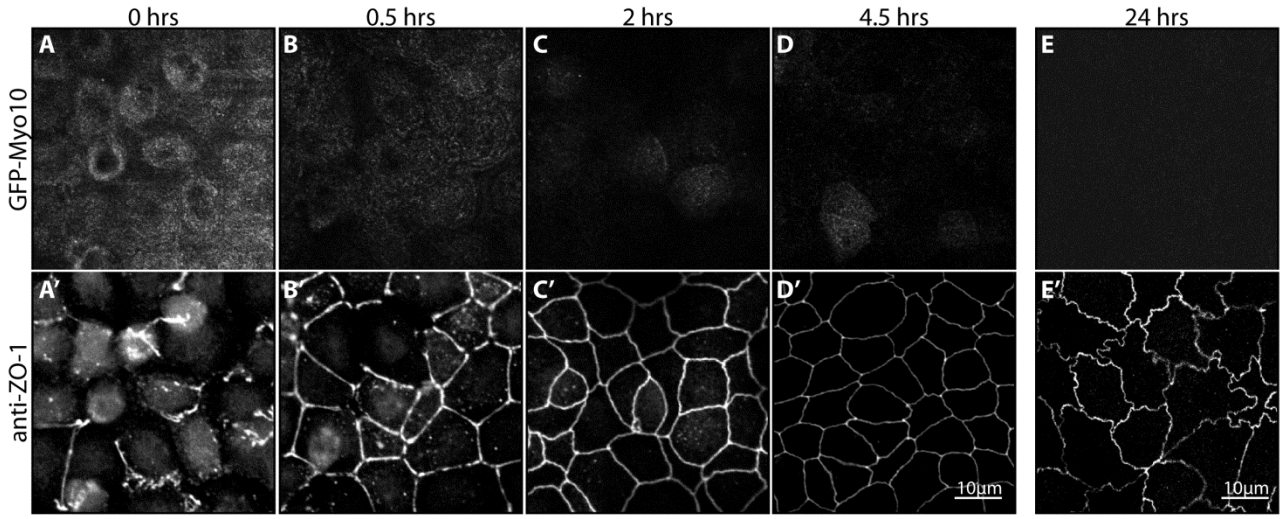

Figure 3.S2 GFP-Myo10 is not detected at the tight junction in MDCK monolayers. Single confocal planes were acquired at the level of the tight junction to show GFP-Myo10 (A-E) and ZO-1 staining (A'-E') during calcium-induced junction assembly. ZO-1 starts to be seen in a continuous pattern at apical junctions at 0.5 hours (B') while GFP-Myo10 is still diffusely distributed within the cytosol (B). GFP-Myo10 is enriched at the lateral membrane at the plane of the apical junctions (C-E). 24 hour images (E,E') were acquired from a separate experiment and again show lack of GFP-Myo10 enrichment at the tight junction in MDCK cells. Images were acquired from the same experiment and field of view as Figure 3.2.

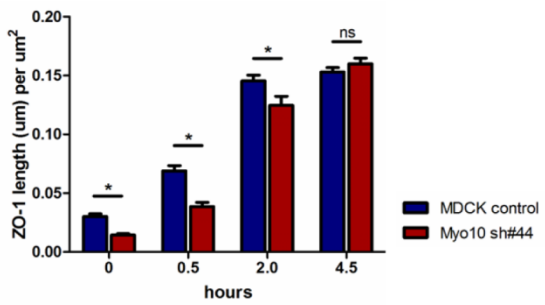

Figure 3.S3 Length measurements show Myo10 knockdown monolayers have less continuous, linear ZO-1 staining during junction assembly. Total length of continuous ZO-1 staining was quantified at different time points during calcium switch (see Supplemental Methods). Myo10 knockdown (sh#44) showed reduced ZO-1 length at each time point until 4.5 hours. * denotes significance of $p<0.05$, and ns = not significant.

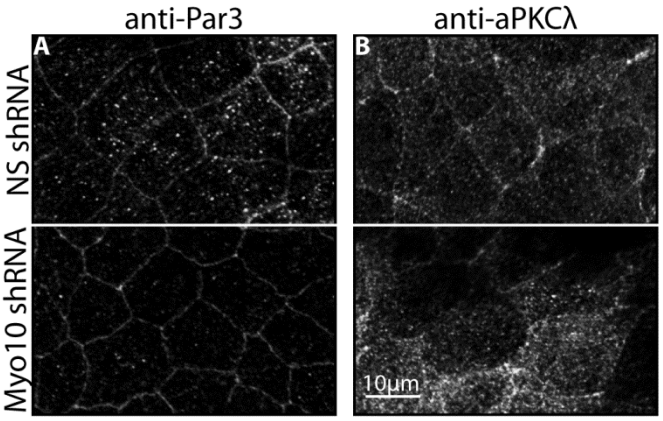

Figure 3.S4 Localization of polarity proteins Par3 and aPKC is unchanged with Myo10 knockdown. In Mature MDCK monolayers (grown for 5 days), there were no apparent differences in localization of anti-Par3 (A) and anti-aPKCλ (B) in Myo10 knockdown cells when compared with NS shRNA-expressing MDCK controls. All images are maximum projections of a confocal stack.

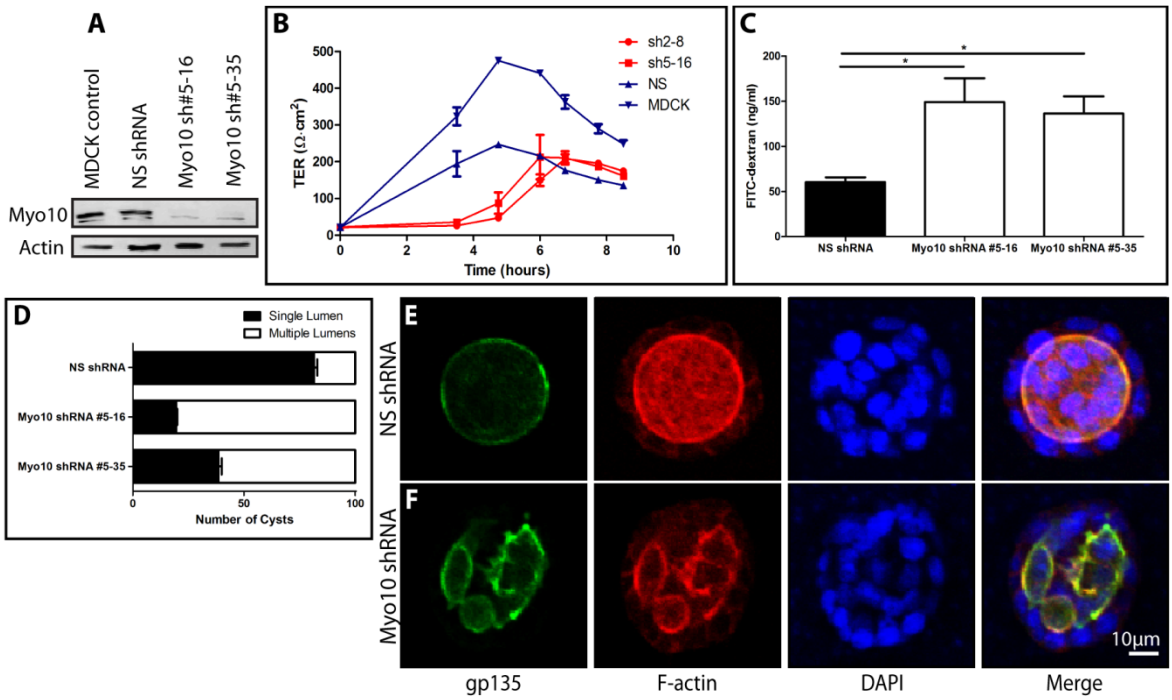

Figure 3.S5 Stable knockdown lines expressing shRNA#2 and shRNA#5 have similar defects in junction assembly and epithelial morphogenesis. (A) Immunoblot of myo10 knockdown using sh#2 and sh#5, and control cell expressing non-specific (NS) shRNA. (B) sh#5 and sh#2 show a similar kinetic delay in peak TER during calcium-switch. (C) Myo10 knockdown (sh#5) results in increased paracellular permeability to 3.0 kD FITC-dextran. (D) In 3D culture, Myo10 knockdown (sh#5) cells form fewer single lumens (~20-40%) compared with ~80% single lumens in control NS shRNA cells. Statistical significance ($p<0.001$) was achieved for NS vs. sh#5-16, NS vs. sh#5-35, and sh#5-16 vs. sh#5-35. (E,F) Apical marker ezrin and F-actin are localized properly in Myo10 shRNA cysts (sh#5-35) (F) compared with NS shRNA control cysts (E).

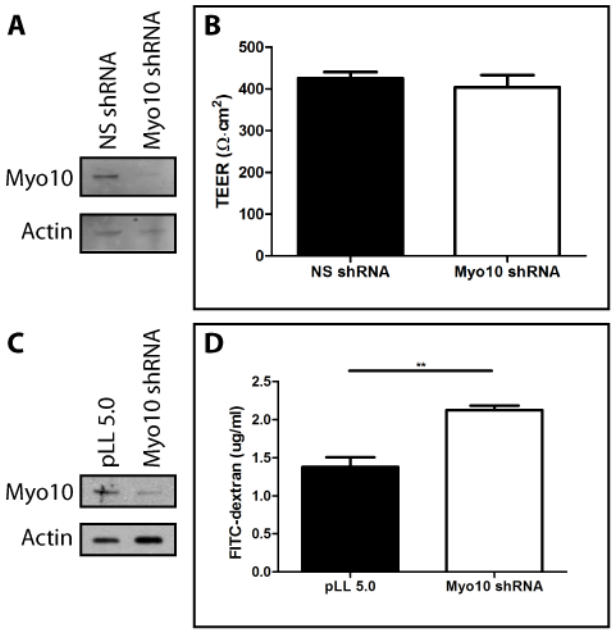

Figure 3.S6 As with MDCK cells, knockdown of Myo10 in Caco-2 cells has no effect on steady state TER but increases paracellular permeability to 3.0 kD FITC-dextran. (A) Immunoblot showing knockdown of Myo10 in Caco-2 BBe1 (human colon adenocarcinoma) cells using lentivirus methods (see Supplemental Methods). (B) No difference in steady state TER is observed in mature monolayers of Caco-2 cells (2 weeks in culture). (C) Immunoblot showing Myo10 knockdown by lentivirus methods; Cacl-2 cells were infected with lentivirus encoding Myo10 shRNA and placed under drug selection to select for infected cells. (D) Myo10 knockdown increases paracellular permeability in mature monolayers of Caco-2 cells (2 weeks in culture). ** denotes significance of p=0.0018.

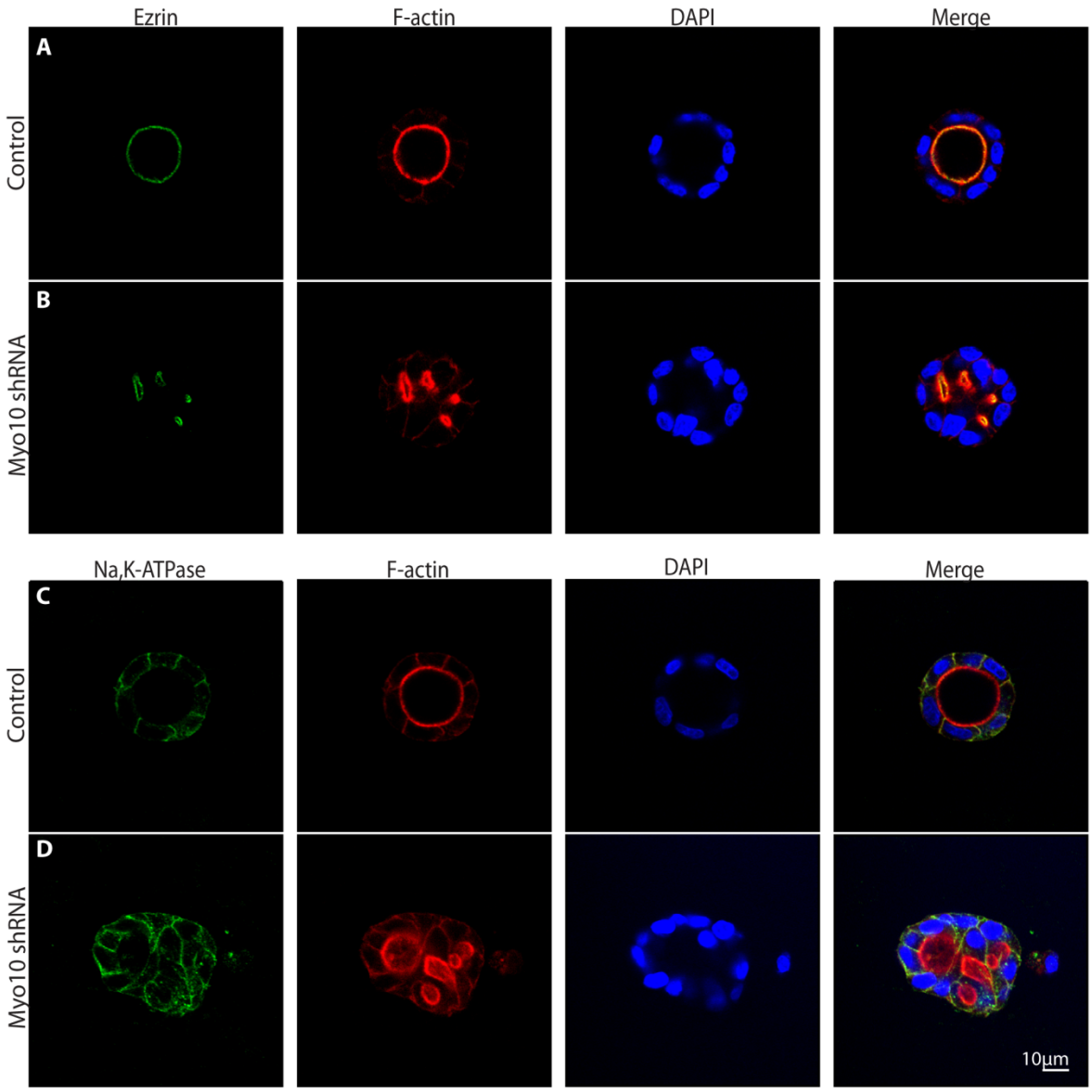

Figure 3.S7 Myo10 knockdown does not affect the localization of ezrin or Na,K-ATPase in MDCK cells grown in 3D culture. Myo10 knockdown (sh#38) and control cells are stained with (A,B) ezrin and actin, and (C,D) Na,K-ATPase and actin. (B,D) Although Myo10 knockdown cysts have multiple lumens, ezrin is properly localized to the apical domain (B), and Na,K-ATPase is properly localized to the basolateral domain (D).

SUPPLEMENTAL METHODS

Quantification of linear ZO-1 staining: Z-stacks of ZO-1 staining from 10 random fields of view were acquired at each time point in Myo10 knockdown and control MDCK monolayers during calcium-switch. From the z-stacks, standard deviation z-projections of ZO-1 staining were generated in ImageJ. Linear ZO-1 was identified in ImageJ using a procedure of enhancing contrast, applying the find edges filter, and generating a binary mask. Punctate ZO-1 staining was filtered out using the despeckle function. Length of linear ZO-1 staining was measured in an automated fashion using the AnalyzeSkeleton ImageJ plugin (Arganda-Carreras et al., Microsc Res Tech 2010), thresholded for all line segments greater than 0.5 μm. Total ZO-1 length was calculated in Microsoft Excel, and statistical analysis was performed using GraphPad Prism 5. This automated method of identifying ZO-1 length was manually validated by hand-tracing total ZO-1 length.

Caco-2 lentivirus Myo10 knockdown using cell sorting: (Supplemental Figure S6; A and B) Human Myo10 shRNA constructs were designed using siDESIGN Center (Dharmacon). Two siRNA constructs were made to target sequences in the motor domain of myosin-X (NM_012334): ggaaaggaattatcacata (bp 1236-1254) and aagtgcgaacggcaaaagaga (bp 4253-4273). One non-specific construct was made: gatcgacttacgacgttat. Forward and reverse oligonucleotides were designed, produced and annealed. The vector pLentiLox 4.0 was digested with XhoI and HpaI. For lentivirus infection, HEK-293 cells (ATCC CRL-1573) were plated at $150x10^4$ cells per 10 cm dish and grown in complete growth medium: DMEM with 10% fetal bovine serum, 100 units/ml penicillin/streptomycin. At 16-18 hours post-plating (day 1), FuGENE reagent (Qiagen), viral promoters pMDL-G/P-RRE, pRSV-REV, pCMV-VSVG,

and pLL shRNA (pool of 2 Myo10 shRNAs or NS shRNA) were added to serum-free DMEM. After incubation for 30 minutes, the DNA and FuGENE were added to the HEK293 cells. The efficiency of transfection was evaluated by screening for GFP fluorescence after 36-48 hours (day 3), and the media was changed to Caco-2 complete growth medium. On day 4, Caco-2 cells were split and replated to ~25% confluency. On day 5, viral media was removed from HEK293 cells and transferred to a 15 ml conical tube. Viral media was spun down at 3500 rpm for 5 minutes. To infect the Caco-2 cells with the lentivirus, viral supernatant was added to the Caco-2 cells, and polybrene (Sigma) at 4 μg/ml was added to the media. Following 8 hour incubation, the viral media was aspirated, discarded and replaced with fresh Caco-2 complete growth medium. On day 7, the infected Caco-2 cells were split into T75 flasks. On day 9, infected cells were sorted by fluorescence activated cell sorting. Caco-2 cells selected for GFP were replated in 10 mm transwell filters at 5000 cells/well. Caco-2 cells were grown for two weeks, changing media every 2-3 days.

Caco-2 lentivirus Myo10 knockdown using antibiotic resistance: (Supplemental Figure S6; C and D) Myo10 shRNA (target sequence: ggaaaggaattatcacata) was cloned into the HpaI/XhoI sites of pLL 5.0 BSR (blasticidin resistance, no GFP), a gift from Dr. Alan Fanning. Myo10 shRNA and empty pLL5.0 were used to infect Caco-2 cells using the above protocol (A). Following infection, Caco-2 cells were grown in 5 μg/ml blasticidin (InvivoGen) to select for infected knockdown or control cells. Selected Caco-2 cells were replated in 10 mm transwell filters at 5000 cells/well. Caco-2 cells were grown for two weeks, removing blasticidin one week prior to the experiment.

Immunoprecipitations: MDCK cells were grown in 10 cm plates to confluence (4-6 days), and calcium switch was performed. At 2 or 4 hours after calcium re-addition, cells were washed once with PBS. 1 ml of RIPA buffer (150 mM NaCl, 50 mM Tris-HCl pH 8, 1% NP-40, 0.5% sodium deoxycholate, 0.1% SDS, 50 mM NaF, 10 mM Na_4P_2O, 0.2 mM sodium orthovanadate, protease inhibitor cocktail (Roche)) or Cadherin IP lysis buffer (150 mM NaCl, 25 mM Tri-HCl pH 7.4,1 mM EDTA, 1% NP-40, 0.25% sodium deoxycholate, 50 mM NaF, 10 mM Na_4P_2O, 0.2 mM sodium orthovanadate, protease inhibitor cocktail) was added to each plate. Cells were scraped into eppendorf tubes and incubated on ice for 30 minutes. Cell lysates were passed through a 27-gauge needle to shear DNA. Cell lysates were centrifuged at 13,000xg for 15 minutes at 4^{o}C. Cell lysates were incubated with Myo10 (Sigma, HPA024223)/E-cadherin (BD Biosciences, 610181) antibody and Gammabind plus sepharose beads (GE Healthcare, Piscataway, NJ) for one hour at 4^{o}C, rotating. For immunoprecipitations of endogenous Myo10 in mature MDCK cells, MDCK cells were grown on 10 cm plates for 6 days. Immunoprecipitation protocol follows as above. The lysis buffer contains 40 mM HEPES pH 7.4, 75 mM KCl, 1% Triton-X, 2 mM K-EGTA, 5 µM latrunculin B, 5 mM ATP, protease inhibitor cocktail. The lysate, beads and antibody were incubated for 4 hours at 4^{o}C. For FLAG tag immunoprecipitation of GFP-Myo10, stable GFP-Myo10 cells were grown to confluence in 10 cm plates, and the lysis buffer contains 50 mM Tris-HCl (pH 7.4), 150 mM NaCl, 1% Triton-X, 2 mM MgCl2, 5 nM latrunculin B, 5 mM ATP, 4 mM DTT, protease inhibitor cocktail. Cells were washed with PBS and incubated in lysis buffer for 10 minutes on ice. Cell lysates were centrifuged for 13,000xg for 15 minutes at 4^{o}C. anti-FLAG M2 agarose beads (Sigma, A2220) were incubated with the cell lysate for 30 minutes at 4^{o}C.

Elutions were collected using 200 µg/µl 3X FLAG peptide (Sigma, F4799; diluted in 50 mM Tris-HCl, 150 mM NaCl, pH 7.9).

MOVIE LEGEND

Movie 3.1 Dynamics of GFP-Myo10 in filopodia-like structures on the basal surface of a confluent layer of MDCK cells during junction assembly. TIRF microscopy was used to image the basal surface of MDCK cells during calcium-switch. Puncta of GFP-Myo10 at the tips of filopodia-like structures show dynamic extension and retraction throughout junction assembly, and are present on the basal surface before E-cadherin localizes to cell-cell contacts. MDCK cells are stably expressing GFP-Myo10 at near endogenous levels. Note that GFP-Myo10 puncta exhibit similar dynamics despite the cells having variable levels of GFP-Myo10 expression. The frame rate is 1 frame/4 minutes with an exposure time of 130 ms. TIRF imaging was performed on an Olympus IX81 inverted microscope with a 60X Apo N, NA 1.49 Oil lens. Images were captured on an ImagEM-1K cooled CCD camera (Hamamatsu). 488 nm laser line was used at 66.29^{o} incident angle and penetration depth of 110 nm. Temperature was maintained at 37^{o}C and CO_2 was injected using a Bioptech closed chamber system (Bioptech, Butler, PA). Cells were plated on 35 mm Delta T dishes. Cells were calcium depleted overnight. To begin calcium-switch, 1.8 mM $CaCl_2$ was added to trigger junction formation. Metamorph software was used to acquire images, adjust contrast, scale images and build the movie. This movie was taken at 3.75 hrs after calcium addition, but similar Myo10 dynamics were observed prior to calcium addition and in mature monolayers. Scale bar = 35 µm.

CHAPTER FOUR

APICO-BASAL TARGETING OF MYOSIN-X IN POLARIZED EPITHELIAL CELLS

INTRODUCTION

Myosin-X (Myo10) is an unconventional myosin that localizes to the tips of filopodia and has been shown to have important functions in filopodia in non-polarized cells. Recently, we found that Myo10 has key functions in junction assembly, maintenance of paracellular permeability, and epithelial morphogenesis in polarized epithelial cells (Liu et al., 2012). We saw that GFP-Myo10 localizes to basolateral puncta in MDCK cells during junction formation. Here, using TIRF microscopy, we show that full-length Myo10 localizes to the tips of actin-based filopodia at the basal surface, and that these basal puncta of Myo10 are extremely dynamic. Interestingly, the Myo10 tail is sufficient for basolateral localization. Although full-length Myo10 was not detected in apical microvilli, GFP-Myo10 HMM (a construct lacking the tail) does localize to apical microvilli. Thus, the PH domains of the tail are necessary and sufficient for Myo10's basolateral localization. Deletion of the PH domains or disruption of phosphatidylinositol binding results in redistribution of Myo10 to the apical domain. Thus, apico-basal targeting of Myo10 is regulated, at least in part, by its PH domains.

In organs such as the kidney and small intestine, epithelial cells line tubular structures in a polarized manner with a lumen-facing apical domain and a basolateral domain contacting neighboring cells and the basement membrane. Apico-basal polarity is established by several conserved signaling pathways: Par3-Par6-aPKC, Scribble-Lgl-Dlg and Crumbs-Stardust-PATJ (McCaffrey and Macara, 2009). These signaling pathways arrange an unequal distribution of proteins between the apical and basolateral domains. Apical domain formation has been studied extensively, as proper apical surface organization is needed for the formation of normal, central lumens in tubules and cysts (Lincz et al., 1997; Olson et al., 1991). However, less is known regarding the establishment of the basolateral domain.

The actin cytoskeleton is a major structural component of the apical domain, cell junctions and basolateral domain. At the apical domain, actin filaments comprise the microvillus core and the underlying terminal web (Mukherjee and Staehelin, 1971). At the cell junction, a dense circumferential ring of actin is apposed to the adherens junction (Hirokawa et al., 1983; Hirokawa and Tilney, 1982). At the basal surface, robust actin bundles constitute stress fibers (Byers et al., 1984). Although often overlooked, the basolateral domain has other actin-based protrusions – sheet-like projections on the lateral membrane and filopodia on the basal surface (Figure 4.1) (Georgiou and Baum, 2010). Basolateral actin-based protrusions are dynamic, and inhibiting actin polymerization eliminates both lateral projections and basal filopodia (Georgiou and Baum, 2010).

The formation of the basolateral domain, like the apical domain, is defined by polarized signals. The structure of the basolateral actin cytoskeleton is regulated by Par proteins, Par3 and Par6 (Georgiou and Baum, 2010) and Dlg/Lgl/Scrib (Discs large/Lethal

giant larvae/Scribble) (Bilder et al., 2003). Also, formation of the basolateral plasma membrane is regulated by the polarized distribution of phosphatidylinositols (Gassama-Diagne et al., 2006). Specifically, phosphatidylinositol-4,5-bisphosphate (PIP2) is found at the apical domain while phosphatidyinositol-3,4,5-triphosphate (PIP3) is basolateral (Martin-Belmonte et al., 2007; Watton and Downward, 1999). Importantly, basolateral filopodia have a critical role in Delta-Notch signaling during Drosophila bristle organization (Cohen et al., 2010). Furthermore, components of the basolateral domain affect overall cell morphology. Defects in basolateral actin-based structures perturb cell morphology (Georgiou and Baum, 2010), and inhibition of endogenous PIP3 production results in abnormally short lateral domains (Gassama-Diagne et al., 2006). The basal surface is also the site of important cell-ECM (extracellular matrix) interactions. For example, basolateral β1-integrins regulate epithelial cell surface polarity in three-dimensional culture (Ojakian and Schwimmer, 1994). Yet, despite our current knowledge, relatively few regulators of the basolateral domain and its associated actin cytoskeleton are known.

Myosin-X (Myo10) is an unconventional myosin that is found at the tips of filopodia and has critical roles in filopodial formation (Berg and Cheney, 2002; Bohil et al., 2006; Kerber et al., 2009). Myo10 is widely expressed in epithelial cells (Berg et al., 2000), and in the kidney, Myo10 localizes to the basolateral domain (Liu et al., 2012) and is biochemically enriched in the basolateral fractions (Yonezawa et al., 2003). Myo10 is organized into a motor, neck and tail (Berg et al., 2000). The motor domain contains actin- and nucleotide-binding regions. The neck domain has three IQ motifs that can bind calmodulin or calmodulin-like protein (CLP), an epithelia-specific calcium-binding protein (Bennett et al.,

2007). The tail domain of Myo10 allows for a variety of unique molecular interactions. Importantly, three pleckstrin homology (PH) domains regulate the interaction of Myo10 with membrane-bound phosphatidylinositol-3,4,5-triphosphate (PIP3) (Mashanov et al., 2004; Plantard et al., 2010). The PH domains have been shown to affect filopodial formation in non-polarized cells (Plantard et al., 2010). The Myo10 tail also has a MyTH4-FERM domain (Myosin Tail Homology 4 domain and band 4.1/ezrin/radixin/moesin domain) that mediates Myo10's interactions with microtubules (Weber et al., 2004; Woolner et al., 2008) and β-integrins (Zhang et al., 2004). β-integrins are known to localize to the basolateral membrane in cultured polarized epithelial cells (Schoenenberger et al., 1994; Schreider et al., 2002).

Myosins function at both apical and basolateral domains. In the small intestine, Myo5b is critical for proper apical domain morphology, as knockout of Myo5b causes microvillar inclusion disease, where microvilli are enclosed in cytoplasmic vacuoles and remaining apical microvilli are morphologically abnormal (Muller et al., 2008). Myosin-VI is needed for basolateral trafficking of tyrosine motif-containing proteins (Au et al., 2007). Finally, Myosin-II is required for the maintenance of the circumferential actin ring at the zonula adherens (Ivanov et al., 2007).

Recently, we found that Myo10 functions in polarized epithelial cells (Liu et al., 2012). Specifically, Myo10 localizes to the lateral membrane during junction assembly and Myo10 knockdown results in defects in junction assembly, paracellular permeability and epithelial morphogenesis. We also found that Myo10 localizes to dynamic basal puncta, which we hypothesize to correspond to the tips of basolateral filopodia. Here, we provide evidence that supports Myo10 localization to the tips of basolateral filopodia. Also, we

demonstrate that the Myo10 tail domain and PH domains are required for basolateral localization. Myo10 constructs lacking either the tail or the PH domains localize to apical microvilli. Similar to the phenotype seen with inhibition of PIP3 production (Gassama-Diagne et al., 2006), preliminary studies show Myo10 knockdown cells are shorter and wider (Appendix I) and suggest a possible role for Myo10 in the regulation of cell morphology.

MATERIALS AND METHODS

Cell culture and Plasmids

Caco-2 BBe1 cells (ATCC, CRL-2102) were cultured in complete media (DMEM high glucose (Gibco/Invitrogen, Carlsbad, CA) with 10% fetal bovine serum (Gibco), 100 units/ml penicillin-streptomycin (Sigma, St. Louis, MO), 10 ug/ml human holo-transferrin (Sigma). Plasmids: Bovine GFP-Myo10, GFP-Myo10-heavy meromyosin (GFP-Myo10 HMM), GFP-Myo10 tail and GFP-Myo10 Headless were previously described (Berg and Cheney, 2002). GFP-Myo10Δ3PH was generated by Taofei Yin, based on constructs previously described (Cox et al., 2002).

Transfection and PI(3)K Inhibition

Caco-2 cells were plated at $7.5x10^4$ cells/well in 10-mm transwell filters with 0.4 µm pore size (Corning, Corning, NY) for two to three days. Caco-2 cells were transfected by Magnetofection with PolyMag beads (Oz Biosciences, Marseille, France). 1.5 µl DNA and 1.5 µl PolyMag beads were added to each well, followed by 15-minute incubation above a

super-magnetic plate (OZ Biosciences). After 48 hours, samples were fixed and prepared for immunofluorescence microscopy. PI3K inhibition experiments were performed by incubating GFP-Myo10-transfected cells with 20 µM LY294002 (Sigma) or 0.15 µM wortmannin (Sigma) for 1 hour at 37^{o}C.

Immunofluorescence Microscopy

Alexa Fluor 568 phalloidin (Invitrogen Molecular Probes) was used to label F-actin. To label focal adhesions, monoclonal anti-vinculin (V9264, Sigma) and mouse anti-paxillin (05-417, Millipore) antibodies were used. Immunofluorescence microscopy was performed as previously described (Liu et al., 2012). Immunofluorescence samples were imaged on an Olympus FLUOVIEW FV 1000 inverted confocal microscope (Center Valley, PA) using a PlanApo 60X Oil, 1.42 NA objective (UNC-Olympus Imaging Research Center). The FV1000 has diode lasers for 405nm, 559nm and 635nm wavelengths, and an Argon laser for 488nm wavelength use. For z-stacks, 640 x 640 pixel, 0.44 µm slices were collected at 4.0 µs/pixel sampling speed in sequential line mode and using Kalman integration.

TIRF Imaging

For TIRF imaging of basolateral filopodia, control MDCK II cells or MDCK II cells stably expressing GFP-Myo10 were transiently transfected with tagRFP-Lifeact (gift from Dr. Jim Bear) using Lipofectamine 2000 (Invitrogen). Cells were plated on 35mm Bioptech Delta T dishes (Bioptechs Inc., Butler, PA) and cultured in complete media for ~3 days or until confluent. Prior to TIRF imaging, media was changed to OptiMEM with 10 mM HEPES, 4%

FBS and penicillin-streptomycin. TIRF imaging was performed on a Nikon TE-2000U inverted microscope equipped with a Nikon TIRF-II illuminator with 18 mm field of view. Images were obtained using a 60X 1.45 NA TIRF objective. TIRF illumination was provided by a 300 mW argon laser and a AOTF was used for rapid wavelength selection and shuttering. Using a 1.45 NA lens with 514 nm light at 63° incidence, the calculated penetration depth of the TIRF field is ~158 nm. Experiments were performed at 37°C. Time-lapse images were acquired at 30 seconds/frame to 2 minutes/frame.

Filopodia Quantification

MDCK cells stably expressing GFP-Myo10 and untreated MDCK II cells were trypsinized from subconfluent cultures and plated at low density onto collagen-coated gridded glass coverslips. Cells were incubated in complete media for two hours at 37^{o}C and 5% CO_2. Cells were fixed with 4% paraformaldehyde in PBS for 30 min at RT, then washed with PBS. Single cells were visualized by DIC microscopy on a Nikon TE-2000U inverted microscope using a 60X TIRF objective. Randomly selected, single cells were imaged. Filopodia number was quantified in ImageJ. From each cell, all thin filopodia-like projections were traced, from the cell edge to the tip of the projection. A filopodium was defined as a projection > 0.5 μm in length. The graph and statistical analysis were generated in GraphPad Prism 5.

Transmission Electron Microscopy

All TEM experiments were performed at the Microscopy Services Laboratory in the Department of Pathology and Laboratory Medicine at UNC-Chapel Hill. Cell monolayers cultured on filter substrates were rinsed with PBS or serum-free medium and fixed in 3% glutaraldehyde/0.1 sodium cacodylate with 0.05% $CaCl_2$, pH 7.4. After three rinses with sodium cacodylate buffer, the monolayers were postfixed for 1 hour in 1% osmium tetroxide/1.25% potassium ferrocyanide in 0.1 sodium cacodylate buffer. After rinsing in deionized water, the cells were dehydrated using increasing concentrations of ethanol (30%, 50%, 75%, 100%, 100%, 10 minutes each) followed by embedment in Polybed 812 epoxy resin (Polysciences, Inc., Warrington, PA). The samples were sectioned perpendicular to the substrate using a diamond knife. 70-nm ultrathin sections were mounted on formvar-carbon filmed 200 mesh copper grids and stained with 4% aqueous uranyl acetate for 15 minutes, followed by Reynolds lead citrate for 7 minutes. Samples were viewed using a LEO EM910 transmission electron microscope operating at 80kV (LEO Electron Microscopy Inc., Thornwood, NY). Digital images were acquired using a Gatan Orius SC1000 CCD Digital Camera and Digital Micrograph 3.11.0 (Gatan, Inc., Pleasanton, CA).

RESULTS

GFP-Myo10 labels the Tips of Basolateral Filopodia in Caco-2 and MDCK cells

For the majority of our experiments, we used Caco-2 cells (human colon adenocarcinoma) cells as a model system. Caco-2 cells have a robust apical cytoskeleton with actin-rich microvilli and terminal web, and a basolateral domain with actin-based

lateral protrusions, basal filopodia, and basal stress fibers (Figure 4.1). Additionally, fully polarized Caco-2 cells grow to be approximately 30 μm tall (Peterson et al., 1993), such that the apical and basolateral domain can be clearly distinguished by confocal microscopy. For Myo10 localization studies, we transiently transfected Caco-2 cells with GFP-Myo10 and other GFP-tagged Myo10 constructs (Figure 4.2). GFP-Myo10 localized at the basolateral domain (Figure 4.3; A and B), cytosolic labeling and strong labeling of the basal surface (Figure 4.3B), although some labeling is also detected on the lateral surfaces. GFP-Myo10 has a striking punctate localization, which we hypothesize to be at the tips of basolateral actin-based filopodia. To verify that the basolateral localization pattern observed in Caco-2 cells was not an artifact of overexpression, we used a Madin-Darby Canine Kidney (MDCK) cell line stably expressing GFP-Myo10 at near endogenous levels. In fixed MDCK cells, we observed the same punctate basolateral localization (Figure 4.3D), in agreement with our observations in transiently transfected Caco-2 cells. GFP-Myo10 was not detected at the apical domain, neither in microvilli nor the terminal web (Figure 4.3D), despite the ability of Myo10 to select for bundled actin (Nagy et al., 2008) in *in vitro* motility assays. The results showing Myo10 at basal puncta in fixed Caco-2 and MDCK cells are consistent with our previously reported results in live MDCK cells stably expressing GFP-Myo10 (Movie 3.1) during calcium-switch.

To determine if puncta of GFP-Myo10 localize specifically to filopodial tips at the basal surface, we transiently transfected GFP-Myo10 stable MDCK cells with tagRFP-Lifeact to label F-actin. Since transfection efficiency is partial, this allows for unambiguous identification of actin-based structures of a single cell within a monolayer. Using live-cell

TIRF microscopy, co-transfection experiments demonstrate GFP-Myo10 labels the tips of actin-labeled protrusions on the basal surface (Figure 4.4; Movie 4.1). To rule out concerns that the basolateral filopodia are a result of filopodia induced by overexpression of GFP-Myo10, we used stable GFP-Myo10 cells expressing near endogenous levels as assessed by immunoblotting. As an additional control, filopodia were quantified in single cells, and there was no significant difference in the average number of filopodia per cell between GFP-Myo10 and MDCK controls (Figure 4.5) (GFP-Myo10: 18.84 ± 1.12 filopodia/cell vs. MDCK control: 20.11 ± 0.99 filopodia/cell). We also confirmed that MDCK cells normally have basolateral filopodia by expressing tagRFP-Lifeact to label basal actin-based protrusions in control MDCK cells (Figure 4.6; Movie 4.2). Finally, to exclude the possibility that Myo10 puncta correspond to focal adhesions, we co-stained GFP-Myo10 stable cells with the focal adhesion markers vinculin and paxillin. GFP-Myo10 does not colocalize with focal adhesion markers at the basal surface of MDCK cells (Figure 4.7), consistent with previously reported results in non-polarized cells (Kerber et al., 2009; Zhang et al., 2004). Together, our results demonstrate Myo10 localizes to the tips of actin-based filopodia on the basal surface of MDCK and Caco-2 cells.

Myo10 Tail is Required for Basolateral Localization

In order to identify the domains that are needed for Myo10's basolateral localization, we performed preliminary targeting experiments using Myo10 deletion constructs. First, we asked whether the tail is needed for basolateral localization. Strikingly, GFP-Myo10 HMM (a construct consisting of the head, neck and alpha helical region but

lacking the rest of the tail; Figure 4.2) localizes predominantly to apical microvilli in Caco-2 cells (Figure 4.8A). GFP-Myo10 HMM colocalizes with F-actin at the apical domain, and little to no GFP-Myo10 HMM was detected at the basal surface (Figure 4.8A).

Next, we tested the GFP-Myo10 Tail construct, which consists of the three PH domains and the MyTH-FERM domain (Figure 4.2). GFP-Myo10 Tail localizes basolaterally, but instead of punctate labeling like full-length Myo10, GFP-Myo10 Tail is distributed throughout the basolateral membrane and does not localize to basal puncta under other cells (Figure 4.8B). Finally, we assessed the localization of GFP-Myo10 Headless (Figure 4.2), which lacks most of the motor but includes the stable alpha helical region (SAH) (Knight et al., 2005) thought to allow Myo10 to dimerize. Similar to GFP-Myo10 Tail, GFP-Myo10 Headless labels the basolateral membrane and appears to co-localize with F-actin (Figure 4.8C).

These results suggest that the tail of Myo10 is necessary and sufficient for localization to the basolateral domain, and the presence of the stable alpha helical region does not restore the punctate basolateral localization of GFP-Myo10 tail.

PH Domains and Phosphatidylinositol Binding are Needed for Basolateral Localization

We next sought to identify the tail domains necessary for the punctate basolateral localization of Myo10. Since the PH domains of Myo10 have high affinity for phosphatidylinositol-3,4,5-triphosphate (PIP3) (Mashanov et al., 2004; Plantard et al., 2010), and PIP3 is a basolateral-specific phosphatidylinositol in polarized epithelial cells (Watton and Downward, 1999; Yu et al., 2003), we hypothesized that the PH domains of

Myo10 are required for its basolateral localization. Consistent with this, we found the PH domains of Myo10 indeed localize to the basolateral domain; GFP-Myo10 3PH (Figure 4.2) labels the basolateral membrane in Caco-2 cells (Figure 4.9A). Like GFP-Myo10 HMM, GFP-Myo10Δ3PH, a deletion construct lacking all three PH domains (Figure 4.2), shows localization to the apical microvilli (Figure 4.9B).

As an alternative method to disrupt PIP3, we treated GFP-Myo10-transfected Caco-2 cells with phosphatidylinositol (PI) 3-kinase inhibitors. In cells treated with LY294002, the punctate basolateral localization of GFP-Myo10 was largely disrupted, and GFP-Myo10 partially relocalized to apical microvilli and cytoplasmic puncta (Figure 4.10). Similar effects were observed in GFP-Myo10 transfected Caco-2 cells treated with wortmannin, another PI 3-kinase inhibitor (data not shown). These results suggest that the PH domains and PIP3 binding are required for localization of Myo10 to basolateral puncta.

DISCUSSION

GFP-Myo10 localizes to Basolateral Filopodia in Polarized Epithelial Cells

Myo10 has well-established roles in filopodial formation and dynamics (Berg and Cheney, 2002; Bohil et al., 2006). In addition, Myo10 is theorized to localize to filopodia by selecting for bundled actin (Nagy et al., 2008). In polarized epithelial cells, there are distinct sets of bundled actin at different parts of the cell: apical microvilli, circumferential actin at cell junctions, lateral infoldings, and basal filopodia (Figure 1.1 and Figure 4.1) (Georgiou and Baum, 2010). We show that GFP-Myo10 is highly dynamic and localizes to tips of actin-based filopodia on the basal surface. Importantly, this striking localization was not due to

the filopodia-inducing activity of Myo10. GFP-Myo10 is expressed at near endogenous levels and does not increase filopodia number, and basal actin-based filopodia are observed in untreated MDCK cells.

Recently, basolateral filopodia have been shown to be important in physiological processes such as tissue patterning (Cohen et al., 2010), and basolateral filopodia share important features with invadopodia, which are actin-based protrusions associated with malignant cancers. Myo10 localizes to invadopodia, and Myo10 knockdown inhibits invadopodia formation (Schoumacher et al., 2010). Thus, it is likely that Myo10 has functional roles in basolateral filopodia of polarized epithelial cells. For example, Myo10 could function during junction assembly in forming initial filopodia-like cell-cell contacts (Vasioukhin et al., 2000). As a molecular motor, Myo10 could, in theory, transport cargoes to the basolateral domain. Given that Myo10 can bind membrane, it could be generating the force needed to maintain actin-based protrusions on the basal surface.

What targets Myo10 to basolateral filopodia rather than apical microvilli? Our data support the hypothesis that Myo10 targets to the basolateral plasma membrane by the tail (and its membrane-binding PH domains), then the motor domain targets Myo10 to the actin bundles of basolateral filopodia.

Myo10 Tail is Sufficient for Localization to the Basolateral Domain

GFP-Myo10 shows striking punctate localization to the tips of basolateral filopodia. We first asked whether the tail was responsible for this basolateral localization. We found that the Myo10 tail localizes to the basolateral membrane in Caco-2 cells. However, unlike

GFP-Myo10, the Myo10 tail localizes along the length of the basolateral membrane rather than in basolateral puncta. From the data presented here, it is likely that the PH domains target the Myo10 tail to the basolateral membrane by binding PIP3. Consistent with this, Lu et al. show that the PH domains also target to the basolateral membrane in MDCK cells (Lu et al., 2011). These results support the hypothesis that Myo10 is first recruited to the basolateral membrane by PH domain-mediated interactions, followed by motor-dependent localization to nearby actin-based filopodia. Our recent work showing transient localization of GFP-Myo10 to lateral membranes during junction assembly (Liu et al., 2012) is also consistent with this hypothesis. Formally, it is possible that deletion of the PH domains could disrupt the folded conformation of Myo10, such that Myo10 is in an unfolded, active state. It is also possible that the MyTH-FERM domain contributes to targeting of the Myo10 tail to the basolateral membrane by binding to β-integrins. Notably, some β-integrins localize along the length of the basolateral membrane (Schoenenberger et al., 1994).

The fact that deletion of the PH domains leads to targeting to microvilli suggests that binding to PIP3 has a dominant role in the basolateral targeting of Myo10, at least in the Caco-2 model used here.

The Motor Domain of Myo10 can bind Microvillar Actin Bundles

Our results show that GFP-Myo10 HMM targets to the apical domain, which demonstrates that the tail is required for basolateral localization of Myo10. GFP-Myo10 HMM appeared to co-localize with the microvillar F-actin. Because of the limited resolution of confocal microscopy in xz- cross-sections (microvilli in MDCK cells are ~1 μm in height), it

was unclear whether GFP-Myo10 labeled only the tips or along the length of microvilli. Additional experiments are needed to determine the precise localization of Myo10 and Myo10 mutant constructs. In order to differentiate between tip or microvilliar length labeling, future experiments could include dissociating the cells for higher resolution imaging of microvilli in the xy-plane. Also, immunogold labeling using an antibody to GFP (antibodies to Myo10 may not be sufficiently robust) can be performed and imaged at higher resolution by electron microscopy. Our observations strongly suggest that the motor domain of Myo10 can move along microvillar actin bundles, but that the PH domains in the tail normally target it basolaterally.

Intriguingly, GFP-Myo10 HMM was rarely observed at basolateral actin bundles. If Myo10 were non-selective for actin bundles, one might have expected the population of GFP-Myo10 HMM to be evenly distributed between apical and basolateral actin bundles; yet, GFP-Myo10 HMM was predominantly found in apical microvilli. One possibility is that the quantity and concentration of F-actin bundles in apical microvilli outweighs the basolateral actin bundles, so that this shifts the population of GFP-Myo10 HMM toward the apical domain. Another possibility could involve the organization of actin bundles, as basolateral actin bundles or stress fibers are not polarized, but rather, the bundles are arranged antiparallel to one another.

PH Domains and PI3K Activation are Needed for Basolateral Localization

The tail of Myo10 has several domains that could contribute to its basolateral localization in polarized epithelial cells. PIP3, found at the basolateral domain, is known to

bind Myo10 with high affinity, and the PH domains of Myo10 localize to the basolateral membrane. Thus, we tested whether deletion of the PH domains affect Myo10's punctate basolateral localization. Similar to results with GFP-Myo10 HMM, GFP-Myo10Δ3PH targets to apical microvilli and co-localizes with F-actin. In preliminary experiments, treatment with PI3K inhibitors partially disrupts GFP-Myo10 localization to basolateral filopodia, with a subpopulation of GFP-Myo10 redistributing to the apical domain or to cytoplasmic puncta. This suggests PI3K activation may be needed for basolateral localization. Further experiments quantifying GFP-Myo10's apico-basal distribution are needed to confirm this result. A partial effect with PI3K inhibitors could be due to the interaction of Myo10 with β-integrins, which are components of adhesive structures found at the basolateral membrane; thus, it is possible that β-integrins contribute to Myo10's localization at the basolateral domain.

Phosphatidylinositols, and PIP3 in particular, have been implicated in establishing the leading and trailing edges of chemotaxing cells, as well as in the polarization of neurons and epithelial cells. Interestingly, Myo10 has been is found in the same location as has been reported for PIP3 in several cell types. PIP3 accumulates at the leading edge in non-polarized cells and induces actin polymerization (Chen et al., 2003). We have observed Myo10 localization at the leading edge of unpolarized epithelial and endothelial cells. Additionally, PIP3 is reported to be enriched in filopodia of neuronal dendrites where Myo10 is also detected (Luikart et al., 2008). Finally, in polarized epithelial cells, PIP3 localizes to the basolateral membrane (Watton and Downward, 1999; Yu et al., 2003). We have also demonstrated that Myo10 localizes to lateral membranes during junction

assembly in MDCK cells (Liu et al., 2012). Further experiments are needed to test whether Myo10 and PIP3 indeed co-localize. PH domains are a unique feature of Myo10 among MyTH-FERM myosins. In comparison, Myo7b, a MyTH-FERM myosin that is expressed in epithelial cells but lacks PH domains, localizes to the tips of microvilli.

Here, we show that GFP-Myo10 has a unique distribution to the tips of basolateral filopodia in fully polarized epithelial cells. The basolateral targeting of Myo10 requires the tail and the PH domains. Intriguingly, GFP-Myo10 HMM and 3PH deletion localizes to apical microvilli, and disruption of PIP3 production showed similar effects. In our working model, full-length Myo10 localizes to the tips of basolateral filopodia via a two-step process (Figure 4.11). Myo10 is present in the cytoplasm as a folded, inactive monomer (Figure 4.11A). Myo10 is targeted to the basolateral membrane as the PH domains bind PIP3 (Figure 4.11B). Binding to PIP3 also results in unfolding and activation of Myo10, which can then dimerize and allow Myo10 move onto actin in basolateral filopodia (Figure 4.11C). However, in the absence of the PH domains, dimerized Myo10-HMM has the ability to move on microvillar actin (Figure 4.11D). Alternatively, it is possible that Myo10 is excluded from certain subpopulations of bundled actin; for example, actin-binding proteins like tropomyosin could "mask" certain bundled actin from Myo10, whereas its absence on other actin bundled arrays would permit Myo10 to bind.

Recent studies have focused on the functional importance of the basolateral domain and basolateral filopodia. Polarized cell morphology is affected by perturbations in the lipid composition of the basolateral domain (Gassama-Diagne et al., 2006). Interestingly,

exogenous PIP3 injected into the apical domain leads to recruitment of basolateral proteins and membrane restructuring at the apical domain (Gassama-Diagne et al., 2006). Also, tissue patterning is regulated by basolateral filopodia that induce lateral inhibition via Delta-Notch signaling (Cohen et al., 2010). In addition, basolateral filopodia are structurally similar and share many of the same molecular components with invadopodia, basal actin-based protrusions characteristic of invasive cancer cells that can breach the basement membrane. Intriguingly, Myo10 is enriched in invadopodia and Myo10 knockdown results in a decreased ability for matrix degradation (Schoumacher et al., 2010). Finally, basolateral filopodia are observed in HGF-induced tubulogenesis in 3D culture (Williams and Clark, 2003), and Myo10 is phosphorylated downstream of HGF stimulation (Hammond et al., 2010). Basolateral filopodia are implicated in several physiological and pathophysiological processes, which suggest functional roles for Myo10 in polarized epithelial cells that remain to be explored.

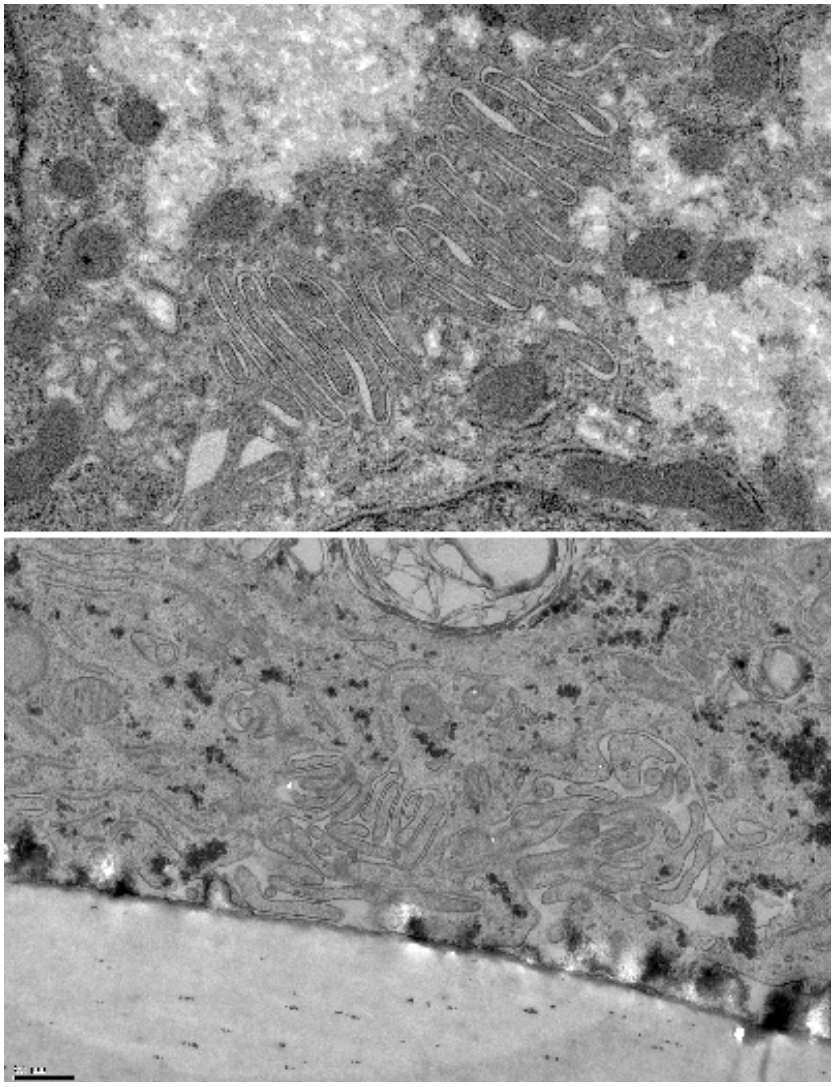

Figure 4.1 Basolateral actin-based protrusions of Caco-2 cells by TEM. (A) Sheet-like protrusions are found at the lateral membrane, interdigitating between neighboring cells. (B) Basal infoldings contact the underlying polycarbonate filter substrate. Scale bar = 0.5 µm. Images were acquired using a Gatan Orius SC1000 CCD Digital Camera and Digital Micrograph 3.11.0 (Microscopy Services Laboratory, UNC Department of Pathology).

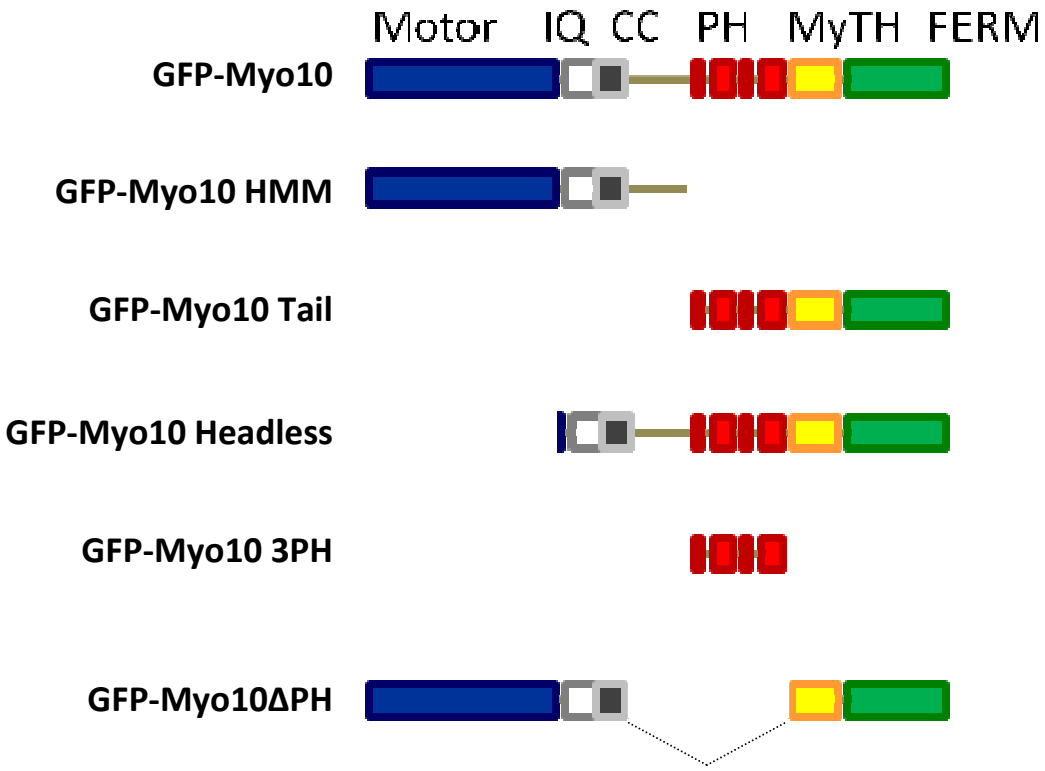

Figure 4.2 Bar diagram of Myo10 constructs. All constructs are in pEGFP-C2 and contain a GFP tag at their amino terminus.

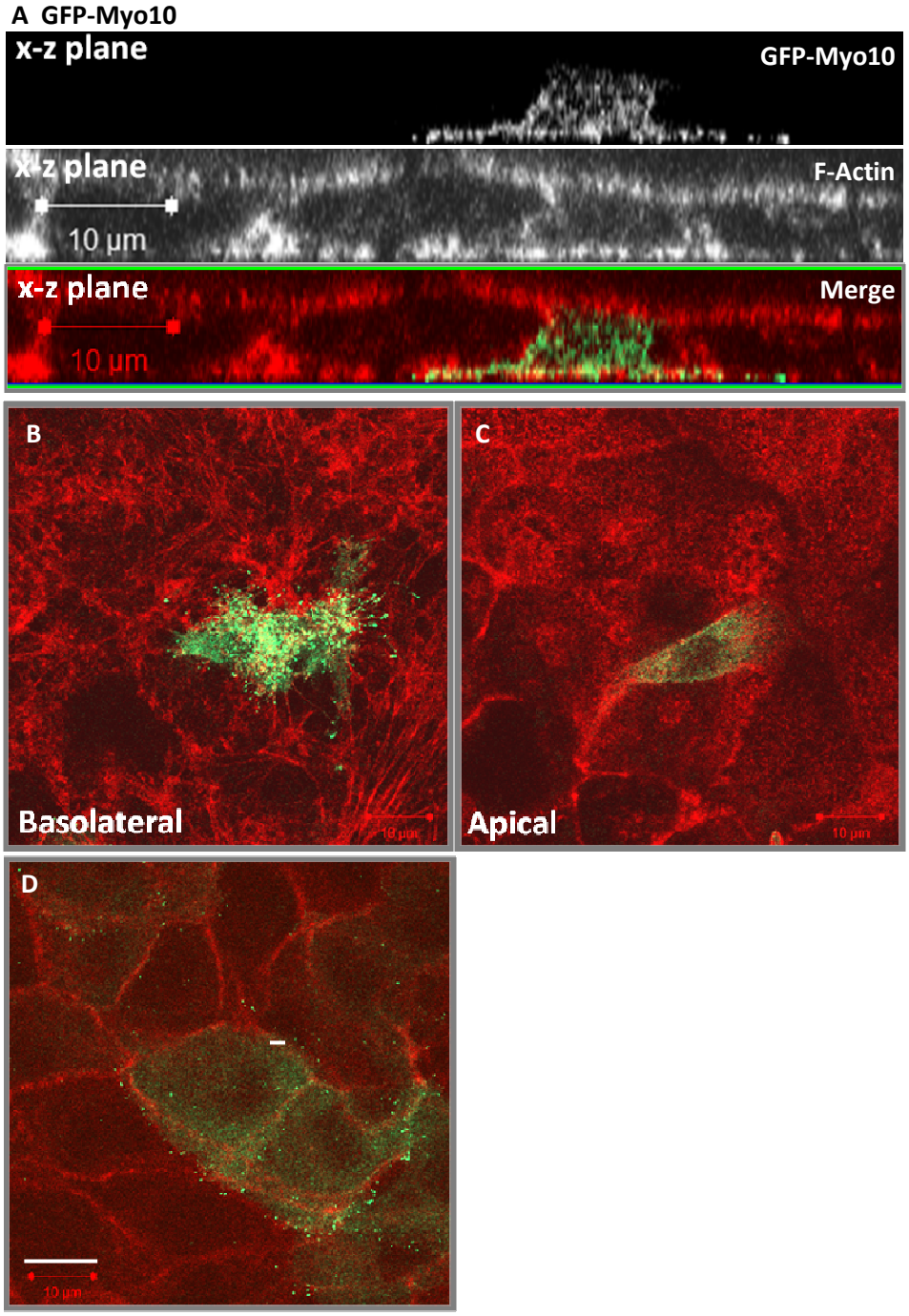

Figure 4.3 GFP-Myo10 localizes to the basolateral domain in Caco-2 and MDCK cells. (A) Cross-section of Caco-2 monolayer shows GFP-Myo10 localizes primarily to the basolateral domain or the cytoplasm. (B) GFP-Myo10 shows punctate staining on the basal surface of Caco-2 cells. (C) Little to no GFP-Myo10 is detected at the apical microvilli, although GFP-Myo10 was present in the cytoplasm. Caco-2 cells were transiently transfected. Note that green dots sometimes extend beneath adjacent cells, raising the possibility that they correspond to the tips of filopodia that have extended beneath adjacent cells. (D) GFP-Myo10 localizes to the basolateral domain in MDCK cells stably expressing GFP-Myo10. xy-plane is taken from the basal surface of an MDCK monolayer (6 days). F-actin is in red. Scale bar = 10 µm.

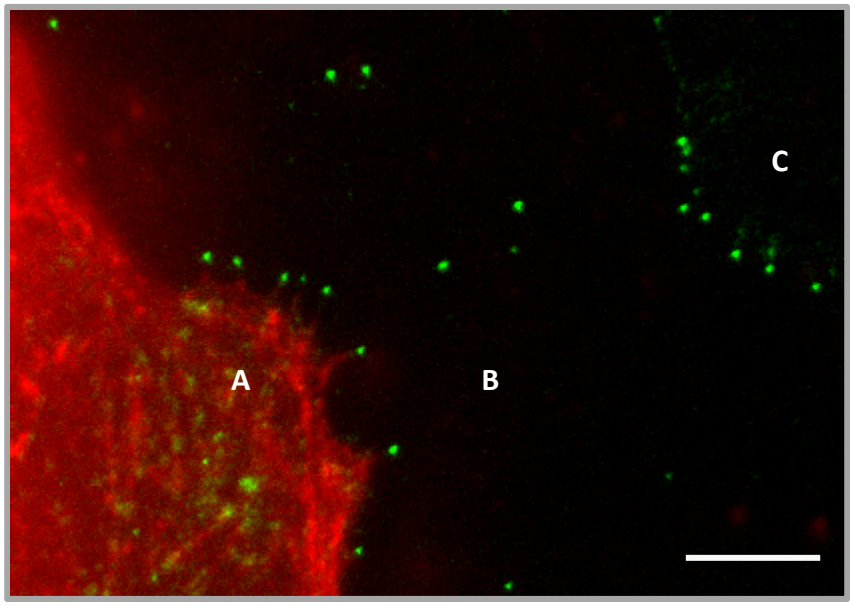

Figure 4.4 GFP-Myo10 localizes to the tips of tagRFP-Lifeact-labeled basal filopodia in an MDCK monolayer. Stably expressing GFP-Myo10 MDCK cells were transfected with tagRFP-Lifeact. TIRF live-cell imaging reveals GFP-Myo10 puncta at the tips of basal actin-based filopodia in cells expressing tagRFP-Lifeact (A) within a monolayer. Autofluorescence was used to determine the outlines of untransfected cells (B) which express little to no GFP-Myo10. (C) Some untransfected cells expressing only GFP-Myo10 showed similar basal puncta of GFP-Myo10. Scale bar = 5 µm.

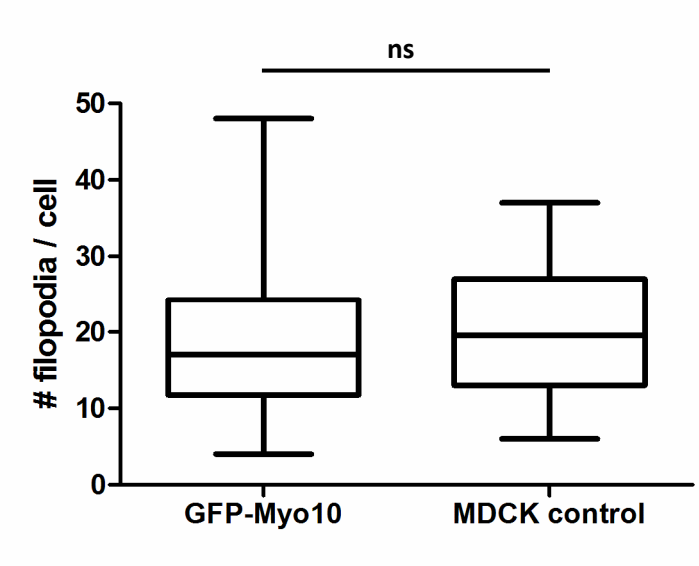

Figure 4.5 Stable expression of GFP-Myo10 at near endogenous levels does not increase filopodia number. Stable GFP-Myo10 cells and untreated MDCK II cells were plated on collagen for two hours before fixation. Single, fixed cells were imaged by DIC. The number of filopodia was quantified by ImageJ. There was no significant (ns) difference in filopodia number between GFP-Myo10 stables and MDCK control cells. 70 cells were quantified in total from three separate experiments.

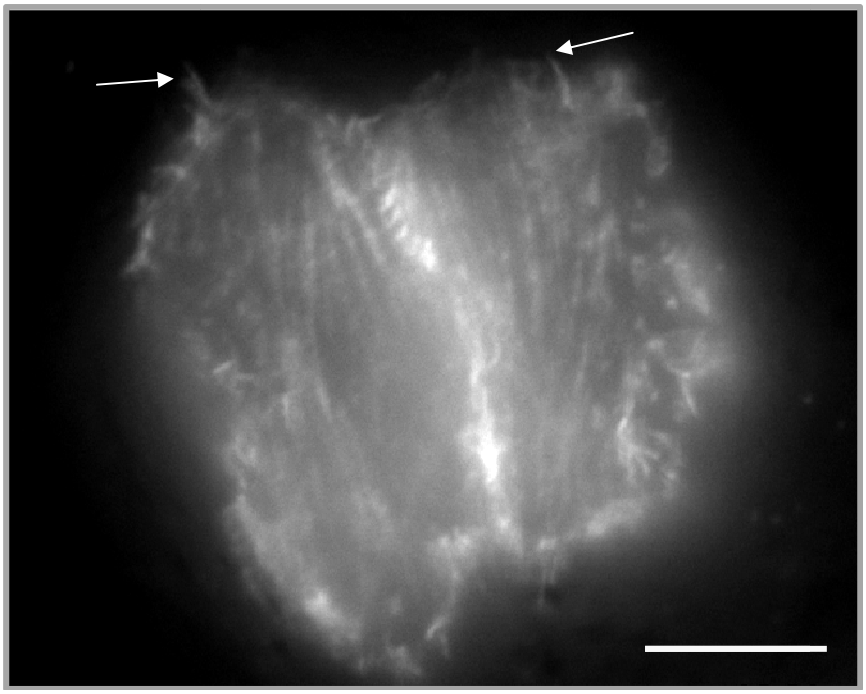

Figure 4.6 MDCK cells not expressing GFP-Myo10 have basal filopodia. MDCK II cells were transfected with tagRFP-Lifeact and cultured to form monolayers on glass dishes. Live-cell TIRF imaging shows dynamic actin-based filopodia (arrows). MDCK cells are in a confluent monolayer, the surrounding cells not expressing tagRFP-Lifeact. Scale bar = 10 µm.

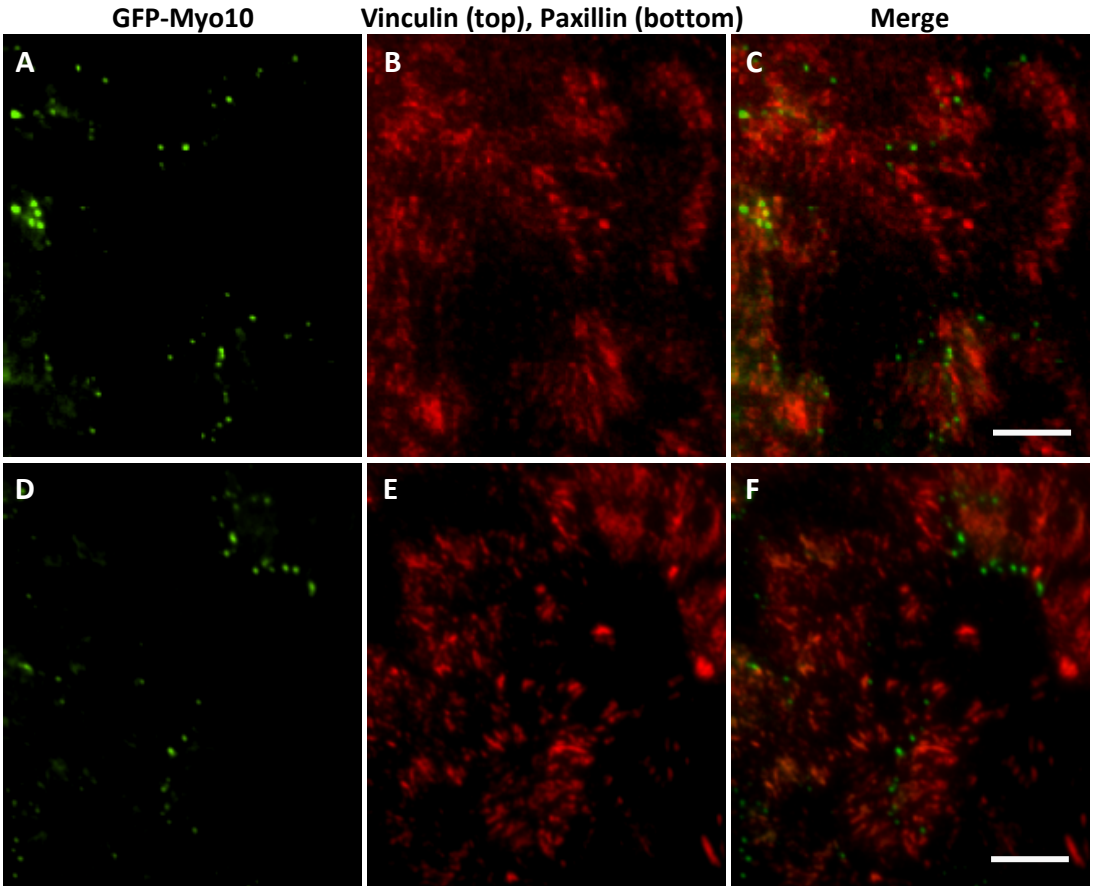

Figure 4.7 GFP-Myo10 does not co-localize with focal adhesion markers, vinculin and paxillin. GFP-Myo10 MDCK cells were fixed and immunolabeled for vinculin and paxillin (red). GFP-Myo10 (A,D) showed little to no colocalization with vinculin (B) or paxillin (E), as indicated in the merge images (C,F). Scale bar = 10 μm.

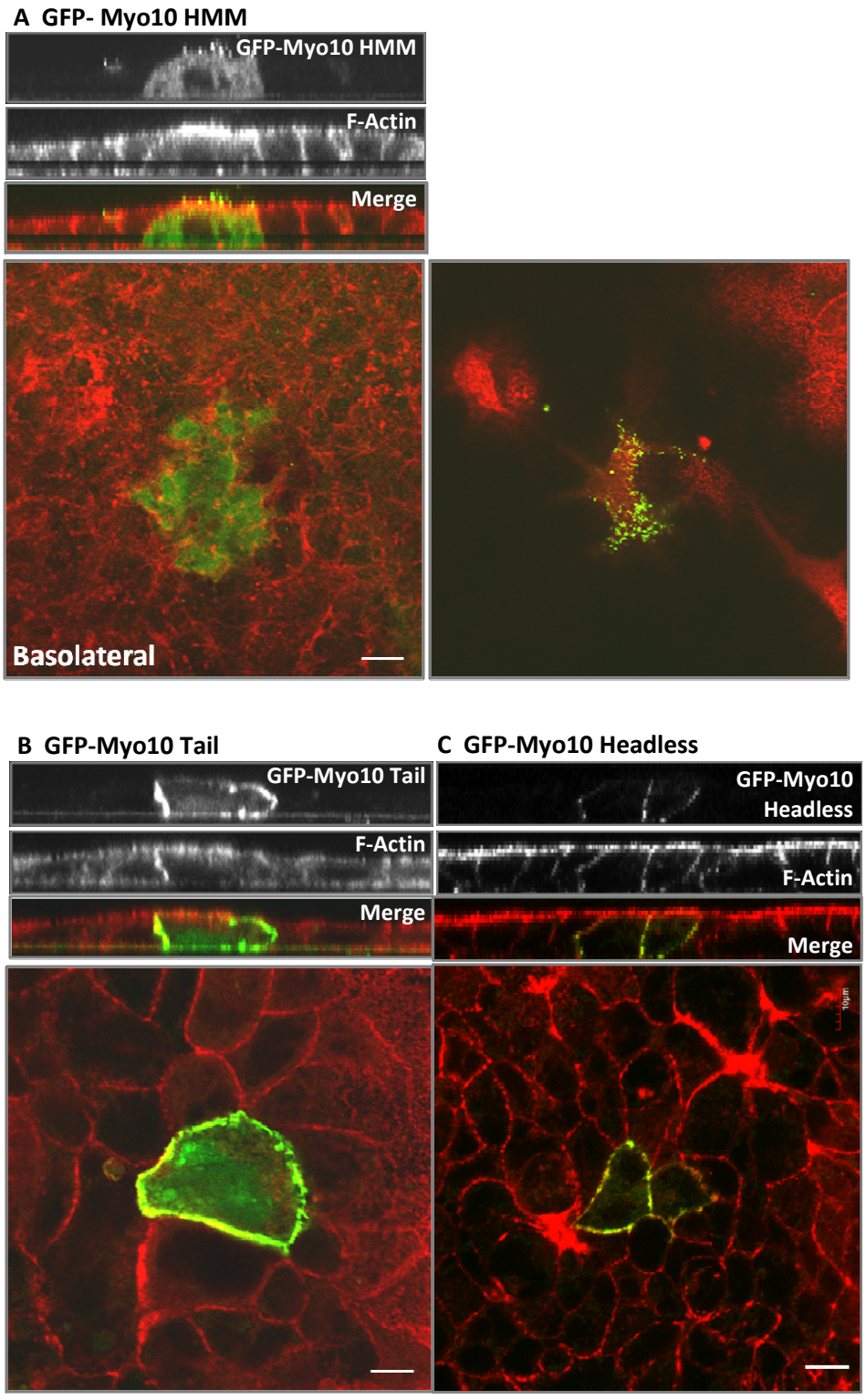

Figure 4.8 The Myo10 Tail is necessary and sufficient for basolateral localization in Caco-2 cells. (A) GFP-Myo10 HMM localizes to the apical domain. F-actin is labeled in red. GFP-Myo10 Tail (B) and GFP-Myo10 Headless (C) localize to the basolateral membrane. xy-plane is taken from mid-section of the cell monolayer. Caco-2 cells were transiently transfected. Scale bar = 10 µm.

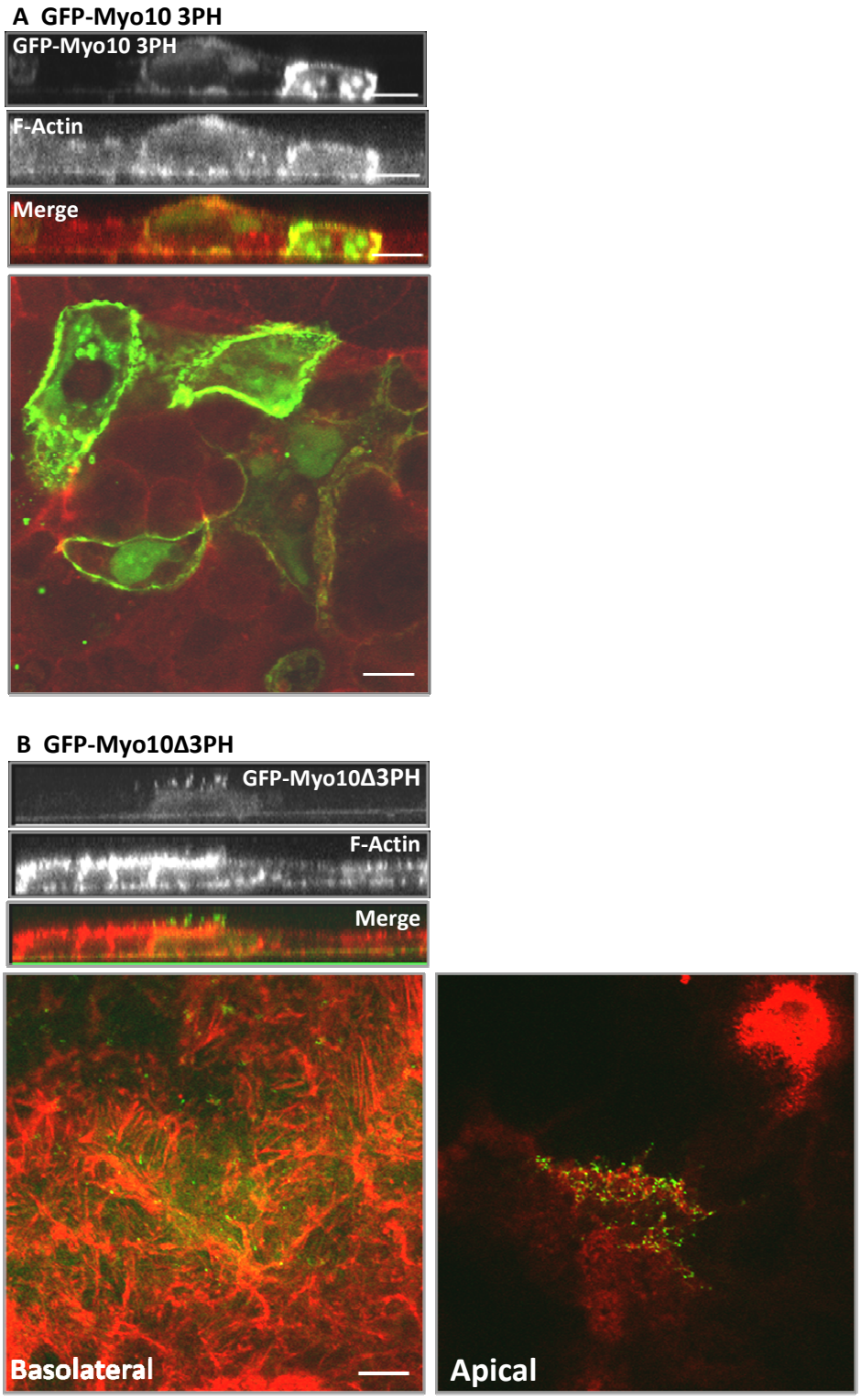

Figure 4.9 PH domain deletion leads to apical localization of Myo10. (A) GFP-Myo10 3PH labels the basolateral membrane and cytoplasm. xy-plane was taken from mid-section of the cell monolayer. (B) GFP-Myo10Δ3PH localizes to the apical microvilli. Caco-2 cells were transiently transfected. F-actin is labeled with phalloidin in red. Scale bar = 10 µm.

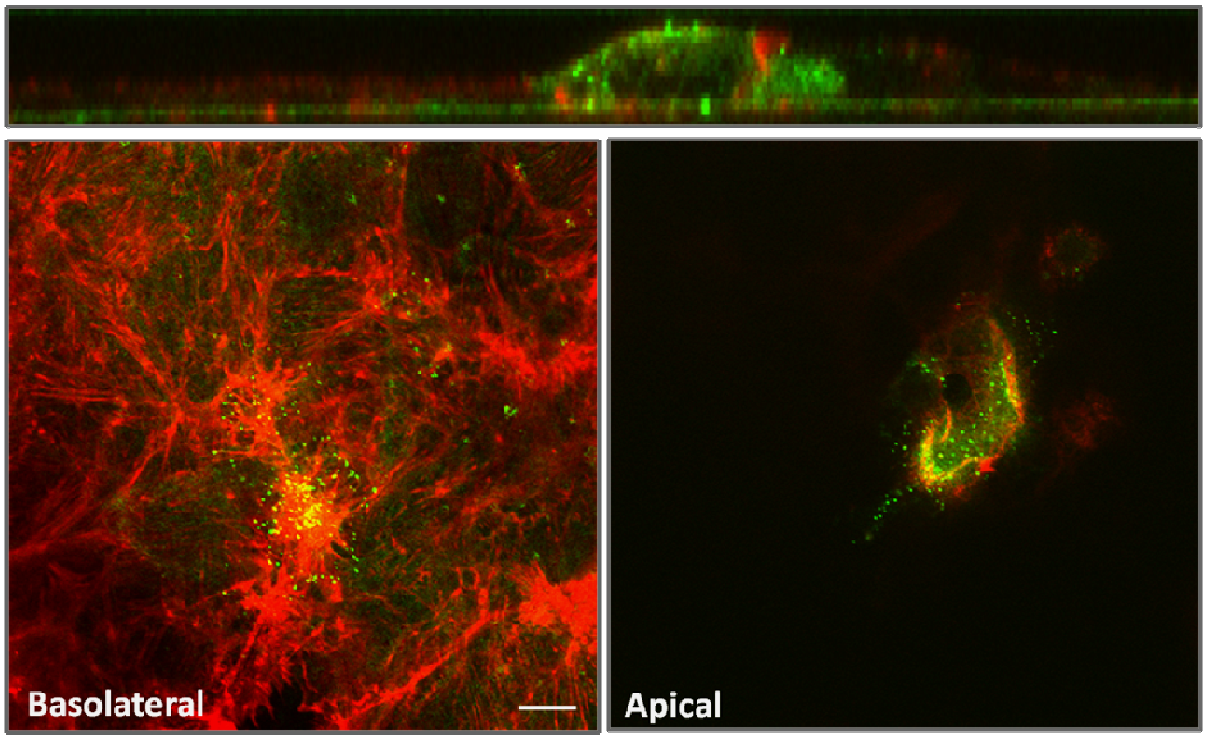

Figure 4.10 PI3K inhibition partially redistributes GFP-Myo10 to the apical domain and to cytoplasmic puncta. Caco-2 cells transfected with GFP-Myo10 were treated with LY294002, and GFP-Myo10 was partially redistributed to the apical domain and to cytoplasmic puncta. Some residual punctate staining remained at the basolateral domain. F-actin is labeled in red. Scale bar = 10 µm.

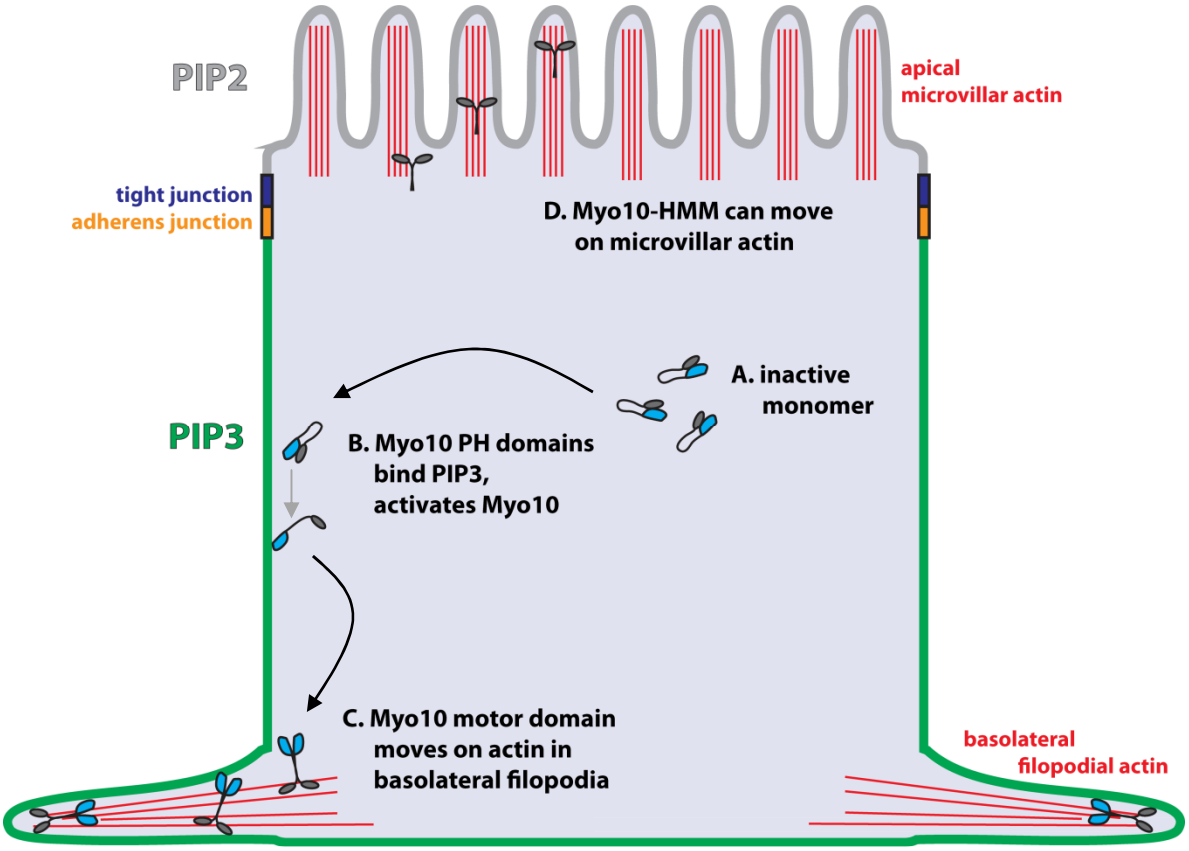

Figure 4.11 Working model for Myo10 targeting to basolateral filopodia in polarized epithelial cells. (A) In the cytoplasm, Myo10 is in a folded, inactive monomer. (B) PIP3 binding to Myo10's PH domains activates and allows for dimerization of Myo10. (C) Dimerized Myo10 targets to basolateral filopodia. (D) In the absence of PH domains, Myo10-HMM can move on microvillar actin.

MOVIE LEGENDS

Movie 4.1 GFP-Myo10 localizes to the tips of tagRFP-Lifeact-labeled filopodia in an MDCK monolayer. Stably expressing GFP-Myo10 MDCK cells (green) were transfected with tagRFP-Lifeact (white). TIRF live-cell imaging reveals GFP-Myo10 puncta at the tips of actin-based filopodia in cells expressing tag-RFP-Lifeact. Three cells are present in the field of view. The left cell expresses GFP-Myo10 and tagRFP-Lifeact. The center cell expresses no GFP-Myo10. Autofluorescence was used to determine the outlines of untransfected cells. The right-most cell expresses GFP-Myo10 only and shows similar basal puncta of GFP-Myo10. Images were collected at 1 frame/30 seconds on a Nikon TE-2000U inverted microscope. Scale bar = 5 μm.

Movie 4.2 MDCK II cells have basal filopodia. MDCK II cells, not expressing GFP-Myo10, were transfected with tagRFP-Lifeact and cultured to form monolayers in glass dishes. Live-cell TIRF imaging shows dynamic actin-based filopodia in cells transfected with tagRFP-Lifeact while surrounding cells do not express tagRFP-Lifeact. Images were collected at 1 frame/30 seconds on a Nikon TE-2000U inverted microscope. Scale bar = 10 μm.

CONCLUSIONS AND FUTURE DIRECTIONS

Conclusions

The experiments presented here are the first in-depth investigations on the role of Myo10 in polarized epithelial cells. We found that Myo10 localizes largely to the basolateral domain in kidney *in vivo*. Using MDCK and Caco-2 cells as model systems, we found that GFP-Myo10 localizes the tips of basolateral filopodia. Furthermore, during junction assembly, GFP-Myo10 transiently localizes to the lateral membrane. Importantly, these studies are the first to identify functional roles for Myo10 in polarized epithelial cells in junction assembly, paracellular permeability and epithelial morphogenesis. Myo10 knockdown cells show a delay in junction assembly, increased paracellular permeability to fluorescent dextrans, and multi-lumen cysts in three-dimensional culture. Furthermore, we found that Myo10 is targeted to the basolateral domain by the tail, and specifically, the PH domains. Excitingly, Myo10 reveals basolateral filopodia and provides a tool by which to characterize and study these lesser known structures in polarized epithelial cells.

How does Myo10 Affect Junction Assembly and Epithelial Morphogenesis?

Although our studies identified functional roles for Myo10 in polarized epithelial cells, the mechanisms of action that result in defects in junction assembly kinetics, paracellular permeability and epithelial morphogenesis remain unclear. Myo10 has critical functions in filopodia, and Myo10's effect on filopodial formation and dynamics could cause

delays in initial cell-cell contact formation during junction assembly. Live-cell imaging of Myo10 knockdown cells using a membrane marker could be utilized to examine specific defects in early junction assembly dynamics. For example, are there fewer filopodia at nascent cell-cell contacts in Myo10 knockdown cells? Moreover, one could identify other proteins that are critical for filopodial formation and ask whether knockdown has similar effects on initial cell-cell contact formation. Of course, any results would be correlative by providing supporting evidence for a filopodial mechanism for proper junction assembly.

During junction assembly and epithelial morphogenesis, Myo10 could be transporting cargoes to the basolateral domain. It is possible that Myo10 is found on vesicles, as GFP-Myo10 showed punctate cytoplasmic localization (Figure 2.4). Further experiments are needed to test whether Myo10 localizes to one or more populations of vesicles. To confirm the presence of dynamic cytoplasmic puncta, live-cell imaging of GFP-Myo10 could be performed, which would also avoid artifacts from fixation or immunostaining. To determine whether cytoplasmic puncta of Myo10 localize to specific membrane compartments, colocalization studies can be performed by co-labeling GFP-Myo10 cells with vesicular compartment markers. In polarized epithelial cells, other myosins such as Myo6 and Myo5B have established trafficking roles. Thus far, Myo10 has not been implicated in vesicular trafficking.

In my experiments in MDCK cells, Myo10 knockdown results in spindle misorientation. Interestingly, a recent *Xenopus* study shows defective spindle positioning with Myo10 knockdown (Woolner and Papalopulu, 2012). There are now several examples in which spindle misorientation is a mechanism that disrupts single lumen formation in

three-dimensional cysts (Hao et al., 2010; Jaffe et al., 2008; Rodriguez-Fraticelli et al., 2010). The majority of Myo10 spindle experiments have been performed in Xenopus oocytes, where the Bement group shows endogenous Myo10 localizing to the mitotic spindle poles (Woolner et al., 2008). Future studies should determine whether Myo10 localizes to the mammalian mitotic spindle as well. Although I have not observed Myo10 at the spindle in subconfluent GFP-Myo10 expressing MDCK cells, a comprehensive screening using mitotic synchronization methods could be performed in the future to confirm this result. Even if Myo10 does not localize to the mitotic spindle in mammalian epithelial cells, Myo10 could still function in spindle orientation. Spindle orientation is thought to be mediated by contacts between astral microtubules and the lateral cortex, and Myo10 can bind microtubules via the MyTH domain. Interestingly, Myo10 localizes to the lateral membrane during junction assembly, as do proteins important for mitosis, i.e. the adaptor protein LGN (leucine-glycine-asparagine repeat protein) (Zheng et al., 2010). It is possible that Myo10 recruits proteins to the lateral membrane. Does Myo10 knockdown affect Pins or LGN localization to the lateral cortex? In future immunostaining experiments, MDCK cysts can be immunolabeled to determine Pins localization in dividing Myo10 knockdown cells.

In addition to controlling for off-target effects, rescue experiments are often used to elucidate the mechanism of action. However, rescue experiments have proven to be difficult due to heterogeneous expression levels, and full length GFP-Myo10 rescue only partially restores the single lumen phenotype observed in 3D culture. Future rescue experiments reintroducing different Myo10 deletion constructs may thus be difficult to interpret – recent work indicates Myo10 is found in a folded, inactive state such that the

motor domain binds the FERM and PH domains of the tail (Umeki et al., 2011). Thus, deletion of certain domains may disrupt Myo10's folded conformation and generate a constitutively active Myo10 motor, rather than the intended effect of deleting specific functional domains. To address this issue, Myo10 point mutations can be used instead, provided that the motor-to-tail interacting sites for the folded conformation are not disrupted.

Myo10 Reveals Basolateral Filopodia in Polarized Epithelial Cells

Basolateral filopodia are an understudied subclass of filopodia, perhaps due to the difficulty in observing basal filopodia within a continuous cell monolayer. Excitingly, Myo10 provides a means to visualize basal filopodia by marking the tips of basolateral filopodia. At present, basolateral filopodia are not well-characterized. To our knowledge, Myo10 and F-actin are the only known components of basolateral filopodia. In this case, what other proteins comprise basolateral filopodia? VASP, known to interact with Myo10, is a candidate to localize to basolateral filopodia. Another candidate is fascin, an actin-bundling protein found in dorsal filopodia of non-polarized cells, but unfortunately, fascin is absent or expressed at very low levels in epithelial cells (Zhang et al., 2008). It is important to determine what molecules are involved in the formation of basolateral filopodia. In non-polarized cells, Myo10 is required for the formation of dorsal and substrate-attached filopodia. Does Myo10 have a similar requisite role in the formation of basolateral filopodia in polarized epithelial cells? In the future, it would be intriguing to test whether Myo10 knockdown affects the number of basolateral filopodia, since Myo10 knockdown

significantly reduces the number of dorsal filopodia in non-polarized cells (Bohil et al., 2006). In contrast, does Myo10 overexpression induce basolateral filopodia? To visualize basolateral filopodia, single cells can be labeled for F-actin by transiently transfecting with fluorescently-tagged Lifeact. Using live-cell imaging, we can ask what proteins affect the dynamics of basolateral filopodia. MDCK cells stably expressing GFP-Myo10 could be instrumental for TIRF imaging of basal filopodia and their dynamics. As lesser known actin-based structures in polarized epithelial cells, initial characterization studies of basolateral filopodia are certainly needed.

Possible Functions for Basolateral Filopodia: Force Generator or Adhesive Complex?

Basolateral filopodia have been recently established as important regulators of tissue patterning in *Drosophila* (Cohen et al., 2010) and cell morphology in cultured epithelial cells (Georgiou and Baum, 2010). What are other possible functional roles for basolateral filopodia, and how does Myo10 fit into these functional processes?

At the basal surface, filopodia could be force generating structures involved in the movement of epithelial cell sheets. Cell monolayers of are dynamic, and the collective and cooperative movement of cells is termed plithotaxis (Trepat and Fredberg, 2011). Recently, the movement of cell sheets has been elegantly demonstrated in a cell culture model. In a three-dimensional collagen culture, epithelial cysts rotate in a coordinated manner (Tanner et al., 2012) where the cells within the cyst cooperate to generate collective cell movement. Interestingly, cysts comprised of cancerous epithelial cells do not rotate in a coordinated fashion. In addition, polarized follicle cells in the *Drosophila* ovary undergo rotation by the

basolateral domain contacting underlying extracellular matrix to promote follicular shape change (Haigo and Bilder, 2011). By contacting the underlying extracellular matrix, basolateral filopodia are prime position to facilitate force generation in epithelial cells. The movement of cell sheets is also important in pathophysiologic conditions such as wound healing. Our preliminary studies suggest Myo10 knockdown slows wound closure (Figure 5.1). Interestingly, in a wound healing model, basal structures called “cryptic lamellipodia” have been observed to crawl and reach beneath neighboring cells, several rows behind the wound edge (Farooqui and Fenteany, 2005). It is possible that these cryptic lamellipodia are present throughout a cell monolayer, and that Myo10 is a component of the cryptic lamellipodia. Future studies should determine whether Myo10 has a functional role in collective cell migration. For example, using the stable Myo10 knockdown lines, it would be straightforward to ask whether Myo10 knockdown cells undergo cyst rotation. As a possible caveat, it is not known whether a multi-lumen cyst will show rotational movement, although this independently poses an interesting question. Another myosin, Myo9B, has been recently implicated in collective cell migration (Omelchenko and Hall, 2012). Myo9B is a RhoGAP (Rho GTPase-activating protein), and Myo9B knockdown results in slower wound closure and a cell scattering phenotype during cell-cell contact formation. These results suggest Myo9B is needed for cell-cell contact expansion and stabilization (Omelchenko and Hall, 2012).

Alternatively, basolateral filopodia could function as part of an adhesion complex. There are a small number of studies that report the observation of ventral “actin waves”, and a recent report by Case and Waterman suggests that these F-actin waves are adhesive

and integrin-based (Case and Waterman, 2011). The adhesive actin waves show progressive recruitment of molecules: first zyxin and VASP appear, followed by paxillin and vinculin, and finally talin and integrin. Since basolateral filopodia and actin waves are both dynamic actin-based basal protrusions, they may be related structures. Since Myo10 sometimes localizes to the cell's leading edge (Berg et al., 2000), it may be a component of actin waves, and Myo10 could function to recruit other proteins to the actin wave. Myo10 was been reported to interact with VASP (Tokuo and Ikebe, 2004), and although Myo10 has not been shown to colocalize with paxillin and vinculin at focal adhesions (Kerber et al., 2009; Zhang et al., 2004), we have not ruled out the possibility that Myo10 transiently localizes to focal complexes, nascent adhesive structures. Also, Myo10 can bind β-integrins, and thus, Myo10 could be involved in building adhesive actin waves at the basal surface. In addition, actin waves rapidly assemble and disassemble (Case and Waterman, 2011), so Myo10 could be engaged in the dynamics of these basal actin-based protrusions.

A Conserved Role for MyTH-FERM Myosins in Cell Adhesion?

The MyTH-FERM family is an ancient group of myosins comprised of Myo7a, Myo7b, Myo10 and Myo15a. They are a phylogenetically conserved myosin family – could there be a conserved functional role for MyTH-FERM myosins? Similar to Myo10, Myo7b is expressed in epithelial cells, but Myo7b localizes apically to the tips of microvilli (Chen et al., 2001). Myo7b's localization at microvillar tips raises the possibility that it is part of an adhesive microvillar tip complex. Both Myo7a and Myo15a have been reported to localize to cell-cell contacts. Myo7a localizes to cell-cell contacts in polarized epithelial cells and a specialized

adhesive structure in testis (Velichkova et al., 2002), while Drosophila Myo15a localizes to newly formed junctions in dorsal closure (Liu et al., 2008). Functionally, Myo7a binds cadherin-23 in stereocilia and likely provides the physical link between stereocilia (Bahloul et al., 2010). Drosophila Myo15a has been reported to interact with DE-cadherin and is important for proper epithelial sheet adhesion and fusion during dorsal closure (Liu et al., 2008). Together, the studies of Myo7a, Myo7b, Myo10 and Myo15a are provocative and allow us to consider a conserved role for MyTH-FERM myosins in cell adhesion.

Myo10 and Cell-Cell Adhesion

Myo10 transiently localizes to lateral membranes during junction assembly (Liu et al., 2012), and Myo10 has been reported to co-transport VE-cadherin in endothelial cells at early stages of cell-cell contact (Almagro et al., 2010). In my experiments, Myo10 knockdown results in a delay in E-cadherin localization to cell-cell contacts during junction assembly. Thus, in epithelial cells, an interaction between Myo10 and E-cadherin could contribute to cell-cell contact formation. Interestingly, other myosins such as Myo6 bind E-cadherin and have functional roles in E-cadherin-based cell-cell contacts (Maddugoda et al., 2007). However, in our preliminary studies, we did not detect an interaction between Myo10 and E-cadherin. Myo10 and E-cadherin immunoprecipitations were performed on MDCK cells during junction assembly and in mature monolayers using several different lysis buffer conditions. In addition, GFP-Myo10 was immunoprecipitated using the FLAG tag, but we did not observe co-immunoprecipitation with E-cadherin. These results do not rule out

the possibility that Myo10 and E-cadherin may interact transiently or under some conditions.

Alternatively, Myo10 could interact with other junction-associated proteins, similar to Myo7a, which binds vezatin, a transmembrane protein at the adherens junction (Kussel-Andermann et al., 2000), and Shroom2, a tight junction-associated protein (Etournay et al., 2007). Given Myo10's localization to cell-cell contacts and effect on junction assembly, further studies exploring the role of Myo10 in cell-cell adhesion are promising.

Myo10 and Cell-ECM Adhesion

Myo10 localizes to the tips of filopodia on the basal surface, and we hypothesize Myo10 is a component of F-actin waves, which are likely integrin-based, adhesive structures on the basal surface. Myo10 can bind β1, β3 and β5 integrins (Zhang et al., 2004), and in MDCK cells, β1, β3 and β4 integrins localize to the basolateral membrane (Schoenenberger et al., 1994). Future experiments could determine whether Myo10 interacts with β-integrins at the basolateral domain. Preliminary experiments suggest Myo10 is not detected at focal adhesions, but is Myo10 found in focal complexes? Also, does Myo10 co-localize with β-integrins in polarized epithelial cells? In unpolarized endothelial cells, Myo10 and β-integrins both localize to filopodia, with β-integrin found slightly behind the Myo10-labeled filopodial tip (Zhang et al., 2004). Functionally, does loss of Myo10 reduce basal surface adhesion to the extracellular matrix? The apico-basal targeting of Myo10 could also be affected, at least in part, by interaction with β-integrins. Myo10 primarily localizes to the

basal surface at steady state, and preliminary targeting experiments show only a partial redistribution of Myo10 to the apical domain when treated with PI3K inhibitors.

Finally, cell-ECM interactions are also important in three-dimensional culture, as epithelial cysts self-assemble such that the basolateral surfaces contact the surrounding extracellular matrix. The precise localization of GFP-Myo10 in 3D cysts remains unclear, probably due to the faint GFP-Myo10 signal and/or increased autofluorescence from the surrounding 3D matrix. We hypothesize that GFP-Myo10 is found at the cell-ECM interface in 3D cysts, similar to GFP-Myo10 localization in two-dimensional monolayers, but future experiments should test this hypothesis in 3D culture.

Interestingly, Myo10 is one of a small number of proteins phosphorylated on tyrosine following HGF (hepatocyte growth factor) stimulation (Hammond et al., 2010); since there is evidence to suggest Myo10 interacts with HGF receptor, and filopodia-like basal protrusions have been implicated in HGF-mediated tubulogenesis (Guo et al., 2008; Williams and Clark, 2003), future experiments should next determine the localization of Myo10 during HGF-induced tubulogenesis in 3D cysts. While Myo10 clearly affects cytogenesis in MDCK cells, does Myo10 have a role in tubulogenesis as well? In preliminary experiments, overall inspection of HGF-stimulated MDCK cysts suggests Myo10 knockdown cells still have ability to form tubules. However, whether the tubules differ in morphology or dynamics remains to be determined.

The work described here is the first extensive examination of Myo10 and its functions in polarized epithelial cells. While defects were observed in junction assembly,

paracellular permeability and epithelial morphogenesis, the precise mechanisms for these defects remain unsolved. Importantly, Myo10 reveals basolateral filopodia, lesser known yet prominent actin-based structures on the basal surface of polarized epithelial cells. GFP-Myo10 serves as an excellent marker for the tips of basolateral filopodia, which provides a valuable imaging tool for future studies. Essential work lies ahead to fully characterize and identify functions for basolateral filopodia, as well as to understand where Myo10 fits into the larger framework of basolateral filopodia.

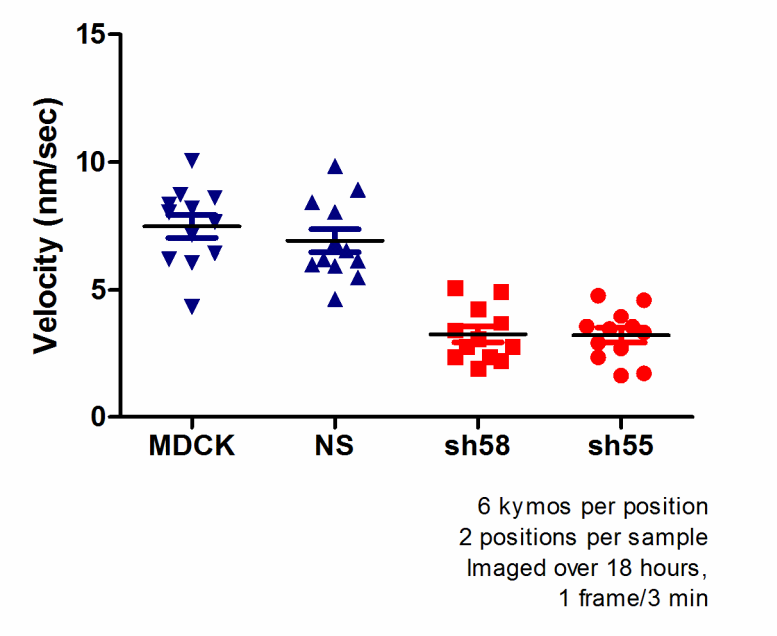

Figure 5.1 In preliminary experiments, Myo10 knockdown slows wound closure. Myo10 stable knockdown lines 58 (shRNA #5) and 55 (shRNA #5) showed reduced velocity of wound closure compared with NS shRNA-expressing and MDCK untreated controls. 3 day old MDCK monolayers were scratch wounded using a P10 pipette tip and imaged immediately over the next 18 hours using the Olympus VivaView incubator microscope at 37^{o}C and 5% CO2. Two random stage positions along the scratch wound were imaged. Wound healing velocities were calculated by preparing kymographs of the leading edge using the Metamorph software. Per stage position, 6 kymographs were prepared. There were two stage positions per condition.

APPENDIX

DOES MYOSIN-X HAVE A ROLE IN MICROVILLI?

INTRODUCTION

Myo10 is an unconventional myosin that is known to have important roles in filopodia (Bohil et al., 2006). Microvilli share some similarities with filopodia, but differ in that they are found at the apical domain of polarized epithelial cells and are involved in absorptive functions. Given that both microvilli and filopodia are slender cellular extensions based on actin bundles, we tested whether Myo10 plays a role in the formation of microvilli using Caco-2 cells, a well-characterized model for microvilli. Immunoblotting demonstrates that Myo10 is present throughout Caco-2 differentiation, Myo10 expression is highest during early stages. To test whether Myo10 function is required for microvillar formation, Myo10 was knocked down by infecting Caco-2 cells with shRNA-expressing lentivirus. Using scanning electron microscopy to visualize the apical surface, Myo10 knockdown showed no obvious effect on the formation of microvilli. Nonetheless, Myo10 knockdown did affect cell morphology, as Myo10 shRNA cells were shorter and wider than control cells. Although knockdown of Myo10 did not affect microvilli, preliminary studies support functions for Myo10 in early development of polarized epithelia as well as proper cell morphology.

Microvilli are finger-like membrane protrusions located on the apical domain of polarized epithelial cells. Microvilli function to absorb nutrients and salts in tissues such as the small intestine, proximal tubules of the kidneys and retinal pigmented epithelia in the eye. Like filopodia and stereocilia, microvilli are structures that are comprised of actin bundles with the plus ends of actin filaments oriented toward the tips of microvilli (Mooseker and Tilney, 1975). The actin core of each microvillus terminates at its base in the terminal web region (Hull and Staehelin, 1979); together, the microvillus and terminal web domain form the brush border. The microvillar actin filaments are cross-linked by actin-bundling proteins, villin and fimbrin, and actin is bound to the surrounding plasma membrane by myosin-1a (Tyska et al., 2005). While the structural components of microvilli have been established and largely understood, the molecular mechanism of microvillar formation remains unclear. Using a human cell culture model, Peterson et al. suggested microvilli develop from filopodia-like precursors (Peterson and Mooseker, 1993). Contrastingly, based on studies using *Drosophila* bristles, Tilney et al. theorized that actin bundles are nucleated and elongate from small electron-dense regions on the apical surface into microvilli (Tilney et al., 2004).

We approached our investigation of microvillar formation by focusing on myosins, which are molecular motors that move in a directed manner along actin filaments. Myosins have important roles in the formation of other actin-bundled structures such as filopodia and stereocilia. Myosin-X is critical for filopodial formation, and myosin-VIIa and myosin-XVa are important for proper stereocilia formation and organization (Belyantseva et al., 2003; Self et al., 1998). Thus, myosins are potentially involved in the formation of actin-

based microvilli. In fact, many classes of myosins have been implicated in several other microvillar processes. Myosin-1a functions to link microvillar actin bundles in to the surrounding membrane and facilitates membrane shedding at tips of microvilli (McConnell and Tyska, 2007; Tyska et al., 2005). Myosin-Vb deficiency has been linked to cases of microvillus inclusion disease, and Myosin-Vb is involved in trafficking and proper localization of apical and basolateral proteins (Muller et al., 2008). Additionally, myosin-VI is involved in clathrin-mediated endocytosis at the apical surface of polarized epithelial cells (Buss et al., 2001a).

Myosin-X (Myo10) is an unconventional molecular motor that moves toward the plus ends of actin filaments (Homma et al., 2001), Myo10 is required for the formation of filopodia (Berg et al., 2000; Bohil et al., 2006). Furthermore, Myo10 localizes to the tips of filopodia and undergoes intrafilopodial motility (Berg and Cheney, 2002), leading to the hypothesis that Myo10 functions as an intrafilopodial transport system to move cargo to the tips of filopodia. Although Myo10 is highly expressed in epithelial tissues such as kidney and small intestine (Berg et al., 2000), the majority of experiments on Myo10 have been performed in non-polarized cells. Intriguingly, Myo10 is a member of the family of MyTH-FERM myosins, which have critical roles in actin-bundled structures such as microvilli and stereocilia (see Chapter 2). Myosin-VIIb localizes to the tips of microvilli (Chen et al., 2001; Wolfrum et al., 1998) while myosin-VIIa and myosin-XV are important for proper formation, elongation and organization of stereocilia (Belyantseva et al., 2005; Liang et al., 1999). Given the critical function of Myo10 in filopodial formation and the requirement for other

MyTH-FERM myosins in bundled actin structures, we tested whether Myo10 localizes to and is needed for the formation of microvilli.

We used human colon adenocarcinoma (Caco-2) cells as a model system to study Myo10 in microvilli. Caco-2 (clone BBe1) cells were advantageous for the study of microvilli because they have a robust brush border (Peterson and Mooseker, 1992). However, a noticeable experimental drawback is the relatively slow developmental time course, which requires two to three weeks for cells to reach full maturity. Another disadvantage of using Caco-2 cells is the low transfection efficiency attained by transient transfection. At 0-2 days post-plating, Caco-2 cells are initially unpolarized, and as the cells spread along the substrate, filopodia and lamellipodia are observed along the cell edges. As cells become polarized, junctional complexes form at the sites of cell-cell contacts, and the apical junctional complexes separate the apical and basolateral domains. The apical domain has an actin-rich brush border comprised of microvilli and the terminal web. At two weeks, fully polarized Caco-2 cells have microvilli that are compact and fairly uniform in length. We also used the LLC-PK1 cell line, a porcine kidney cell line derived from the proximal tubule (Perantoni and Berman, 1979), to study Myo10 in microvilli.

Here, we characterize the localization and expression pattern of Myo10 in Caco-2 cells. We find that Myo10 shows varying levels of expression and localization patterns based on the degree of Caco-2 cell maturation. Interestingly, we find that Myo10 is expressed at highest levels at early stages in Caco-2 development. Although preliminary experiments showed Myo10 antibody 117 stained microvilli, further investigation revealed that this antibody cross-reacts with ezrin, a particularly abundant protein in microvilli. Using new

antibodies directed against different portions of Myo10, we detected little to no endogenous Myo10 in microvilli, and Myo10 knockdown studies suggest Myo10 is not needed for formation of microvilli. However, Myo10 does appear to affect cell morphology as Myo10 knockdown cells are shorter and wider than control cells. Although our studies here do not support a role for Myo10 in apical microvilli, the Caco-2 expression studies presented here encouraged us to turn our attention to Myo10 during early stages of epithelia development.

MATERIALS AND METHODS

Cell culture

Caco-2 BBe1 cells (ATCC, Manassas, VA) were cultured in complete growth medium: DMEM (Invitrogen/Gibco, Grand Island, NY) supplemented with 10% fetal bovine serum (Sigma, St. Louis, MO), 100 units/ml penicillin-streptomycin (Sigma) and 10 µg/ml human holo-transferrin (Sigma). LLC-PK1 cells (ATCC) were cultured in complete growth medium: DMEM supplemented with 10% FBS and 100 units/ml penicillin-streptomycin. Caco-2 cells were maintained at 37°C and 5% CO_2. Caco-2 cells were passaged every 2-3 days. Caco-2 cells were split by trypsin addition (Sigma) followed by a 10-minute incubation at 37°C. Caco-2 cells were replated to approximately 25% confluency. The media was changed every 2-3 days.

Plasmids and Constructs

shRNA constructs were designed using siDESIGN Center (Dharmacon). Two siRNA constructs were designed against target sequences in the motor domain of human myosin-X (NM_012334): GGAAAGGAATTATCACATA (bp 1236-1254) and AAGTGCGAACGGCAAAAGAGA (bp 4253-4273). One non-specific siRNA construct was made against the target sequence, GATCGACTTACGACGTTAT, which does not recognize any gene in human, rat or mouse genomes. Forward and reverse oligonucleotides were designed, produced and annealed. The pLentiLox 4.0 vector (Rubinson et al., 2003) was digested with restriction enzymes XhoI and HpaI. Oligonucleotides were ligated with pLentiLox 4.0, and clones were tested by restriction digest with XbaI and NotI. Positive clones were confirmed by DNA sequencing.

The Myo10 putative dominant negative construct in pEGFP-C2 consists of the stable alpha helical region of Myo10 (bp 2434-2836; aa 812-946), generated by PCR from human Myo10 (Bohil et al., 2006). Immunoblot analysis shows a band at approximately 55 kD, the expected molecular weight of GFP-Myo10 coiled coil.

Immunofluorescence

For immunofluorescence experiments, we used a 19-day time course of Caco-2 or LLC-PK1 cells with time points at 1, 2, 3, 6, 8, 10, 13, 15, 17 and 19 days. For each time point, cells were counted with a haemocytomer after trypsinization. Samples at all time points were replated at $7.5x10^4$ cells/well in 10-mm transwell filters with 0.4 µm pore size (Corning, Lowell, MA). The time course was setup such that the longest time point, 19 days,

was plated up to 19 days. At day 19, all samples were rinsed twice with PBS before fixation with 4% paraformaldehyde (EMS, Hatfield, PA) in PBS for 20 minutes at 37°C. Cells were rinsed with PBS three times for 15 minutes each. Samples were permeabilized with 0.5% Triton-X (Sigma) in PBS for 10 minutes at room temperature followed by three 15-minute washes in PBS. Samples were blocked by incubating in 5% heat-inactivated goat serum (Sigma) with 0.05% sodium azide for 2 hours at room temperature. Primary antibody was added at 0.8-1.0 μg/ml in 5% goat serum and incubated overnight. Antibodies used were 117 rabbit anti-Myo10, SDI rabbit anti-Myo10 (2243.00.02, SDIX, Newark, DE), Sigma rabbit anti-Myo10 (Sigma, HPA024223), mouse anti-villin (1D2C3, abcam, Cambridge, MA), mouse anti-ezrin (abcam, 3C12), rabbit non-immune IgG (Sigma) and mouse non-immune IgG (Sigma). After three 15-minute washes in PBS, samples were incubated overnight with fluorescently-tagged secondary antibody at 0.75 μg/ml in 5% goat serum. The samples were washed with 0.66 μl/ml fluorescently-tagged phalloidin at 1:500 dilution (Invitrogen Molecular Probes) for 20 minutes. After three additional 15-minute washes in PBS, the filters were cut out of the plastic transwell holders using a scalpel, filters were mounted cell-side up onto slides with Gel-mount mounting medium (EMS), and sealed with a No. 1.5 thickness cover glass (Fisher Scientific, Pittsburgh, PA). Mounting medium was allowed to dry overnight before visualization on the Zeiss LSM 510 confocal inverted microscope (UNC Neuroscience Center).

Myo10 Lentivirus Knockdown and Dominant Negative Expression

To generate lentivirus, HEK293 cells (ATCC, CRL-1573) were plated at $150x10^4$ cells per 100-mm dish and cultured in complete growth medium: DMEM supplemented with 10% fetal bovine serum, 100 units/ml penicillin-streptomycin. At 16-18 hours post-plating (day 1), FuGENE reagent (Qiagen, Germantown, MD), viral promoters pMDL-G/P-RRE, pRSV-REV, pCMV-VSVG, and pLL shRNA (Myo10 shRNA or NS shRNA) were added to serum-free DMEM. After incubation for 30 minutes, the DNA and FuGENE were added to the HEK293 cells. Transfection efficiency was evaluated by screening for GFP fluorescence after 36-48 hours (day 3), and the media was changed to Caco-2 complete growth medium. On day 4, Caco-2 cells were split and replated to ~25% confluency. On day 5, viral media was collected from HEK293 cells and transferred to a 15 ml conical tube. Viral media was spun down at 3500 rpm for five minutes and filtered through a 0.45 μm filter (Millipore, Billerica, MA). For lentiviral infection of Caco-2 cells, the undiluted viral supernatant was added to Caco-2 cells, and polybrene (Sigma) at 4 μg/ml was added to the media. After an 8-hour incubation, the virus-containing media was aspirated, discarded and replaced with Caco-2 complete growth medium. On day 7, the infected Caco-2 cells were split into T75 flasks (Corning). On day 9, GFP-expressing infected cells were selected by fluorescence-activated cell sorting. Selected Caco-2 cells were replated in 10-mm transwell filters at 5000 cells/well and in 6-well plates at 20,000 cells/well. Caco-2 cells were grown for two weeks, changing media every 2-3 days.

Immunoblotting

During the 19-day time course, Caco-2 or LLC-PK1 cells were replated onto 6-well dishes at $20x10^4$ cells/well for immunoblot analysis. On day 19, all samples were lysed with 200 µl lysis buffer (40 mM HEPES pH 7.4, 75 mM KCl, 1% Triton-X 100, 2 mM K-EGTA, fresh 5X protease inhibitor cocktail EDTA-free (Roche)), scraped and transferred into an eppendorf tube. Hot LSB (Laemmli Sample Buffer) was added up to 1X dilution, and samples were immediately heated at 95°C for 5-8 minutes. Samples were either used immediately or flash frozen in liquid nitrogen and stored at -80°C. Samples were loaded into a 5-12% Bis-Tris gel (Invitrogen). Following gel electrophoresis, the protein was transferred onto a nitrocellulose membrane in an XCell SureLock Electrophoresis system (Invitrogen), at 140 volts for ~90 minutes using a PowerPac Basic power supply (BioRad). The membrane was incubated in 5% dry milk in TBST (50 mM Tris, 150 mM NaCl, 0.05% Tween 20, pH 7.5) for 30 minutes followed by primary antibody, 1:1000 dilution for rabbit anti-actin (Sigma) or 1:3,000 for mouse anti-villin (abcam) for at least one hour. The membrane was for blotted for actin or villin as loading controls. The blot was washed three times in 1X TBST for 10 minutes each. HRP secondary antibody (Jackson Laboratories, Bar Harbor, ME) at 1:10,000 was added to the membrane for 50 minutes. After three 10-minute washes in TBST, the developing solution (West Pico Luminescent Reagents, Thermo Fisher Scientific, Rockford, IL) was added at 1:1 before developing. The intensities of the actin bands were quantified using Adobe Photoshop. Using the loading control quantification, volumes of time course samples were adjusted to obtain equal total protein loading. The new membrane was immunoblotted for Myo10 using 117 (1 µg/ml) or SDI (0.8 µg/ml).

Scanning Electron Microscopy

After two weeks, the GFP-sorted lentivirus-infected Caco-2 cells on transwell filters were washed three times with PBS and fixed overnight using 2% paraformaldehyde and 0.5% glutaraldehyde. Cells were incrementally dehydrated by incremental washes in 50%, 75%, 90% and 100% ethanol. Ethanol was removed from samples by critical point drying, and samples were coated with a ~10 nm layer of 60% gold / 40% palladium. Filters were cut out of the plastic transwell holders and mounted onto carbon-coated aluminum stubs (EMS) for scanning electron microscopy. SEM was performed on a Zeiss Supra 25 Field Emission Scanning Electron Microscope (Microscopy Services Laboratory, Department of Pathology and Laboratory Medicine, UNC Chapel Hill). For each sample, low-power fields of view at 10,000X magnification were captured, and at least 20 random high-power 25,000X fields of view were captured.

Microvillar Morphology

Random, high-power (25,000X) SEM fields of view were used for microvillar analysis. The number of microvilli was quantified by selecting a 2µm x 2µm square on each high-power image, its position remaining constant in from image to image. An alternative square was selected if the edge of a cell clearly crossed through the square, cracks on the cell surface ran through the square, or if artifact was present, such as debris or obstruction. A microvillus was counted if the entire length of the microvillus resided within the square or if the base of a microvillus began inside and continued outside the square.

Statistical Analysis

The number of microvilli was averaged for each treatment case and was analyzed by single-variable ANOVA. If significant, Tukey's method was performed as *post hoc* comparison tests. When comparing GFP-Myo10-CC and GFP alone treatment cases, t-test analyses were performed to determine significance. In all cases, p value<0.01 was defined as statistically significant.

Immunoprecipitation

Two 100-mm plates of 2 week old Caco-2 monolayers were washed twice with PBS and lysed with 1 ml lysis buffer (40 mM HEPES pH 7.4, 75 mM KCl, 1% Triton-X-100, 2 mM K-EGTA, fresh 5X protease inhibitor, 5 µM latrunculin B, 5 mM ATP). Plates were scraped and lysate transferred to an eppendorf tube. The lysate was passed through a 27-gauge needle several times to shear the cells and DNA. The lysate was ultracentrifuged at 100,000g for 15 minutes at 4°C. Beads were prepared by adding 50 µl Gammabind beads plus Sepharose (GE Healthcare, UK) to six eppendorf tubes. 200 µl PBS was added to the beads, and beads were pelleted by low-speed centrifugation. PBS was aspirated and washes were repeated twice. 200 µl of lysis buffer was added to the beads followed by pelleting and aspiration of the lysis buffer. Lysate supernatant was added to tubes 2-4. 18 µg antibody to Myo10 or the protein to be pulled-down, i.e. ezrin, was added to tubes 3 and 5. 18 µg non-immune antibody was added to tubes 4 and 6. Volumes in all tubes were raised to 500 µl with lysis buffer. Each experiment is setup such that tube 3 is the IP lane and remaining tubes are controls. Tube 1 is beads alone, tube 2 is beads + lysate, tube 3 is beads + lysate + IP

antibody, tube 4 is beads + lysate + non-immune antibody, tube 5 is beads + IP antibody, and tube 6 is beads + non-immune antibody. Tubes were incubated for 4-5 hours, rotating, at 4°C. To pellet the beads, tubes were centrifuged at 5000 rpm for 3 minutes. Tube 3 supernatant was transferred to a new tube. The supernatant from remaining tubes was aspirated. The beads were washed three times with PBS. 100 µl PBS and 25 µl 5X LSB was added to each tube and heated at 95°C for 5 minutes. Beads were pellet prior to running on SDS-PAGE gel.

Proteomics analysis

An immunoprecipitation was performed using Myo10 antibody 117 from 2-week old Caco-2 monolayers, as described above. The gel of the immunoprecipitation lane (beads + lysate + IP antibody) was stained with 0.1% Coomassie R-250 in 10% acetic acid for 1.5 hours, rocking. The gel was destained with several washes in 10% acetic acid. The stained gel was sent to the UNC Proteomics Center for analysis by mass spectrometry and MADLI-TOF peptide sequencing.

RESULTS

Myo10 is Expressed at High Levels in Early Stage Caco-2 Cells

Immunoblotting of the Caco-2 cell developmental time course shows endogenous Myo10 is present at all time points, and expression levels vary based on degree of maturation (Figure A.1). Highest Myo10 expression levels are observed between 3-6 days post-plating, and levels decrease as Caco-2 cells mature. As a control, villin expression was

quantified, and as expected, increasing villin levels in Caco-2 cells correlates with maturation of microvilli. All protein levels were normalized against F-actin loading controls. Consistent with these results, a Caco-2 microarray study shows higher Myo10 mRNA levels at early stages of Caco-2 cell development (Halbleib et al., 2007). In LLC-PK1 cells and MDCK cells, full length Myo10 protein expression did not differ between time points (data not shown).

Full-length Myo10 was detected using two different antibodies, 117 and SDI, which yielded similar results. However, in addition to the full-length endogenous Myo10 (~237 kDa), 117 detects an extra band at 75 kDa with a higher signal intensity than the full-length Myo10 band in both Caco-2 and MDCK cells (Figure A.2).

Ezrin is identified as the 75 kDa band detected by 117 anti-Myo10

The identity of the 75 kDa band was inadvertently discovered during our search to identify binding partners for Myo10. We performed immunoprecipitation experiments with Myo10 antibody, and immunoblotting with an anti-ezrin antibody recognized a 75 kDa band. However, when I performed the reverse immunoprecipitation using the anti-ezrin antibody, immunoblotting with 117 anti-Myo10 recognized the 75 kD band but not the full-length Myo10 band (Figure A.3). Proteomic analysis identified the 75 kD band as ezrin and radixin, and ezrin was quantified as more abundant than radixin in Caco-2 cells (Figure A.4). To confirm these results, we probed bacterially expressed ezrin, and the 117 antibody was also found to react with this (data not shown). As a possible explanation for the cross-reactivity with ezrin, the 117 Myo10 antibody was made against its predicted coiled-coil

region (Berg et al., 2000), and ezrin contains a coiled-coil region as well (Turunen et al., 1998). We thus used different Myo10 antibodies for subsequent experiments. Immunoprecipitation using Myo10 antibodies from SDI and Sigma did not co-immunoprecipitate the 75 kDa band (data not shown).

Myo10 Is Not Detected in Microvilli of Mature Caco-2 Cells

The immunofluorescence experiments using the SDI anti-Myo10 antibody demonstrate that, as Caco-2 cells become fully polarized (11 days), little to no Myo10 is detected in the actin-rich microvilli of the apical surface (Figure A.5). Instead, this antibody labeled diffuse cytoplasmic puncta in the basolateral portion of the cell. Non-immune antibody immunostaining does not show localization to cytoplasmic puncta.

Myo10 Knockdown does not affect number of microvilli

Since microvilli are hypothesized to develop from filopodia, we tested whether Myo10 is needed for the formation of microvilli. Myo10 knockdown was achieved by infecting Caco-2 cells with shRNA-expressing lentivirus. Lentivirus shRNA knockdown has the advantage of long-term shRNA expression by stably integrating into the host genome. ~40% of cells were infected with the shRNA-expressing lentivirus, as identified by GFP labeling. The infected cells were fluorescence-activated cell sorted (FACS) to select for GFP-shRNA expressing cells. Immunoblotting indicated that Myo10 continued to be knocked down by ~80-90% using shRNA lentivirus in Caco-2 cells at two weeks post-plating (Figure A.6).

Although preliminary scanning electron microscopy (SEM) experiments had suggested that Myo10 knockdown decreased the number of microvilli, the lentivirus-treated Caco-2 cultures used in those experiments were contaminated with mesenchymal HEK293 cells used to produce the lentivirus. After resolving the contamination issue by harvesting virus via filtration rather than centrifugation, Myo10 knockdown cells did not show a statistically significant decrease in number of microvilli.

Myo10 Knockdown Cells Differ in Cell Morphology

Since Myo10 knockdown did not appear to affect number of microvilli, we next asked whether Myo10 knockdown affects overall cell morphology. To measure changes in cell morphology, cell area and cell height were examined (Figure A.7). To quantify cell area, Caco-2 monolayers expressing Myo10 or NS shRNA were immunostained for ZO-1, and cell area was measured using the junction borders delineated by ZO-1 staining. Myo10 knockdown cells showed increased cell area versus control cells (Myo10 shRNA: 150.9 ± 19.42 μm^2 vs. NS shRNA 251.2 ± 35.01 μm^2). This result using GFP-cell sorted Caco-2 knockdown cells was verified with antibiotic-selected Caco-2 knockdown cells (Myo10 shRNA: 170.0 ± 12.9 µm vs. NS shRNA: 310.8 ± 30.9 µm). Furthermore, Myo10 knockdown cells were shorter than control cells (Myo10 shRNA: 15.02 ± 0.9 µm vs. pLL 5.0: 26.17 ± 0.9 µm), as measured using transmission electron micrographs of cross-sections through Caco-2 monolayers.

DISCUSSION

Myo10 is Expressed at Highest Levels at Early Stages in Caco-2 Cells

During the developmental time course of Caco-2 cells, Myo10 is expressed at all time points, yet Myo10 expression varies over time. At early stages, Myo10 expression increases and peaks between 3-6 days. Myo10 levels then decrease and level off as Caco-2 cells mature. These results are in agreement with microarray studies that found high Myo10 mRNA levels at early stages of Caco-2 development (Halbleib et al., 2007). Since Myo10 expression is highest between 3-6 days, this could support a functional role for Myo10 at early stages of Caco-2 development. Interestingly, high Myo10 expression levels correlate with the presence of abundant actin-based filopodia and lamellipodia in early stage, spreading Caco-2 cells. Myo10 localizes to the tips of filopodia and at the edge of lamellipodia (Berg et al., 2000), and Myo10 is needed for formation of filopodia. Thus, it is possible that Myo10 is involved in filopodial and lamellipodial processes, such as cell spreading and initial cell-cell contact formation, at early stages in Caco-2 cells. In addition, microvilli begin to develop at early stages in Caco-2 cells, so it was also possible is that high Myo10 expression correlated with a role in microvillar formation. Conversely, lower levels of Myo10 are expressed in mature, polarized Caco-2 cells when apical microvilli are the predominant actin-based structure, as evidenced by increased villin expression. However, low expression levels do not rule out a role for Myo10 in mature, polarized epithelial cells as Myo10 is a ubiquitous but generally low abundance protein (Berg et al., 2000). Thus, Myo10 expression data presented here suggests a functional role for Myo10 in early stages of polarized epithelial cell development.

Myo10 Labels the Basolateral Domain in Polarized Caco-2 Cells

In mature Caco-2 cells, the majority of anti-Myo10 (SDI) immunostaining was basolateral and cytoplasmic, and the staining pattern was strongly punctate rather than diffuse. This localization of endogenous Myo10 is likely specific, as staining with the non-immune antibody showed a significantly weaker, more diffuse signal. Also, similar staining patterns were observed using two Myo10 antibodies, SDI and Sigma. Furthermore, GFP-Myo10 also shows some punctate localization in MDCK cells (Figures 3.1 and 3.S1).

Our studies indicate endogenous Myo10 is not enriched in apical microvilli, yet we cannot rule out trace amounts of Myo10 in microvilli that are below our level of detection. Consistent with these results, biochemical fractionation studies of polarized epithelial tissue show that Myo10 fractionated in the basolateral fraction of kidney lysates (Yonezawa et al., 2003). In addition, McConnell et al. failed to detect Myo10 in the brush border fraction from mouse small intestine, although get did detect 14 other myosins (McConnell et al., 2011). Friedman lab has also reported that GFP-Myo10 does not localize to stereocilia in cultured hair cells (Kitajiri et al., 2010).

Thus far, the identity of the Myo10-labelled cytoplasmic puncta is uncertain. One possibility is that Myo10 is present on cytoplasmic vesicles. While Myo10 has not been implicated in trafficking roles, other unconventional myosins, such as Myo6, Myo5B and Myo5C, have known functional roles in endocytosis, membrane trafficking and exocytosis (Tuxworth and Titus, 2000). Alternatively, one could hypothesize that inactive Myo10 localizes to a vesicular compartment until needed by the cell. To determine whether Myo10

indeed localizes to cytoplasmic vesicles, future experiments could include immunostaining for vesicular compartment markers and assessing for colocalization with Myo10. However, it is formally possible that the cytoplasmic puncta are an artifact of immunostaining or fixation. To address this issue, Caco-2 cells transiently transfected with fluorescently-tagged Myo10 or stable GFP-Myo10 MDCK cells can be imaged using live-cell spinning disc microscopy. Although further experiments are needed to definitively characterize Myo10-labelled cytoplasmic puncta, the results presented here indicate that Myo10 is not enriched in apical microvilli.

Myo10 Is Not Needed for Formation of Apical Microvilli

Since microvilli have been theorized to develop from filopodia and Myo10 is necessary for filopodial formation, we tested whether knockdown of Myo10 inhibits the formation of microvilli. Our data thus far shows that Myo10 knockdown does not affect the number of apical microvilli as assayed by scanning electron microscopy. Thus, our results support the view that Myo10 is not needed for the formation of microvilli. Instead, these results suggest that microvilli and filopodia are distinct structures with different mechanisms of formation. However, it is formally possible that the amount of Myo10 in microvilli is below our threshold level of detection, in which case, a knockout mouse is needed to obtain conclusive results.

These studies highlight a fundamental question: what is the difference between filopodia and microvilli? After all, filopodia and microvilli are both actin-based structures, and oftentimes the nomenclature is used interchangeably; for example, surface protrusions

on cells in suspension, i.e. leukocytes, have been referred to as either microvilli or filopodia. Yet, there are clear differences between filopodia found on the dorsal surface of non-polarized cells and apical microvilli in polarized epithelial cells. Filopodia are dynamic, and among filopodia, the length and number of actin filaments within the core actin bundle can vary considerably. In contrast, polarized epithelial cells have microvilli – fundamentally apical structures with a core of approximately 20 actin filaments (Mooseker, 1985), and microvilli maintain a constant height of 1-2 μm. The rate of retrograde flow is slower in microvilli (~7 nm/min) than in filopodia (10-100 nm/sec) (Kerber et al., 2009; Nambiar et al., 2010). Both filopodia and microvilli are composed of actin bundles, but interestingly, different proteins cross-link the actin filaments. Fascin is a major actin crosslinker in most filopodia, whereas fimbrin and villin bundle actin in intestinal microvilli. Although filopodia and microvilli are similar actin-based structures, our investigations with Myo10 suggest that their mechanisms of formation may differ.

Myo10 May Be Needed for Proper Cell Morphology

Preliminary cell morphology analysis of shows that Myo10 knockdown cells have increased cell area and decreased cell height compared with control cells. Our observations are similar to the defect reported for inhibition of phosphatidylinositol (3,4,5)-triphosphate (PIP3) production in MDCK cells (Gassama-Diagne et al., 2006). Phospholipids are segregated in polarized epithelial cells such that PIP3 is restricted to the basolateral domain (Martin-Belmonte et al., 2007). Since Myo10 binds PIP3 via its PH domain region, it is plausible for Myo10 to affect cell morphology through its interaction with basolateral PIP3.

The PH domains of Myo10 have been recently shown to target to the basolateral domain in polarized epithelial cells (Lu et al., 2011). Perhaps Myo10 recruits binding partners to the basolateral membrane via targeting by PIP3.

Interestingly, Myo10 knockdown results in an increase in cell area in non-polarized cells (Bohil et al., 2006). In non-polarized cells, it has been postulated that the loss of filopodia increases the amount of available cell membrane (previously used to make filopodia), which results in a larger cell area. Although our results suggest Myo10 does not affect the formation of microvilli, which would provide large amount of available cell membrane, Myo10 may be important for other actin-based protrusive structures in polarized epithelial cells. Notably, in polarized epithelial cells, basolateral filopodia and sheet-like lateral membrane protrusions have been observed (Georgiou and Baum, 2010). In future studies, it would be important to determine whether Myo10 functions in basolateral filopodia or lateral protrusions and to correlate this with the defect in cell morphology.

Alternatively, it is possible the observed changes in cell morphology results from Myo10 knockdown cells developing at a slower rate. Myo10 is necessary for proper spindle orientation (Weber et al., 2004), which in turn, will affects the process of cell division. Normally, as polarized epithelial cells grow increasingly taller and more compact as cells divide and form monolayers. Thus, the shorter and wider cell phenotype could result from Myo10 knockdown cells observed at an earlier stage of maturation. In order to address this concern, we plated Caco-2 cells at confluent densities. Other controls could include immunoblotting for polarized epithelial differentiation markers such as sucrose-isomaltase

or dipeptidyl peptidase IV (DPP-IV). Also, epithelial monolayer could be cultured for longer time periods to ensure that cell height of the monolayer has fully stabilized.

Myo10, a motor protein critical for the formation of filopodia, is highly expressed in epithelial tissues. Yet, the role of Myo10 in polarized epithelia is relatively unknown. Here, we present initial characterization of Myo10 expression in Caco-2 cells, and we test the hypothesis that Myo10 is needed for microvillar formation. Notably, Myo10 is expressed at high levels early in Caco-2 development. Localization studies indicate Myo10 is not enriched in microvilli, which is consistent with a recent proteomic analysis that failed to detect Myo10 in the apical domain of intestinal cells (McConnell et al., 2011); instead, Myo10 is found in the basolaterally. Moreover, in my experiments, Myo10 knockdown does not affect the formation of microvilli. Interestingly, Myo10 may have a role in cell morphology as Myo10 knockdown led to shorter and wider cells in both Caco-2 and MDCK cultures. Our studies raise the issue of how filopodia and microvilli differ. Although filopodia and microvilli are both actin-based structures, our studies suggest that formation of filopodia and microvilli are likely regulated by different mechanisms. Thus, we consider microvilli as a fundamentally apical structure.

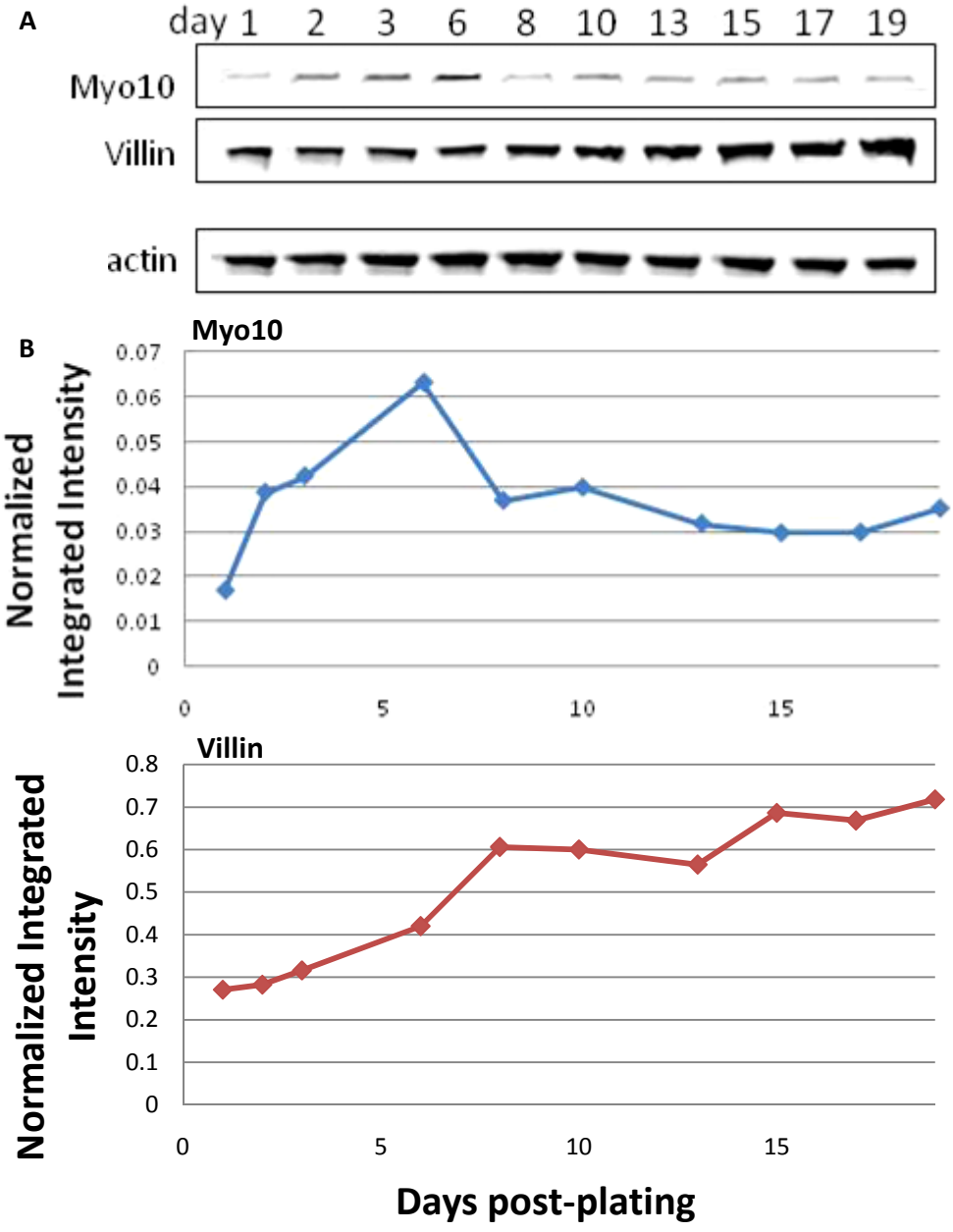

Figure A.1 Myo10 is expressed in Caco-2 cells with peak expression at early stages. (A) Immunoblotting of a Caco-2 time course over 19 days using the SDI antibody shows that Myo10 is expressed at all time points with a peak at ~6 days. Villin, a microvillar marker, was used as a control for microvillar maturation; as expected, villin expression increased as Caco-2 cells matured. Actin was used as a loading control. (B) Myo10 (blue) and villin (red) expression levels were quantified using the LI-COR Odyssey imaging software by measuring the integrated intensity and normalizing for protein loading with actin. (n = 6)

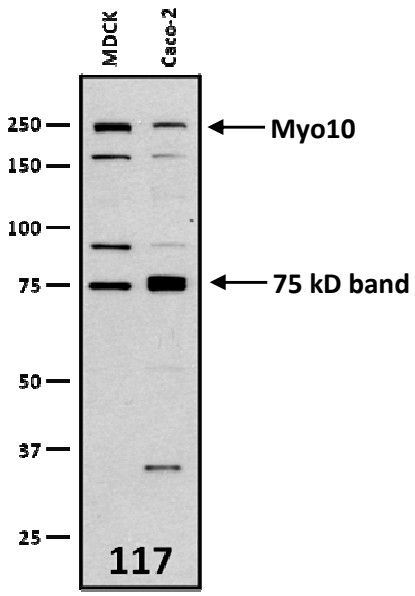

Figure A.2 anti-Myo10 antibody 117 detects full-length Myo10 and additional bands in MDCK and Caco-2 cells. Immunoblotting in Caco-2 and MDCK cells recognizes full-length Myo10 at approximately 250 kD. 117 antibody also detects additional bands at lower molecular weights. In particular, there is an extra band at 75 kD, the intensity of which is significantly stronger than that of full-length Myo10.

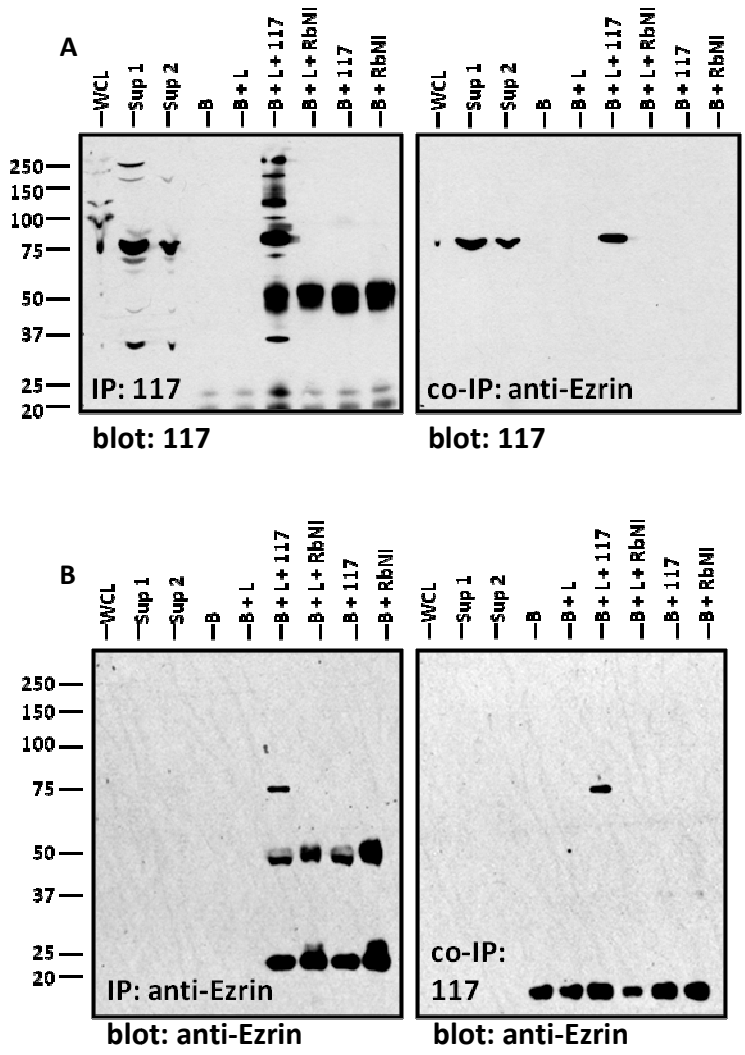

Figure A.3 Ezrin co-immunoprecipitates with Myo10, but only the 75 kD band co-immunoprecipitates with Ezrin. (A) Immunoprecipitation with 117 anti-Myo10 shows that full-length Myo10 and the 75 kD band are immunoprecipitated and detected with 117; ezrin also co-immunoprecipitates with 117 but not with non-immune IgG. (B) When the reverse IP is performed, the 75 kD band, but not full-length Myo10, co-immunoprecipitates with ezrin, confirming that anti-Myo10 117 cross-reacts with ezrin. WCL = whole cell lysate; Sup 1 = supernatant 1 (after low-speed spin); Sup 2 = supernatant 2 (unbound to beads); B = beads; L = lysate; RbNI = rabbit non-immune antibody.

A

B

Protein Name	Species	Database Accession ID [1]	MW (Da)	Peptide Count [2]
Villin 2.- Homo sapiens (Human).	Homo sapiens	Q6NUR7_HUMAN	69198.6	35
BC047109 NID: - Homo sapiens	Homo sapiens	AAH47109	68522.3	23

Figure A.4 Ezrin is the 75kD band detected by the Myo10 antibody 117. (A) Coomassie stain of proteins immunoprecipitated with Myo10 antibody 117. The ~75 kD band was sent for mass spectrometry and proteomics analysis. (B) Results from the proteomics analysis identifies Ezrin (accession ID: Q6NUR7_HUMAN) and Radixin (accession ID: AAH47109). “Peptide count” refers to the number of peptides that match peptides from theoretical digest.

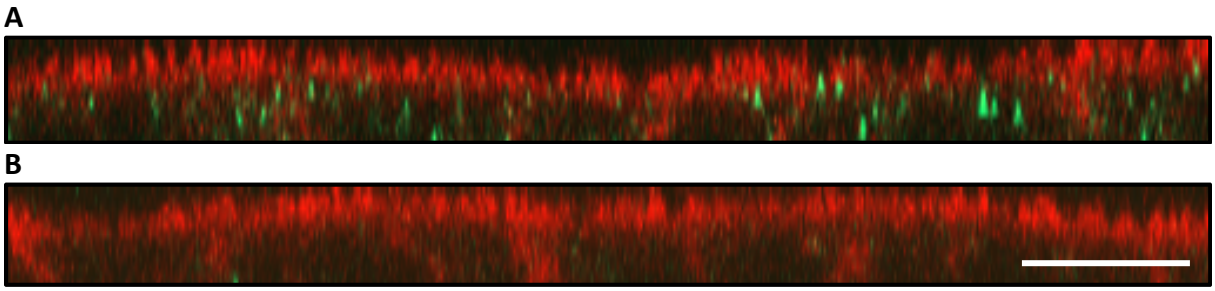

Figure A.5 Immunostaining shows little or no endogenous Myo10 is detected in microvilli of Caco-2 cell monolayers. (A) SDI anti-Myo10 (green) is not enriched in microvilli, but rather, endogenous Myo10 localizes to cytoplasmic puncta. F-actin is labeled in red. Images are confocal xz-sections from 11-day Caco-2 monolayers. (B) Non-immune control. Scale bar = 10 µm.

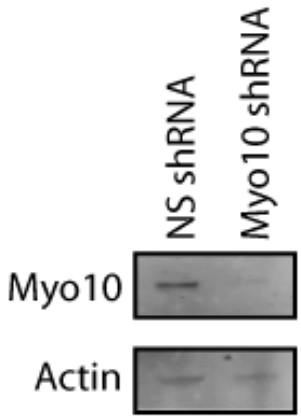

Figure A.6 Myo10 is knocked down by shRNA lentivirus methods (with filtration of viral supernatant). Immunoblot shows mature Caco-2 cells (2 weeks) infected with Myo10 shRNA are knocked down for Myo10 when compared with Caco-2 cells infected with control NS shRNA lentivirus. Actin was used as a loading control.

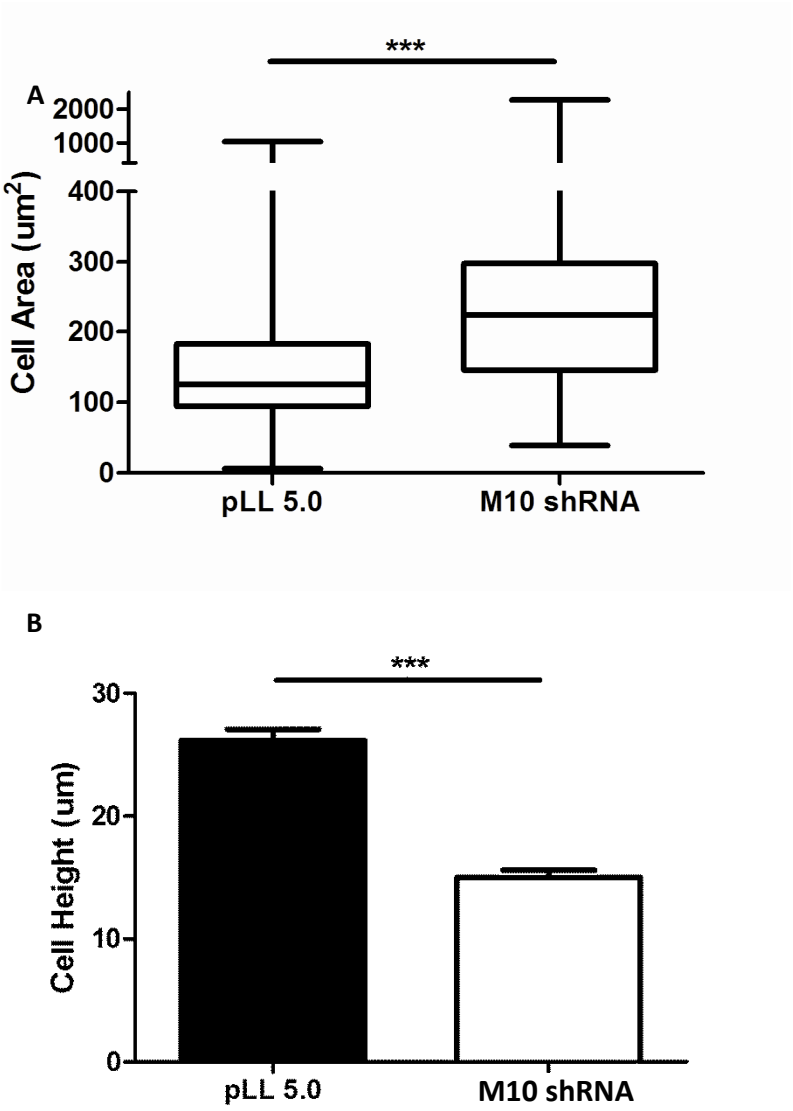

Figure A.7 Myo10 knockdown by lentivirus in Caco-2 cells shows (A) increased cell area and (B) reduced cell height. Increased cell area and reduced cell height in shRNA transfected Myo10 knockdown cells were consistent with lentivirus knockdown results. Caco-2 cells were knocked down for Myo10 using shRNA nucleofection. Cells were plated at confluent densities and allowed to grow for one week. Cell area was measured by ZO-1 staining using immunofluorescence. pLL 5.0 = control lentivirus vector. (n=2)

REFERENCES

Abouhamed, M., K. Grobe, I.V. San, S. Thelen, U. Honnert, M.S. Balda, K. Matter, and M. Bahler. 2009. Myosin IXa regulates epithelial differentiation and its deficiency results in hydrocephalus. *Mol Biol Cell*. 20:5074-5085.

Adams, C.L., W.J. Nelson, and S.J. Smith. 1996. Quantitative analysis of cadherin-catenin-actin reorganization during development of cell-cell adhesion. *J Cell Biol*. 135:1899-1911.

Adato, A., D. Weil, H. Kalinski, Y. Pel-Or, H. Ayadi, C. Petit, M. Korostishevsky, and B. Bonne-Tamir. 1997. Mutation profile of all 49 exons of the human myosin VIIA gene, and haplotype analysis, in Usher 1B families from diverse origins. *Am J Hum Genet*. 61:813-821.

Albanesi, J.P., M. Coue, H. Fujisaki, and E.D. Korn. 1985. Effect of actin filament length and filament number concentration on the actin-activated ATPase activity of Acanthamoeba myosin I. *J Biol Chem*. 260:13276-13280.

Almagro, S., C. Durmort, A. Chervin-Petinot, S. Heyraud, M. Dubois, O. Lambert, C. Maillefaud, E. Hewat, J.P. Schaal, P. Huber, and D. Gulino-Debrac. 2010. The motor protein myosin-X transports VE-cadherin along filopodia to allow the formation of early endothelial cell-cell contacts. *Mol Cell Biol*. 30:1703-1717.

Anderson, J.M., and C.M. Van Itallie. 2009. Physiology and function of the tight junction. *Cold Spring Harb Perspect Biol*. 1:a002584.

Ando-Akatsuka, Y., S. Yonemura, M. Itoh, M. Furuse, and S. Tsukita. 1999. Differential behavior of E-cadherin and occludin in their colocalization with ZO-1 during the establishment of epithelial cell polarity. *J Cell Physiol*. 179:115-125.

Arganda-Carreras, I., R. Fernandez-Gonzalez, A. Munoz-Barrutia, and C. Ortiz-De-Solorzano. 2010. 3D reconstruction of histological sections: Application to mammary gland tissue. *Microsc Res Tech*. 73:1019-1029.

Au, J.S., C. Puri, G. Ihrke, J. Kendrick-Jones, and F. Buss. 2007. Myosin VI is required for sorting of AP-1B-dependent cargo to the basolateral domain in polarized MDCK cells. *J Cell Biol*. 177:103-114.

Avraham, K.B., T. Hasson, K.P. Steel, D.M. Kingsley, L.B. Russell, M.S. Mooseker, N.G. Copeland, and N.A. Jenkins. 1995. The mouse Snell's waltzer deafness gene encodes an unconventional myosin required for structural integrity of inner ear hair cells. *Nat Genet*. 11:369-375.

Baas, A.F., J. Kuipers, N.N. van der Wel, E. Batlle, H.K. Koerten, P.J. Peters, and H.C. Clevers. 2004. Complete polarization of single intestinal epithelial cells upon activation of LKB1 by STRAD. *Cell*. 116:457-466.

Bahloul, A., V. Michel, J.P. Hardelin, S. Nouaille, S. Hoos, A. Houdusse, P. England, and C. Petit. 2010. Cadherin-23, myosin VIIa and harmonin, encoded by Usher syndrome type I genes, form a ternary complex and interact with membrane phospholipids. *Hum Mol Genet*. 19:3557-3565.

Balda, M.S., L. Gonzalez-Mariscal, R.G. Contreras, M. Macias-Silva, M.E. Torres-Marquez, J.A. Garcia-Sainz, and M. Cereijido. 1991. Assembly and sealing of tight junctions: possible participation of G-proteins, phospholipase C, protein kinase C and calmodulin. *J Membr Biol*. 122:193-202.

Balda, M.S., J.A. Whitney, C. Flores, S. Gonzalez, M. Cereijido, and K. Matter. 1996. Functional dissociation of paracellular permeability and transepithelial electrical resistance and disruption of the apical-basolateral intramembrane diffusion barrier by expression of a mutant tight junction membrane protein. *J Cell Biol*. 134:1031-1049.

Belyantseva, I.A., E.T. Boger, and T.B. Friedman. 2003. Myosin XVa localizes to the tips of inner ear sensory cell stereocilia and is essential for staircase formation of the hair bundle. *Proc Natl Acad Sci U S A*. 100:13958-13963.

Belyantseva, I.A., E.T. Boger, S. Naz, G.I. Frolenkov, J.R. Sellers, Z.M. Ahmed, A.J. Griffith, and T.B. Friedman. 2005. Myosin-XVa is required for tip localization of whirlin and differential elongation of hair-cell stereocilia. *Nat Cell Biol*. 7:148-156.

Bement, W.M., T. Hasson, J.A. Wirth, R.E. Cheney, and M.S. Mooseker. 1994a. Identification and overlapping expression of multiple unconventional myosin genes in vertebrate cell types. *Proc Natl Acad Sci U S A*. 91:6549-6553.

Bement, W.M., J.A. Wirth, and M.S. Mooseker. 1994b. Cloning and mRNA expression of human unconventional myosin-IC. A homologue of amoeboid myosins-I with a single IQ motif and an SH3 domain. *J Mol Biol*. 243:356-363.

Bennett, R.D., A.S. Mauer, and E.E. Strehler. 2007. Calmodulin-like protein increases filopodia-dependent cell motility via up-regulation of myosin-10. *J Biol Chem*. 282:3205-3212.

Berg, J.S., and R.E. Cheney. 2002. Myosin-X is an unconventional myosin that undergoes intrafilopodial motility. *Nat Cell Biol*. 4:246-250.

Berg, J.S., B.H. Derfler, C.M. Pennisi, D.P. Corey, and R.E. Cheney. 2000. Myosin-X, a novel myosin with pleckstrin homology domains, associates with regions of dynamic actin. *J Cell Sci*. 113 Pt 19:3439-3451.

Berg, J.S., B.C. Powell, and R.E. Cheney. 2001. A millennial myosin census. *Mol Biol Cell*. 12:780-794.

Bilder, D., M. Schober, and N. Perrimon. 2003. Integrated activity of PDZ protein complexes regulates epithelial polarity. *Nat Cell Biol*. 5:53-58.

Boeda, B., A. El-Amraoui, A. Bahloul, R. Goodyear, L. Daviet, S. Blanchard, I. Perfettini, K.R. Fath, S. Shorte, J. Reiners, A. Houdusse, P. Legrain, U. Wolfrum, G. Richardson, and C. Petit. 2002. Myosin VIIa, harmonin and cadherin 23, three Usher I gene products that cooperate to shape the sensory hair cell bundle. *EMBO J*. 21:6689-6699.

Bohil, A.B., B.W. Robertson, and R.E. Cheney. 2006. Myosin-X is a molecular motor that functions in filopodia formation. *Proc Natl Acad Sci U S A*. 103:12411-12416.

Boller, K., D. Vestweber, and R. Kemler. 1985. Cell-adhesion molecule uvomorulin is localized in the intermediate junctions of adult intestinal epithelial cells. *J Cell Biol*. 100:327-332.

Bolz, H., B. von Brederlow, A. Ramirez, E.C. Bryda, K. Kutsche, H.G. Nothwang, M. Seeliger, C.S.C.M. del, M.C. Vila, O.P. Molina, A. Gal, and C. Kubisch. 2001. Mutation of CDH23, encoding a new member of the cadherin gene family, causes Usher syndrome type 1D. *Nat Genet*. 27:108-112.

Booth, A.G., and A.J. Kenny. 1976. Proteins of the kidney microvillus membrane. Identification of subunits after sodium dodecylsullphate/polyacrylamide-gel electrophoresis. *Biochem J*. 159:395-407.

Braga, V.M., and A.S. Yap. 2005. The challenges of abundance: epithelial junctions and small GTPase signalling. *Curr Opin Cell Biol*. 17:466-474.

Breshears, L.M., D. Wessels, D.R. Soll, and M.A. Titus. 2010. An unconventional myosin required for cell polarization and chemotaxis. *Proc Natl Acad Sci U S A*. 107:6918-6923.

Bresnick, A.R. 1999. Molecular mechanisms of nonmuscle myosin-II regulation. *Curr Opin Cell Biol*. 11:26-33.

Bridges, C., and T. Morgan. 1919. Contributions to the genetics of Drosophila melanogaster. II. The second-chromosome group of mutant characters. *Carnegie Inst Washington Publ*. 278:123-304.

Bruewer, M., A.M. Hopkins, M.E. Hobert, A. Nusrat, and J.L. Madara. 2004. RhoA, Rac1, and Cdc42 exert distinct effects on epithelial barrier via selective structural and biochemical modulation of junctional proteins and F-actin. *Am J Physiol Cell Physiol*. 287:C327-335.

Bruewer, M., A. Luegering, T. Kucharzik, C.A. Parkos, J.L. Madara, A.M. Hopkins, and A. Nusrat. 2003. Proinflammatory cytokines disrupt epithelial barrier function by apoptosis-independent mechanisms. *J Immunol*. 171:6164-6172.

Buss, F., S.D. Arden, M. Lindsay, J.P. Luzio, and J. Kendrick-Jones. 2001a. Myosin VI isoform localized to clathrin-coated vesicles with a role in clathrin-mediated endocytosis. *EMBO J*. 20:3676-3684.

Buss, F., J. Kendrick-Jones, C. Lionne, A.E. Knight, G.P. Cote, and J. Paul Luzio. 1998. The localization of myosin VI at the golgi complex and leading edge of fibroblasts and its phosphorylation and recruitment into membrane ruffles of A431 cells after growth factor stimulation. *J Cell Biol*. 143:1535-1545.

Buss, F., J.P. Luzio, and J. Kendrick-Jones. 2001b. Myosin VI, a new force in clathrin mediated endocytosis. *FEBS Lett*. 508:295-299.

Byers, H.R., G.E. White, and K. Fujiwara. 1984. Organization and function of stress fibers in cells in vitro and in situ. A review. *Cell Muscle Motil*. 5:83-137.

Capaldo, C.T., and I.G. Macara. 2007. Depletion of E-cadherin disrupts establishment but not maintenance of cell junctions in Madin-Darby canine kidney epithelial cells. *Mol Biol Cell*. 18:189-200.

Case, L.B., and C.M. Waterman. 2011. Adhesive F-actin waves: a novel integrin-mediated adhesion complex coupled to ventral actin polymerization. *PLoS One*. 6:e26631.

Cereijido, M., E.S. Robbins, W.J. Dolan, C.A. Rotunno, and D.D. Sabatini. 1978. Polarized monolayers formed by epithelial cells on a permeable and translucent support. *J Cell Biol*. 77:853-880.

Chatterjee, A., S. Chaudhuri, G. Saha, S. Gupta, and R. Chowdhury. 2004. Effect of bile on the cell surface permeability barrier and efflux system of Vibrio cholerae. *J Bacteriol*. 186:6809-6814.

Chen, L., C. Janetopoulos, Y.E. Huang, M. Iijima, J. Borleis, and P.N. Devreotes. 2003. Two phases of actin polymerization display different dependencies on PI(3,4,5)P3 accumulation and have unique roles during chemotaxis. *Mol Biol Cell*. 14:5028-5037.

Chen, Z.Y., T. Hasson, P.M. Kelley, B.J. Schwender, M.F. Schwartz, M. Ramakrishnan, W.J. Kimberling, M.S. Mooseker, and D.P. Corey. 1996. Molecular cloning and domain structure of human myosin-VIIa, the gene product defective in Usher syndrome 1B. *Genomics*. 36:440-448.

Chen, Z.Y., T. Hasson, D.S. Zhang, B.J. Schwender, B.H. Derfler, M.S. Mooseker, and D.P. Corey. 2001. Myosin-VIIb, a novel unconventional myosin, is a constituent of microvilli in transporting epithelia. *Genomics*. 72:285-296.

Cheney, R.E., and M.S. Mooseker. 1992. Unconventional myosins. *Curr Opin Cell Biol*. 4:27-35.

Chiba, H., N. Sakai, M. Murata, M. Osanai, T. Ninomiya, T. Kojima, and N. Sawada. 2006. The nuclear receptor hepatocyte nuclear factor 4alpha acts as a morphogen to induce the formation of microvilli. *J Cell Biol*. 175:971-980.

Chieregatti, E., A. Gartner, H.E. Stoffler, and M. Bahler. 1998. Myr 7 is a novel myosin IX-RhoGAP expressed in rat brain. *J Cell Sci*. 111 (Pt 24):3597-3608.

Citi, S., H. Sabanay, J. Kendrick-Jones, and B. Geiger. 1989. Cingulin: characterization and localization. *J Cell Sci*. 93 (Pt 1):107-122.

Claude, P. 1978. Morphological factors influencing transepithelial permeability: a model for the resistance of the zonula occludens. *J Membr Biol*. 39:219-232.

Cohen, M., M. Georgiou, N.L. Stevenson, M. Miodownik, and B. Baum. 2010. Dynamic filopodia transmit intermittent Delta-Notch signaling to drive pattern refinement during lateral inhibition. *Dev Cell*. 19:78-89.

Conti, M.A., S. Even-Ram, C. Liu, K.M. Yamada, and R.S. Adelstein. 2004. Defects in cell adhesion and the visceral endoderm following ablation of nonmuscle myosin heavy chain II-A in mice. *J Biol Chem*. 279:41263-41266.

Cordenonsi, M., F. D'Atri, E. Hammar, D.A. Parry, J. Kendrick-Jones, D. Shore, and S. Citi. 1999. Cingulin contains globular and coiled-coil domains and interacts with ZO-1, ZO-2, ZO-3, and myosin. *J Cell Biol*. 147:1569-1582.

Cox, D., J.S. Berg, M. Cammer, J.O. Chinegwundoh, B.M. Dale, R.E. Cheney, and S. Greenberg. 2002. Myosin X is a downstream effector of PI(3)K during phagocytosis. *Nat Cell Biol*. 4:469-477.

De La Cruz, E.M., E.M. Ostap, and H.L. Sweeney. 2001. Kinetic mechanism and regulation of myosin VI. *J Biol Chem*. 276:32373-32381.

Demontis, F., and C. Dahmann. 2007. Apical and lateral cell protrusions interconnect epithelial cells in live Drosophila wing imaginal discs. *Dev Dyn*. 236:3408-3418.

den Elzen, N., C.V. Buttery, M.P. Maddugoda, G. Ren, and A.S. Yap. 2009. Cadherin adhesion receptors orient the mitotic spindle during symmetric cell division in mammalian epithelia. *Mol Biol Cell*. 20:3740-3750.

Deng, W., K. Leaper, and M. Bownes. 1999. A targeted gene silencing technique shows that Drosophila myosin VI is required for egg chamber and imaginal disc morphogenesis. *J Cell Sci*. 112 (Pt 21):3677-3690.

Deol, M.S., and M.C. Green. 1966. Snell's waltzer, a new mutation affecting behaviour and the inner ear in the mouse. *Genet Res*. 8:339-345.

DeRosier, D.J., and L.G. Tilney. 2000. F-actin bundles are derivatives of microvilli: What does this tell us about how bundles might form? *J Cell Biol*. 148:1-6.

Di Palma, F., R.H. Holme, E.C. Bryda, I.A. Belyantseva, R. Pellegrino, B. Kachar, K.P. Steel, and K. Noben-Trauth. 2001. Mutations in Cdh23, encoding a new type of cadherin, cause stereocilia disorganization in waltzer, the mouse model for Usher syndrome type 1D. *Nat Genet*. 27:103-107.

Drees, F., S. Pokutta, S. Yamada, W.J. Nelson, and W.I. Weis. 2005. Alpha-catenin is a molecular switch that binds E-cadherin-beta-catenin and regulates actin-filament assembly. *Cell*. 123:903-915.

Drenckhahn, D., and R. Dermietzel. 1988. Organization of the actin filament cytoskeleton in the intestinal brush border: a quantitative and qualitative immunoelectron microscope study. *J Cell Biol*. 107:1037-1048.

Ebermann, I., H.P. Scholl, P. Charbel Issa, E. Becirovic, J. Lamprecht, B. Jurklies, J.M. Millan, E. Aller, D. Mitter, and H. Bolz. 2007. A novel gene for Usher syndrome type 2: mutations in the long isoform of whirlin are associated with retinitis pigmentosa and sensorineural hearing loss. *Hum Genet*. 121:203-211.

Etournay, R., I. Zwaenepoel, I. Perfettini, P. Legrain, C. Petit, and A. El-Amraoui. 2007. Shroom2, a myosin-VIIa- and actin-binding protein, directly interacts with ZO-1 at tight junctions. *J Cell Sci*. 120:2838-2850.

Fanning, A.S., C. Van Itallie, and J.M. Anderson. 2012. Zonula Occludens (ZO)-1 and -2 Regulate Apical Cell Structure and the Zonula Adherens Cytoskeleton in Polarized Epithelia. *Mol Biol Cell*. 23:577-590.

Farooqui, R., and G. Fenteany. 2005. Multiple rows of cells behind an epithelial wound edge extend cryptic lamellipodia to collectively drive cell-sheet movement. *J Cell Sci*. 118:51-63.

Faul, C., K. Asanuma, E. Yanagida-Asanuma, K. Kim, and P. Mundel. 2007. Actin up: regulation of podocyte structure and function by components of the actin cytoskeleton. *Trends Cell Biol*. 17:428-437.

Ferrary, E., M. Cohen-Tannoudji, G. Pehau-Arnaudet, A. Lapillonne, R. Athman, T. Ruiz, L. Boulouha, F. El Marjou, A. Doye, J.J. Fontaine, C. Antony, C. Babinet, D. Louvard, F. Jaisser, and S. Robine. 1999. In vivo, villin is required for Ca(2+)-dependent F-actin disruption in intestinal brush borders. *J Cell Biol*. 146:819-830.

Fish, E.M., and B.A. Molitoris. 1994. Alterations in epithelial polarity and the pathogenesis of disease states. *N Engl J Med*. 330:1580-1588.

Friedman, T.B., Y. Liang, J.L. Weber, J.T. Hinnant, T.D. Barber, S. Winata, I.N. Arhya, and J.H. Asher, Jr. 1995. A gene for congenital, recessive deafness DFNB3 maps to the pericentromeric region of chromosome 17. *Nat Genet*. 9:86-91.

Gassama-Diagne, A., W. Yu, M. ter Beest, F. Martin-Belmonte, A. Kierbel, J. Engel, and K. Mostov. 2006. Phosphatidylinositol-3,4,5-trisphosphate regulates the formation of the basolateral plasma membrane in epithelial cells. *Nat Cell Biol*. 8:963-970.

Gassler, N., C. Rohr, A. Schneider, J. Kartenbeck, A. Bach, N. Obermuller, H.F. Otto, and F. Autschbach. 2001. Inflammatory bowel disease is associated with changes of enterocytic junctions. *Am J Physiol Gastrointest Liver Physiol*. 281:G216-228.

Geisbrecht, E.R., and D.J. Montell. 2002. Myosin VI is required for E-cadherin-mediated border cell migration. *Nat Cell Biol*. 4:616-620.

Georgiou, M., and B. Baum. 2010. Polarity proteins and Rho GTPases cooperate to spatially organise epithelial actin-based protrusions. *J Cell Sci*. 123:1089-1098.

Gibson, F., J. Walsh, P. Mburu, A. Varela, K.A. Brown, M. Antonio, K.W. Beisel, K.P. Steel, and S.D. Brown. 1995. A type VII myosin encoded by the mouse deafness gene shaker-1. *Nature*. 374:62-64.

Gillespie, P.G., J.P. Albanesi, M. Bahler, W.M. Bement, J.S. Berg, D.R. Burgess, B. Burnside, R.E. Cheney, D.P. Corey, E. Coudrier, P. de Lanerolle, J.A. Hammer, T. Hasson, J.R. Holt, A.J. Hudspeth, M. Ikebe, J. Kendrick-Jones, E.D. Korn, R. Li, J.A. Mercer, R.A. Milligan, M.S. Mooseker, E.M. Ostap, C. Petit, T.D. Pollard, J.R. Sellers, T. Soldati, and M.A. Titus. 2001. Myosin-I nomenclature. *J Cell Biol*. 155:703-704.

Goligorsky, M.S., W. Lieberthal, L. Racusen, and E.E. Simon. 1993. Integrin receptors in renal tubular epithelium: new insights into pathophysiology of acute renal failure. *Am J Physiol*. 264:F1-8.

Golomb, E., X. Ma, S.S. Jana, Y.A. Preston, S. Kawamoto, N.G. Shoham, E. Goldin, M.A. Conti, J.R. Sellers, and R.S. Adelstein. 2004. Identification and characterization of nonmuscle myosin II-C, a new member of the myosin II family. *J Biol Chem*. 279:2800-2808.

Gonzalez-Mariscal, L., B. Chavez de Ramirez, and M. Cereijido. 1985. Tight junction formation in cultured epithelial cells (MDCK). *J Membr Biol*. 86:113-125.

Gorman, S.W., N.B. Haider, U. Grieshammer, R.E. Swiderski, E. Kim, J.W. Welch, C. Searby, S. Leng, R. Carmi, V.C. Sheffield, and D.M. Duhl. 1999. The cloning and developmental expression of unconventional myosin IXA (MYO9A) a gene in the Bardet-Biedl syndrome (BBS4) region at chromosome 15q22-q23. *Genomics*. 59:150-160.

Gumbiner, B., and K. Simons. 1986. A functional assay for proteins involved in establishing an epithelial occluding barrier: identification of a uvomorulin-like polypeptide. *J Cell Biol*. 102:457-468.

Gumbiner, B., and K. Simons. 1987. The role of uvomorulin in the formation of epithelial occluding junctions. *Ciba Found Symp*. 125:168-186.

Guo, Q., B. Xia, S. Moshiach, C. Xu, Y. Jiang, Y. Chen, Y. Sun, J.M. Lahti, and X.A. Zhang. 2008. The microenvironmental determinants for kidney epithelial cyst morphogenesis. *Eur J Cell Biol*. 87:251-266.

Haigo, S.L., and D. Bilder. 2011. Global tissue revolutions in a morphogenetic movement controlling elongation. *Science*. 331:1071-1074.

Halbleib, J.M., A.M. Saaf, P.O. Brown, and W.J. Nelson. 2007. Transcriptional modulation of genes encoding structural characteristics of differentiating enterocytes during development of a polarized epithelium in vitro. *Mol Biol Cell*. 18:4261-4278.

Hammond, D.E., R. Hyde, I. Kratchmarova, R.J. Beynon, B. Blagoev, and M.J. Clague. 2010. Quantitative analysis of HGF and EGF-dependent phosphotyrosine signaling networks. *J Proteome Res*. 9:2734-2742.

Hanono, A., D. Garbett, D. Reczek, D.N. Chambers, and A. Bretscher. 2006. EPI64 regulates microvillar subdomains and structure. *J Cell Biol*. 175:803-813.

Hao, Y., Q. Du, X. Chen, Z. Zheng, J.L. Balsbaugh, S. Maitra, J. Shabanowitz, D.F. Hunt, and I.G. Macara. 2010. Par3 controls epithelial spindle orientation by aPKC-mediated phosphorylation of apical Pins. *Curr Biol*. 20:1809-1818.

Harris, T.J., and U. Tepass. 2010. Adherens junctions: from molecules to morphogenesis. *Nat Rev Mol Cell Biol*. 11:502-514.

Hartman, M.A., D. Finan, S. Sivaramakrishnan, and J.A. Spudich. 2011. Principles of unconventional Myosin function and targeting. *Annu Rev Cell Dev Biol*. 27:133-155.

Hartsock, A., and W.J. Nelson. 2008. Adherens and tight junctions: structure, function and connections to the actin cytoskeleton. *Biochim Biophys Acta*. 1778:660-669.

Hasson, T. 2003. Myosin VI: two distinct roles in endocytosis. *J Cell Sci*. 116:3453-3461.

Hasson, T., M.B. Heintzelman, J. Santos-Sacchi, D.P. Corey, and M.S. Mooseker. 1995. Expression in cochlea and retina of myosin VIIa, the gene product defective in Usher syndrome type 1B. *Proc Natl Acad Sci U S A*. 92:9815-9819.

Hirokawa, N., and J.E. Heuser. 1981. Quick-freeze, deep-etch visualization of the cytoskeleton beneath surface differentiations of intestinal epithelial cells. *J Cell Biol*. 91:399-409.

Hirokawa, N., T.C. Keller, 3rd, R. Chasan, and M.S. Mooseker. 1983. Mechanism of brush border contractility studied by the quick-freeze, deep-etch method. *J Cell Biol*. 96:1325-1336.

Hirokawa, N., and L.G. Tilney. 1982. Interactions between actin filaments and between actin filaments and membranes in quick-frozen and deeply etched hair cells of the chick ear. *J Cell Biol*. 95:249-261.

Homma, K., J. Saito, R. Ikebe, and M. Ikebe. 2001. Motor function and regulation of myosin X. *J Biol Chem*. 276:34348-34354.

Hull, B.E., and L.A. Staehelin. 1979. The terminal web. A reevaluation of its structure and function. *J Cell Biol*. 81:67-82.

Iizumi, Y., H. Sagara, Y. Kabe, M. Azuma, K. Kume, M. Ogawa, T. Nagai, P.G. Gillespie, C. Sasakawa, and H. Handa. 2007. The enteropathogenic E. coli effector EspB facilitates microvillus effacing and antiphagocytosis by inhibiting myosin function. *Cell Host Microbe*. 2:383-392.

Irvine, E.J., and J.K. Marshall. 2000. Increased intestinal permeability precedes the onset of Crohn's disease in a subject with familial risk. *Gastroenterology*. 119:1740-1744.

Ivanov, A.I. 2008. Actin motors that drive formation and disassembly of epithelial apical junctions. *Front Biosci*. 13:6662-6681.

Ivanov, A.I., M. Bachar, B.A. Babbin, R.S. Adelstein, A. Nusrat, and C.A. Parkos. 2007. A unique role for nonmuscle myosin heavy chain IIA in regulation of epithelial apical junctions. *PLoS One*. 2:e658.

Ivanov, A.I., A.M. Hopkins, G.T. Brown, K. Gerner-Smidt, B.A. Babbin, C.A. Parkos, and A. Nusrat. 2008. Myosin II regulates the shape of three-dimensional intestinal epithelial cysts. *J Cell Sci*. 121:1803-1814.

Ivanov, A.I., D. Hunt, M. Utech, A. Nusrat, and C.A. Parkos. 2005. Differential roles for actin polymerization and a myosin II motor in assembly of the epithelial apical junctional complex. *Mol Biol Cell*. 16:2636-2650.

Ivanov, A.I., I.C. McCall, C.A. Parkos, and A. Nusrat. 2004. Role for actin filament turnover and a myosin II motor in cytoskeleton-driven disassembly of the epithelial apical junctional complex. *Mol Biol Cell*. 15:2639-2651.

Jaffe, A.B., and A. Hall. 2005. Rho GTPases: biochemistry and biology. *Annu Rev Cell Dev Biol*. 21:247-269.

Jaffe, A.B., N. Kaji, J. Durgan, and A. Hall. 2008. Cdc42 controls spindle orientation to position the apical surface during epithelial morphogenesis. *J Cell Biol*. 183:625-633.

Kametani, Y., and M. Takeichi. 2007. Basal-to-apical cadherin flow at cell junctions. *Nat Cell Biol*. 9:92-98.

Kellerman, P.S., R.A. Clark, C.A. Hoilien, S.L. Linas, and B.A. Molitoris. 1990. Role of microfilaments in maintenance of proximal tubule structural and functional integrity. *Am J Physiol*. 259:F279-285.

Kerber, M.L., and R.E. Cheney. 2011. Myosin-X: a MyTH-FERM myosin at the tips of filopodia. *J Cell Sci*. 124:3733-3741.

Kerber, M.L., D.T. Jacobs, L. Campagnola, B.D. Dunn, T. Yin, A.D. Sousa, O.A. Quintero, and R.E. Cheney. 2009. A novel form of motility in filopodia revealed by imaging myosin-X at the single-molecule level. *Curr Biol*. 19:967-973.

Kiehart, D.P., J.D. Franke, M.K. Chee, R.A. Montague, T.L. Chen, J. Roote, and M. Ashburner. 2004. Drosophila crinkled, mutations of which disrupt morphogenesis and cause lethality, encodes fly myosin VIIA. *Genetics*. 168:1337-1352.

Kitajiri, S., T. Sakamoto, I.A. Belyantseva, R.J. Goodyear, R. Stepanyan, I. Fujiwara, J.E. Bird, S. Riazuddin, Z.M. Ahmed, J.E. Hinshaw, J. Sellers, J.R. Bartles, J.A. Hammer, 3rd, G.P. Richardson, A.J. Griffith, G.I. Frolenkov, and T.B. Friedman. 2010. Actin-bundling protein TRIOBP forms resilient rootlets of hair cell stereocilia essential for hearing. *Cell*. 141:786-798.

Knight, P.J., K. Thirumurugan, Y. Yu, F. Wang, A.P. Kalverda, W.F. Stafford, 3rd, J.R. Sellers, and M. Peckham. 2005. The predicted coiled-coil domain of myosin 10 forms a novel elongated domain that lengthens the head. *J Biol Chem*. 280:34702-34708.

Kollmar, M. 2006. Thirteen is enough: the myosins of Dictyostelium discoideum and their light chains. *BMC Genomics*. 7:183.

Kovacs, M., J. Toth, C. Hetenyi, A. Malnasi-Csizmadia, and J.R. Sellers. 2004. Mechanism of blebbistatin inhibition of myosin II. *J Biol Chem*. 279:35557-35563.

Kovacs, M., F. Wang, A. Hu, Y. Zhang, and J.R. Sellers. 2003. Functional divergence of human cytoplasmic myosin II: kinetic characterization of the non-muscle IIA isoform. *J Biol Chem*. 278:38132-38140.

Kovacs, M., F. Wang, and J.R. Sellers. 2005. Mechanism of action of myosin X, a membrane-associated molecular motor. *J Biol Chem*. 280:15071-15083.

Krasnow, M.A., and W.J. Nelson. 2002. Tube morphogenesis. *Trends Cell Biol*. 12:351.

Krendel, M., S.V. Kim, T. Willinger, T. Wang, M. Kashgarian, R.A. Flavell, and M.S. Mooseker. 2009. Disruption of Myosin 1e promotes podocyte injury. *J Am Soc Nephrol*. 20:86-94.

Kussel-Andermann, P., A. El-Amraoui, S. Safieddine, S. Nouaille, I. Perfettini, M. Lecuit, P. Cossart, U. Wolfrum, and C. Petit. 2000. Vezatin, a novel transmembrane protein, bridges myosin VIIA to the cadherin-catenins complex. *EMBO J*. 19:6020-6029.

Kwon, M., S.A. Godinho, N.S. Chandhok, N.J. Ganem, A. Azioune, M. Thery, and D. Pellman. 2008. Mechanisms to suppress multipolar divisions in cancer cells with extra centrosomes. *Genes Dev*. 22:2189-2203.

Laprise, P., P. Chailler, M. Houde, J.F. Beaulieu, M.J. Boucher, and N. Rivard. 2002. Phosphatidylinositol 3-kinase controls human intestinal epithelial cell differentiation by promoting adherens junction assembly and p38 MAPK activation. *J Biol Chem*. 277:8226-8234.

Laukoetter, M.G., M. Bruewer, and A. Nusrat. 2006. Regulation of the intestinal epithelial barrier by the apical junctional complex. *Curr Opin Gastroenterol*. 22:85-89.

Liang, Y., A. Wang, I.A. Belyantseva, D.W. Anderson, F.J. Probst, T.D. Barber, W. Miller, J.W. Touchman, L. Jin, S.L. Sullivan, J.R. Sellers, S.A. Camper, R.V. Lloyd, B. Kachar, T.B. Friedman, and R.A. Fridell. 1999. Characterization of the human and mouse unconventional myosin XV genes responsible for hereditary deafness DFNB3 and shaker 2. *Genomics*. 61:243-258.

Liburd, N., M. Ghosh, S. Riazuddin, S. Naz, S. Khan, Z. Ahmed, Y. Liang, P.S. Menon, T. Smith, A.C. Smith, K.S. Chen, J.R. Lupski, E.R. Wilcox, L. Potocki, and T.B. Friedman. 2001. Novel mutations of MYO15A associated with profound deafness in consanguineous families and moderately severe hearing loss in a patient with Smith-Magenis syndrome. *Hum Genet*. 109:535-541.

Limouze, J., A.F. Straight, T. Mitchison, and J.R. Sellers. 2004. Specificity of blebbistatin, an inhibitor of myosin II. *J Muscle Res Cell Motil*. 25:337-341.

Lin, H.P., H.M. Chen, S.Y. Wei, L.Y. Chen, L.H. Chang, Y.J. Sun, S.Y. Huang, and J.C. Hsu. 2007. Cell adhesion molecule Echinoid associates with unconventional myosin VI/Jaguar motor to regulate cell morphology during dorsal closure in Drosophila. *Dev Biol*. 311:423-433.

Lincz, L.F., A. Buret, and G.F. Burns. 1997. Formation of spheroid structures in a human colon carcinoma cell line involves a complex series of intercellular rearrangements. *Differentiation*. 61:261-274.

Liu, K.C., D.T. Jacobs, B.D. Dunn, A.S. Fanning, and R.E. Cheney. 2012. Myosin-X Functions in Polarized Epithelial Cells. *Mol Biol Cell*. 23:1675-1687.

Liu, R., S. Woolner, J.E. Johndrow, D. Metzger, A. Flores, and S.M. Parkhurst. 2008. Sisyphus, the Drosophila myosin XV homolog, traffics within filopodia transporting key sensory and adhesion cargos. *Development*. 135:53-63.

Liu, X.Z., J. Walsh, P. Mburu, J. Kendrick-Jones, M.J. Cope, K.P. Steel, and S.D. Brown. 1997. Mutations in the myosin VIIA gene cause non-syndromic recessive deafness. *Nat Genet*. 16:188-190.

Lloyd, R.V., S. Vidal, L. Jin, S. Zhang, K. Kovacs, E. Horvath, B.W. Scheithauer, E.T. Boger, R.A. Fridell, and T.B. Friedman. 2001. Myosin XVA expression in the pituitary and in other neuroendocrine tissues and tumors. *Am J Pathol*. 159:1375-1382.

Lord, E., and W. Gates. 1929. Shaker, a new mutation of the house mouse. *Am Naturalist*. 63:435-442.

Lu, Q., J. Yu, J. Yan, Z. Wei, and M. Zhang. 2011. Structural basis of the myosin X PH1(N)-PH2-PH1(C) tandem as a specific and acute cellular PI(3,4,5)P(3) sensor. *Mol Biol Cell*. 22:4268-4278.

Luikart, B.W., W. Zhang, G.A. Wayman, C.H. Kwon, G.L. Westbrook, and L.F. Parada. 2008. Neurotrophin-dependent dendritic filopodial motility: a convergence on PI3K signaling. *J Neurosci*. 28:7006-7012.

Ma, X., J. Bao, and R.S. Adelstein. 2007. Loss of cell adhesion causes hydrocephalus in nonmuscle myosin II-B-ablated and mutated mice. *Mol Biol Cell*. 18:2305-2312.

Madara, J.L. 1987. Intestinal absorptive cell tight junctions are linked to cytoskeleton. *Am J Physiol*. 253:C171-175.

Madara, J.L. 1998. Regulation of the movement of solutes across tight junctions. *Annu Rev Physiol*. 60:143-159.

Madara, J.L., D. Barenberg, and S. Carlson. 1986. Effects of cytochalasin D on occluding junctions of intestinal absorptive cells: further evidence that the cytoskeleton may influence paracellular permeability and junctional charge selectivity. *J Cell Biol*. 102:2125-2136.

Maddugoda, M.P., M.S. Crampton, A.M. Shewan, and A.S. Yap. 2007. Myosin VI and vinculin cooperate during the morphogenesis of cadherin cell cell contacts in mammalian epithelial cells. *J Cell Biol*. 178:529-540.

Mahoney, P.A., U. Weber, P. Onofrechuk, H. Biessmann, P.J. Bryant, and C.S. Goodman. 1991. The fat tumor suppressor gene in Drosophila encodes a novel member of the cadherin gene superfamily. *Cell*. 67:853-868.

Mangold, S., S.K. Wu, S.J. Norwood, B.M. Collins, N.A. Hamilton, P. Thorn, and A.S. Yap. 2011. Hepatocyte growth factor acutely perturbs actin filament anchorage at the epithelial zonula adherens. *Curr Biol*. 21:503-507.

Manor, U., A. Disanza, M. Grati, L. Andrade, H. Lin, P.P. Di Fiore, G. Scita, and B. Kachar. 2011. Regulation of stereocilia length by myosin XVa and whirlin depends on the actin-regulatory protein Eps8. *Curr Biol*. 21:167-172.

Mao, Y., C. Rauskolb, E. Cho, W.L. Hu, H. Hayter, G. Minihan, F.N. Katz, and K.D. Irvine. 2006. Dachs: an unconventional myosin that functions downstream of Fat to regulate growth, affinity and gene expression in Drosophila. *Development*. 133:2539-2551.

Mao, Y., A.L. Tournier, P.A. Bates, J.E. Gale, N. Tapon, and B.J. Thompson. 2011. Planar polarization of the atypical myosin Dachs orients cell divisions in Drosophila. *Genes Dev*. 25:131-136.

Martin-Belmonte, F., A. Gassama, A. Datta, W. Yu, U. Rescher, V. Gerke, and K. Mostov. 2007. PTEN-mediated apical segregation of phosphoinositides controls epithelial morphogenesis through Cdc42. *Cell*. 128:383-397.

Mashanov, G.I., D. Tacon, M. Peckham, and J.E. Molloy. 2004. The spatial and temporal dynamics of pleckstrin homology domain binding at the plasma membrane measured by imaging single molecules in live mouse myoblasts. *J Biol Chem*. 279:15274-15280.

McCaffrey, L.M., and I.G. Macara. 2009. Widely conserved signaling pathways in the establishment of cell polarity. *Cold Spring Harb Perspect Biol*. 1:a001370.

McCarthy, K.M., S.A. Francis, J.M. McCormack, J. Lai, R.A. Rogers, I.B. Skare, R.D. Lynch, and E.E. Schneeberger. 2000. Inducible expression of claudin-1-myc but not occludin-VSV-G results in aberrant tight junction strand formation in MDCK cells. *J Cell Sci*. 113 Pt 19:3387-3398.

McConnell, R.E., A.E. Benesh, S. Mao, D.L. Tabb, and M.J. Tyska. 2011. Proteomic analysis of the enterocyte brush border. *Am J Physiol Gastrointest Liver Physiol*. 300:G914-926.

McConnell, R.E., and M.J. Tyska. 2007. Myosin-1a powers the sliding of apical membrane along microvillar actin bundles. *J Cell Biol*. 177:671-681.

McNeil, E., C.T. Capaldo, and I.G. Macara. 2006. Zonula occludens-1 function in the assembly of tight junctions in Madin-Darby canine kidney epithelial cells. *Mol Biol Cell*. 17:1922-1932.

Mele, C., P. Iatropoulos, R. Donadelli, A. Calabria, R. Maranta, P. Cassis, S. Buelli, S. Tomasoni, R. Piras, M. Krendel, S. Bettoni, M. Morigi, M. Delledonne, C. Pecoraro, I. Abbate, M.R. Capobianchi, F. Hildebrandt, E. Otto, F. Schaefer, F. Macciardi, F. Ozaltin, S. Emre, T. Ibsirlioglu, A. Benigni, G. Remuzzi, and M. Noris. 2011. MYO1E mutations and childhood familial focal segmental glomerulosclerosis. *N Engl J Med*. 365:295-306.

Mermall, V., P.L. Post, and M.S. Mooseker. 1998. Unconventional myosins in cell movement, membrane traffic, and signal transduction. *Science*. 279:527-533.

Millo, H., K. Leaper, V. Lazou, and M. Bownes. 2004. Myosin VI plays a role in cell-cell adhesion during epithelial morphogenesis. *Mech Dev*. 121:1335-1351.

Molitoris, B.A. 1991. Ischemia-induced loss of epithelial polarity: potential role of the actin cytoskeleton. *Am J Physiol*. 260:F769-778.

Mooseker, M.S. 1985. Organization, chemistry, and assembly of the cytoskeletal apparatus of the intestinal brush border. *Annu Rev Cell Biol*. 1:209-241.

Mooseker, M.S., and L.G. Tilney. 1975. Organization of an actin filament-membrane complex. Filament polarity and membrane attachment in the microvilli of intestinal epithelial cells. *J Cell Biol*. 67:725-743.

Morris, S.M., S.D. Arden, R.C. Roberts, J. Kendrick-Jones, J.A. Cooper, J.P. Luzio, and F. Buss. 2002. Myosin VI binds to and localises with Dab2, potentially linking receptor-mediated endocytosis and the actin cytoskeleton. *Traffic*. 3:331-341.

Mukherjee, T.M., and L.A. Staehelin. 1971. The fine-structural organization of the brush border of intestinal epithelial cells. *J Cell Sci*. 8:573-599.

Muller, T., M.W. Hess, N. Schiefermeier, K. Pfaller, H.L. Ebner, P. Heinz-Erian, H. Ponstingl, J. Partsch, B. Rollinghoff, H. Kohler, T. Berger, H. Lenhartz, B. Schlenck, R.J. Houwen, C.J. Taylor, H. Zoller, S. Lechner, O. Goulet, G. Utermann, F.M. Ruemmele, L.A. Huber, and A.R. Janecke. 2008. MYO5B mutations cause microvillus inclusion disease and disrupt epithelial cell polarity. *Nat Genet*. 40:1163-1165.

Muza-Moons, M.M., E.E. Schneeberger, and G.A. Hecht. 2004. Enteropathogenic Escherichia coli infection leads to appearance of aberrant tight junctions strands in the lateral membrane of intestinal epithelial cells. *Cell Microbiol*. 6:783-793.

Nagy, S., B.L. Ricca, M.F. Norstrom, D.S. Courson, C.M. Brawley, P.A. Smithback, and R.S. Rock. 2008. A myosin motor that selects bundled actin for motility. *Proc Natl Acad Sci U S A*. 105:9616-9620.

Nal, N., Z.M. Ahmed, E. Erkal, O.M. Alper, G. Luleci, O. Dinc, A.M. Waryah, Q. Ain, S. Tasneem, T. Husnain, P. Chattaraj, S. Riazuddin, E. Boger, M. Ghosh, M. Kabra, R.J. Morell, and T.B. Friedman. 2007. Mutational spectrum of MYO15A: the large N-terminal extension of myosin XVA is required for hearing. *Hum Mutat*. 28:1014-1019.

Nambiar, R., R.E. McConnell, and M.J. Tyska. 2010. Myosin motor function: the ins and outs of actin-based membrane protrusions. *Cell Mol Life Sci*. 67:1239-1254.

Nelson, W.J. 2008. Regulation of cell-cell adhesion by the cadherin-catenin complex. *Biochem Soc Trans*. 36:149-155.

Nielsen, J.S., M.L. Graves, S. Chelliah, A.W. Vogl, C.D. Roskelley, and K.M. McNagny. 2007. The CD34-related molecule podocalyxin is a potent inducer of microvillus formation. *PLoS One*. 2:e237.

Nielsen, S., J. Frokiaer, D. Marples, T.H. Kwon, P. Agre, and M.A. Knepper. 2002. Aquaporins in the kidney: from molecules to medicine. *Physiol Rev*. 82:205-244.

Nishikawa, S., K. Homma, Y. Komori, M. Iwaki, T. Wazawa, A. Hikikoshi Iwane, J. Saito, R. Ikebe, E. Katayama, T. Yanagida, and M. Ikebe. 2002. Class VI myosin moves processively along actin filaments backward with large steps. *Biochem Biophys Res Commun*. 290:311-317.

Noguchi, T., M. Lenartowska, and K.G. Miller. 2006. Myosin VI stabilizes an actin network during Drosophila spermatid individualization. *Mol Biol Cell*. 17:2559-2571.

Ojakian, G.K., and R. Schwimmer. 1994. Regulation of epithelial cell surface polarity reversal by beta 1 integrins. *J Cell Sci*. 107 (Pt 3):561-576.

Olson, A.D., T. Pysher, and R.S. Bienkowski. 1991. Organization of intestinal epithelial cells into multicellular structures requires laminin and functional actin microfilaments. *Exp Cell Res*. 192:543-549.

Omelchenko, T., and A. Hall. 2012. Myosin-IXA Regulates Collective Epithelial Cell Migration by Targeting RhoGAP Activity to Cell-Cell Junctions. *Curr Biol*. 22:278-288.

Oshitani, N., K. Watanabe, S. Nakamura, Y. Fujiwara, K. Higuchi, and T. Arakawa. 2005. Dislocation of tight junction proteins without F-actin disruption in inactive Crohn's disease. *Int J Mol Med*. 15:407-410.

Perantoni, A., and J.J. Berman. 1979. Properties of Wilms' tumor line (TuWi) and pig kidney line (LLC-PK1) typical of normal kidney tubular epithelium. *In Vitro*. 15:446-454.

Perez-Moreno, M., C. Jamora, and E. Fuchs. 2003. Sticky business: orchestrating cellular signals at adherens junctions. *Cell*. 112:535-548.

Peterson, M.D., W.M. Bement, and M.S. Mooseker. 1993. An in vitro model for the analysis of intestinal brush border assembly. II. Changes in expression and localization of brush border proteins during cell contact-induced brush border assembly in Caco-2BBe cells. *J Cell Sci*. 105:461-472.

Peterson, M.D., and M.S. Mooseker. 1992. Characterization of the enterocyte-like brush border cytoskeleton of the C2BBe clones of the human intestinal cell line, Caco-2. *J Cell Sci*. 102 (Pt 3):581-600.

Peterson, M.D., and M.S. Mooseker. 1993. An in vitro model for the analysis of intestinal brush border assembly. I. Ultrastructural analysis of cell contact-induced brush border assembly in Caco-2BBe cells. *J Cell Sci*. 105 (Pt 2):445-460.

Phichith, D., M. Travaglia, Z. Yang, X. Liu, A.B. Zong, D. Safer, and H.L. Sweeney. 2009. Cargo binding induces dimerization of myosin VI. *Proc Natl Acad Sci U S A*. 106:17320-17324.

Pi, X., R. Ren, R. Kelley, C. Zhang, M. Moser, A.B. Bohil, M. Divito, R.E. Cheney, and C. Patterson. 2007. Sequential roles for myosin-X in BMP6-dependent filopodial extension, migration, and activation of BMP receptors. *J Cell Biol*. 179:1569-1582.

Plantard, L., A. Arjonen, J.G. Lock, G. Nurani, J. Ivaska, and S. Stromblad. 2010. PtdIns(3,4,5)P is a regulator of myosin-X localization and filopodia formation. *J Cell Sci*. 123:3525-3534.

Podolsky, D.K. 2002. Inflammatory bowel disease. *N Engl J Med*. 347:417-429.

Probst, F.J., R.A. Fridell, Y. Raphael, T.L. Saunders, A. Wang, Y. Liang, R.J. Morell, J.W. Touchman, R.H. Lyons, K. Noben-Trauth, T.B. Friedman, and S.A. Camper. 1998. Correction of deafness in shaker-2 mice by an unconventional myosin in a BAC transgene. *Science*. 280:1444-1447.

Qin, Y., W.H. Meisen, Y. Hao, and I.G. Macara. 2010. Tuba, a Cdc42 GEF, is required for polarized spindle orientation during epithelial cyst formation. *J Cell Biol*. 189:661-669.

Redowicz, M.J. 2001. Regulation of nonmuscle myosins by heavy chain phosphorylation. *J Muscle Res Cell Motil*. 22:163-173.

Reinhard, J., A.A. Scheel, D. Diekmann, A. Hall, C. Ruppert, and M. Bahler. 1995. A novel type of myosin implicated in signalling by rho family GTPases. *EMBO J*. 14:697-704.

Ridley, A.J. 1996. Rho: theme and variations. *Curr Biol*. 6:1256-1264.

Robblee, J.P., A.O. Olivares, and E.M. de la Cruz. 2004. Mechanism of nucleotide binding to actomyosin VI: evidence for allosteric head-head communication. *J Biol Chem*. 279:38608-38617.

Rock, R.S., S.E. Rice, A.L. Wells, T.J. Purcell, J.A. Spudich, and H.L. Sweeney. 2001. Myosin VI is a processive motor with a large step size. *Proc Natl Acad Sci U S A*. 98:13655-13659.

Rodriguez-Fraticelli, A.E., S. Vergarajauregui, D.J. Eastburn, A. Datta, M.A. Alonso, K. Mostov, and F. Martin-Belmonte. 2010. The Cdc42 GEF Intersectin 2 controls mitotic spindle orientation to form the lumen during epithelial morphogenesis. *J Cell Biol*. 189:725-738.

Rogers, M.S., and E.E. Strehler. 2001. The tumor-sensitive calmodulin-like protein is a specific light chain of human unconventional myosin X. *J Biol Chem*. 276:12182-12189.

Rogulja, D., C. Rauskolb, and K.D. Irvine. 2008. Morphogen control of wing growth through the Fat signaling pathway. *Dev Cell*. 15:309-321.

Roland, J.T., D.M. Bryant, A. Datta, A. Itzen, K.E. Mostov, and J.R. Goldenring. 2011. Rab GTPase-Myo5B complexes control membrane recycling and epithelial polarization. *Proc Natl Acad Sci U S A*. 108:2789-2794.

Rosenfeld, S.S., J. Xing, L.Q. Chen, and H.L. Sweeney. 2003. Myosin IIb is unconventionally conventional. *J Biol Chem*. 278:27449-27455.

Rubinson, D.A., C.P. Dillon, A.V. Kwiatkowski, C. Sievers, L. Yang, J. Kopinja, D.L. Rooney, M. Zhang, M.M. Ihrig, M.T. McManus, F.B. Gertler, M.L. Scott, and L. Van Parijs. 2003. A lentivirus-based system to functionally silence genes in primary mammalian cells, stem cells and transgenic mice by RNA interference. *Nat Genet*. 33:401-406.

Sahly, I., A. El-Amraoui, M. Abitbol, C. Petit, and J.L. Dufier. 1997. Expression of myosin VIIA during mouse embryogenesis. *Anat Embryol (Berl)*. 196:159-170.

Sakai, T., N. Umeki, R. Ikebe, and M. Ikebe. 2011. Cargo binding activates myosin VIIA motor function in cells. *Proc Natl Acad Sci U S A*. 108:7028-7033.

Saotome, I., M. Curto, and A.I. McClatchey. 2004. Ezrin is essential for epithelial organization and villus morphogenesis in the developing intestine. *Dev Cell*. 6:855-864.

Sasaki, H., C. Matsui, K. Furuse, Y. Mimori-Kiyosue, M. Furuse, and S. Tsukita. 2003. Dynamic behavior of paired claudin strands within apposing plasma membranes. *Proc Natl Acad Sci U S A*. 100:3971-3976.

Schluter, M.A., C.S. Pfarr, J. Pieczynski, E.L. Whiteman, T.W. Hurd, S. Fan, C.J. Liu, and B. Margolis. 2009. Trafficking of Crumbs3 during cytokinesis is crucial for lumen formation. *Mol Biol Cell*. 20:4652-4663.

Schneeberger, E.E., and R.D. Lynch. 2004. The tight junction: a multifunctional complex. *Am J Physiol Cell Physiol*. 286:C1213-1228.

Schoenenberger, C.A., A. Zuk, G.M. Zinkl, D. Kendall, and K.S. Matlin. 1994. Integrin expression and localization in normal MDCK cells and transformed MDCK cells lacking apical polarity. *J Cell Sci*. 107 (Pt 2):527-541.

Schoumacher, M., R.D. Goldman, D. Louvard, and D.M. Vignjevic. 2010. Actin, microtubules, and vimentin intermediate filaments cooperate for elongation of invadopodia. *J Cell Biol*. 189:541-556.

Schreider, C., G. Peignon, S. Thenet, J. Chambaz, and M. Pincon-Raymond. 2002. Integrin-mediated functional polarization of Caco-2 cells through E-cadherin--actin complexes. *J Cell Sci*. 115:543-552.

Seiler, C., O. Ben-David, S. Sidi, O. Hendrich, A. Rusch, B. Burnside, K.B. Avraham, and T. Nicolson. 2004. Myosin VI is required for structural integrity of the apical surface of sensory hair cells in zebrafish. *Dev Biol*. 272:328-338.

Self, T., M. Mahony, J. Fleming, J. Walsh, S.D. Brown, and K.P. Steel. 1998. Shaker-1 mutations reveal roles for myosin VIIA in both development and function of cochlear hair cells. *Development*. 125:557-566.

Self, T., T. Sobe, N.G. Copeland, N.A. Jenkins, K.B. Avraham, and K.P. Steel. 1999. Role of myosin VI in the differentiation of cochlear hair cells. *Dev Biol*. 214:331-341.

Senften, M., M. Schwander, P. Kazmierczak, C. Lillo, J.B. Shin, T. Hasson, G.S. Geleoc, P.G. Gillespie, D. Williams, J.R. Holt, and U. Muller. 2006. Physical and functional interaction between protocadherin 15 and myosin VIIa in mechanosensory hair cells. *J Neurosci*. 26:2060-2071.

Shearer, A.E., M.S. Hildebrand, J.A. Webster, K. Kahrizi, N.C. Meyer, K. Jalalvand, S. Arzhanginy, W.J. Kimberling, D. Stephan, M. Bahlo, R.J. Smith, and H. Najmabadi. 2009. Mutations in the first MyTH4 domain of MYO15A are a common cause of DFNB3 hearing loss. *Laryngoscope*. 119:727-733.

Shen, L., E.D. Black, E.D. Witkowski, W.I. Lencer, V. Guerriero, E.E. Schneeberger, and J.R. Turner. 2006. Myosin light chain phosphorylation regulates barrier function by remodeling tight junction structure. *J Cell Sci*. 119:2095-2106.

Shen, L., and J.R. Turner. 2005. Actin depolymerization disrupts tight junctions via caveolae-mediated endocytosis. *Mol Biol Cell*. 16:3919-3936.

Shen, L., C.R. Weber, D.R. Raleigh, D. Yu, and J.R. Turner. 2011. Tight junction pore and leak pathways: a dynamic duo. *Annu Rev Physiol*. 73:283-309.

Shewan, A.M., M. Maddugoda, A. Kraemer, S.J. Stehbens, S. Verma, E.M. Kovacs, and A.S. Yap. 2005. Myosin 2 is a key Rho kinase target necessary for the local concentration of E-cadherin at cell-cell contacts. *Mol Biol Cell*. 16:4531-4542.

Shifflett, D.E., D.R. Clayburgh, A. Koutsouris, J.R. Turner, and G.A. Hecht. 2005. Enteropathogenic E. coli disrupts tight junction barrier function and structure in vivo. *Lab Invest*. 85:1308-1324.

Shin, K., S. Straight, and B. Margolis. 2005. PATJ regulates tight junction formation and polarity in mammalian epithelial cells. *J Cell Biol*. 168:705-711.

Simons, M., M. Wang, O.W. McBride, S. Kawamoto, K. Yamakawa, D. Gdula, R.S. Adelstein, and L. Weir. 1991. Human nonmuscle myosin heavy chains are encoded by two genes located on different chromosomes. *Circ Res*. 69:530-539.

Skowron, J.F., W.M. Bement, and M.S. Mooseker. 1998. Human brush border myosin-I and myosin-Ic expression in human intestine and Caco-2BBe cells. *Cell Motil Cytoskeleton*. 41:308-324.

Smutny, M., H.L. Cox, J.M. Leerberg, E.M. Kovacs, M.A. Conti, C. Ferguson, N.A. Hamilton, R.G. Parton, R.S. Adelstein, and A.S. Yap. 2010. Myosin II isoforms identify distinct functional modules that support integrity of the epithelial zonula adherens. *Nat Cell Biol*. 12:696-702.

Smutny, M., S.K. Wu, G.A. Gomez, S. Mangold, A.S. Yap, and N.A. Hamilton. 2011. Multicomponent analysis of junctional movements regulated by myosin II isoforms at the epithelial zonula adherens. *PLoS One*. 6:e22458.

Soldati, T. 2003. Unconventional myosins, actin dynamics and endocytosis: a menage a trois? *Traffic*. 4:358-366.

Sousa, A.D., and R.E. Cheney. 2005. Myosin-X: a molecular motor at the cell's fingertips. *Trends Cell Biol*. 15:533-539.

Sousa, S., D. Cabanes, A. El-Amraoui, C. Petit, M. Lecuit, and P. Cossart. 2004. Unconventional myosin VIIa and vezatin, two proteins crucial for Listeria entry into epithelial cells. *J Cell Sci*. 117:2121-2130.

Stafford, W.F., M.L. Walker, J.A. Trinick, and L.M. Coluccio. 2005. Mammalian class I myosin, Myo1b, is monomeric and cross-links actin filaments as determined by hydrodynamic studies and electron microscopy. *Biophys J*. 88:384-391.

Stevenson, B.R., and D.A. Begg. 1994. Concentration-dependent effects of cytochalasin D on tight junctions and actin filaments in MDCK epithelial cells. *J Cell Sci*. 107 (Pt 3):367-375.

Stevenson, B.R., J.D. Siliciano, M.S. Mooseker, and D.A. Goodenough. 1986. Identification of ZO-1: a high molecular weight polypeptide associated with the tight junction (zonula occludens) in a variety of epithelia. *J Cell Biol*. 103:755-766.

Sun, Y., O. Sato, F. Ruhnow, M.E. Arsenault, M. Ikebe, and Y.E. Goldman. 2010. Single-molecule stepping and structural dynamics of myosin X. *Nat Struct Mol Biol*. 17:485-491.

Svitkina, T.M., A.B. Verkhovsky, K.M. McQuade, and G.G. Borisy. 1997. Analysis of the actin-myosin II system in fish epidermal keratocytes: mechanism of cell body translocation. *J Cell Biol*. 139:397-415.

Tacon, D., P.J. Knight, and M. Peckham. 2004. Imaging myosin 10 in cells. *Biochem Soc Trans*. 32:689-693.

Takai, Y., and H. Nakanishi. 2003. Nectin and afadin: novel organizers of intercellular junctions. *J Cell Sci*. 116:17-27.

Tanner, K., H. Mori, R. Mroue, A. Bruni-Cardoso, and M.J. Bissell. 2012. Coherent angular motion in the establishment of multicellular architecture of glandular tissues. *Proc Natl Acad Sci U S A*. 109:1973-1978.

Terry, S.J., C. Zihni, A. Elbediwy, E. Vitiello, I.V. Leefa Chong San, M.S. Balda, and K. Matter. 2011. Spatially restricted activation of RhoA signalling at epithelial junctions by p114RhoGEF drives junction formation and morphogenesis. *Nat Cell Biol*. 13:159-166.

Tilney, L.G., P.S. Connelly, and G.M. Guild. 2004. Microvilli appear to represent the first step in actin bundle formation in Drosophila bristles. *J Cell Sci*. 117:3531-3538.

Todi, S.V., J.D. Franke, D.P. Kiehart, and D.F. Eberl. 2005. Myosin VIIA defects, which underlie the Usher 1B syndrome in humans, lead to deafness in Drosophila. *Curr Biol*. 15:862-868.

Tokuo, H., and M. Ikebe. 2004. Myosin X transports Mena/VASP to the tip of filopodia. *Biochem Biophys Res Commun*. 319:214-220.

Tokuo, H., K. Mabuchi, and M. Ikebe. 2007. The motor activity of myosin-X promotes actin fiber convergence at the cell periphery to initiate filopodia formation. *J Cell Biol*. 179:229-238.

Toyoshima, F., and E. Nishida. 2007. Integrin-mediated adhesion orients the spindle parallel to the substratum in an EB1- and myosin X-dependent manner. *EMBO J*. 26:1487-1498.

Trepat, X., and J.J. Fredberg. 2011. Plithotaxis and emergent dynamics in collective cellular migration. *Trends Cell Biol*. 21:638-646.

Troeger, H., H.J. Epple, T. Schneider, U. Wahnschaffe, R. Ullrich, G.D. Burchard, T. Jelinek, M. Zeitz, M. Fromm, and J.D. Schulzke. 2007. Effect of chronic Giardia lamblia infection on epithelial transport and barrier function in human duodenum. *Gut*. 56:328-335.

Turunen, O., M. Sainio, J. Jaaskelainen, O. Carpen, and A. Vaheri. 1998. Structure-function relationships in the ezrin family and the effect of tumor-associated point mutations in neurofibromatosis 2 protein. *Biochim Biophys Acta*. 1387:1-16.

Tuxworth, R.I., and M.A. Titus. 2000. Unconventional myosins: anchors in the membrane traffic relay. *Traffic*. 1:11-18.

Tyska, M.J., A.T. Mackey, J.D. Huang, N.G. Copeland, N.A. Jenkins, and M.S. Mooseker. 2005. Myosin-1a is critical for normal brush border structure and composition. *Mol Biol Cell*. 16:2443-2457.

Tzolovsky, G., H. Millo, S. Pathirana, T. Wood, and M. Bownes. 2002. Identification and phylogenetic analysis of Drosophila melanogaster myosins. *Mol Biol Evol*. 19:1041-1052.

Uhlen, M., E. Bjorling, C. Agaton, C.A. Szigyarto, B. Amini, E. Andersen, A.C. Andersson, P. Angelidou, A. Asplund, C. Asplund, L. Berglund, K. Bergstrom, H. Brumer, D. Cerjan, M. Ekstrom, A. Elobeid, C. Eriksson, L. Fagerberg, R. Falk, J. Fall, M. Forsberg, M.G. Bjorklund, K. Gumbel, A. Halimi, I. Hallin, C. Hamsten, M. Hansson, M. Hedhammar, G. Hercules, C. Kampf, K. Larsson, M. Lindskog, W. Lodewyckx, J. Lund, J. Lundeberg, K. Magnusson, E. Malm, P. Nilsson, J. Odling, P. Oksvold, I. Olsson, E. Oster, J. Ottosson, L. Paavilainen, A. Persson, R. Rimini, J. Rockberg, M. Runeson, A. Sivertsson, A. Skollermo, J. Steen, M. Stenvall, F. Sterky, S. Stromberg, M. Sundberg, H. Tegel, S. Tourle, E. Wahlund, A. Walden, J. Wan, H. Wernerus, J. Westberg, K. Wester, U. Wrethagen, L.L. Xu, S. Hober, and F. Ponten. 2005. A human protein atlas for normal and cancer tissues based on antibody proteomics. *Mol Cell Proteomics*. 4:1920-1932.

Umeda, K., T. Matsui, M. Nakayama, K. Furuse, H. Sasaki, M. Furuse, and S. Tsukita. 2004. Establishment and characterization of cultured epithelial cells lacking expression of ZO-1. *J Biol Chem*. 279:44785-44794.

Umeki, N., H.S. Jung, T. Sakai, O. Sato, R. Ikebe, and M. Ikebe. 2011. Phospholipid-dependent regulation of the motor activity of myosin X. *Nat Struct Mol Biol*. 18:783-788.

Umeki, N., H.S. Jung, S. Watanabe, T. Sakai, X.D. Li, R. Ikebe, R. Craig, and M. Ikebe. 2009. The tail binds to the head-neck domain, inhibiting ATPase activity of myosin VIIA. *Proc Natl Acad Sci U S A*. 106:8483-8488.

Vaezi, A., C. Bauer, V. Vasioukhin, and E. Fuchs. 2002. Actin cable dynamics and Rho/Rock orchestrate a polarized cytoskeletal architecture in the early steps of assembling a stratified epithelium. *Dev Cell*. 3:367-381.

Van Itallie, C.M., and J.M. Anderson. 2006. Claudins and epithelial paracellular transport. *Annu Rev Physiol*. 68:403-429.

Van Itallie, C.M., A.S. Fanning, A. Bridges, and J.M. Anderson. 2009. ZO-1 stabilizes the tight junction solute barrier through coupling to the perijunctional cytoskeleton. *Mol Biol Cell*. 20:3930-3940.

Vasioukhin, V., C. Bauer, M. Yin, and E. Fuchs. 2000. Directed actin polymerization is the driving force for epithelial cell-cell adhesion. *Cell*. 100:209-219.

Velichkova, M., J. Guttman, C. Warren, L. Eng, K. Kline, A.W. Vogl, and T. Hasson. 2002. A human homologue of Drosophila kelch associates with myosin-VIIa in specialized adhesion junctions. *Cell Motil Cytoskeleton*. 51:147-164.

Waddington, C. 1940. The genetic control of wing development in Drosophila. *J Genet*. 45:75-139.

Wakabayashi, Y., Y. Takahashi, Y. Kikkawa, H. Okano, Y. Mishima, T. Ushiki, H. Yonekawa, and R. Kominami. 1998. A novel type of myosin encoded by the mouse deafness gene shaker-2. *Biochem Biophys Res Commun*. 248:655-659.

Wang, A., Y. Liang, R.A. Fridell, F.J. Probst, E.R. Wilcox, J.W. Touchman, C.C. Morton, R.J. Morell, K. Noben-Trauth, S.A. Camper, and T.B. Friedman. 1998. Association of unconventional myosin MYO15 mutations with human nonsyndromic deafness DFNB3. *Science*. 280:1447-1451.

Wang, F., M. Kovacs, A. Hu, J. Limouze, E.V. Harvey, and J.R. Sellers. 2003. Kinetic mechanism of non-muscle myosin IIB: functional adaptations for tension generation and maintenance. *J Biol Chem*. 278:27439-27448.

Watanabe, S., R. Ikebe, and M. Ikebe. 2006. Drosophila myosin VIIA is a high duty ratio motor with a unique kinetic mechanism. *J Biol Chem*. 281:7151-7160.

Watanabe, T.M., H. Tokuo, K. Gonda, H. Higuchi, and M. Ikebe. 2010. Myosin-X induces filopodia by multiple elongation mechanism. *J Biol Chem*. 285:19605-19614.

Watton, S.J., and J. Downward. 1999. Akt/PKB localisation and 3' phosphoinositide generation at sites of epithelial cell-matrix and cell-cell interaction. *Curr Biol*. 9:433-436.

Weber, K.L., A.M. Sokac, J.S. Berg, R.E. Cheney, and W.M. Bement. 2004. A microtubule-binding myosin required for nuclear anchoring and spindle assembly. *Nature*. 431:325-329.

Wei, S.Y., L.M. Escudero, F. Yu, L.H. Chang, L.Y. Chen, Y.H. Ho, C.M. Lin, C.S. Chou, W. Chia, J. Modolell, and J.C. Hsu. 2005. Echinoid is a component of adherens junctions that cooperates with DE-Cadherin to mediate cell adhesion. *Dev Cell*. 8:493-504.

Wei, Z., J. Yan, Q. Lu, L. Pan, and M. Zhang. 2011. Cargo recognition mechanism of myosin X revealed by the structure of its tail MyTH4-FERM tandem in complex with the DCC P3 domain. *Proc Natl Acad Sci U S A*. 108:3572-3577.

Weil, D., S. Blanchard, J. Kaplan, P. Guilford, F. Gibson, J. Walsh, P. Mburu, A. Varela, J. Levilliers, M.D. Weston, and et al. 1995. Defective myosin VIIA gene responsible for Usher syndrome type 1B. *Nature*. 374:60-61.

Weil, D., G. Levy, I. Sahly, F. Levi-Acobas, S. Blanchard, A. El-Amraoui, F. Crozet, H. Philippe, M. Abitbol, and C. Petit. 1996. Human myosin VIIA responsible for the Usher 1B syndrome: a predicted membrane-associated motor protein expressed in developing sensory epithelia. *Proc Natl Acad Sci U S A*. 93:3232-3237.

Wells, A.L., A.W. Lin, L.Q. Chen, D. Safer, S.M. Cain, T. Hasson, B.O. Carragher, R.A. Milligan, and H.L. Sweeney. 1999. Myosin VI is an actin-based motor that moves backwards. *Nature*. 401:505-508.

Weston, M.D., P.M. Kelley, L.D. Overbeck, M. Wagenaar, D.J. Orten, T. Hasson, Z.Y. Chen, D. Corey, M. Mooseker, J. Sumegi, C. Cremers, C. Moller, S.G. Jacobson, M.B. Gorin, and W.J. Kimberling. 1996. Myosin VIIA mutation screening in 189 Usher syndrome type 1 patients. *Am J Hum Genet*. 59:1074-1083.

Williams, M.J., and P. Clark. 2003. Microscopic analysis of the cellular events during scatter factor/hepatocyte growth factor-induced epithelial tubulogenesis. *J Anat*. 203:483-503.

Wolfrum, U., X. Liu, A. Schmitt, I.P. Udovichenko, and D.S. Williams. 1998. Myosin VIIa as a common component of cilia and microvilli. *Cell Motil Cytoskeleton*. 40:261-271.

Woolner, S., and W.M. Bement. 2009. Unconventional myosins acting unconventionally. *Trends Cell Biol*. 19:245-252.

Woolner, S., L.L. O'Brien, C. Wiese, and W.M. Bement. 2008. Myosin-10 and actin filaments are essential for mitotic spindle function. *J Cell Biol*. 182:77-88.

Woolner, S., and N. Papalopulu. 2012. Spindle Position in Symmetric Cell Divisions during Epiboly Is Controlled by Opposing and Dynamic Apicobasal Forces. *Dev Cell*. 24:775-787.

Wu, L., L. Pan, Z. Wei, and M. Zhang. 2011. Structure of MyTH4-FERM domains in myosin VIIa tail bound to cargo. *Science*. 331:757-760.

Yamada, S., S. Pokutta, F. Drees, W.I. Weis, and W.J. Nelson. 2005. Deconstructing the cadherin-catenin-actin complex. *Cell*. 123:889-901.

Yang, Y., M. Kovacs, T. Sakamoto, F. Zhang, D.P. Kiehart, and J.R. Sellers. 2006. Dimerized Drosophila myosin VIIa: a processive motor. *Proc Natl Acad Sci U S A*. 103:5746-5751.

Yonezawa, S., N. Yoshizaki, M. Sano, A. Hanai, S. Masaki, T. Takizawa, T. Kageyama, and A. Moriyama. 2003. Possible involvement of myosin-X in intercellular adhesion: importance of serial pleckstrin homology regions for intracellular localization. *Dev Growth Differ*. 45:175-185.

Yu, W., L.E. O'Brien, F. Wang, H. Bourne, K.E. Mostov, and M.M. Zegers. 2003. Hepatocyte growth factor switches orientation of polarity and mode of movement during morphogenesis of multicellular epithelial structures. *Mol Biol Cell*. 14:748-763.

Zhang, F.R., L.H. Tao, Z.Y. Shen, Z. Lv, L.Y. Xu, and E.M. Li. 2008. Fascin expression in human embryonic, fetal, and normal adult tissue. *J Histochem Cytochem*. 56:193-199.

Zhang, H., J.S. Berg, Z. Li, Y. Wang, P. Lang, A.D. Sousa, A. Bhaskar, R.E. Cheney, and S. Stromblad. 2004. Myosin-X provides a motor-based link between integrins and the cytoskeleton. *Nat Cell Biol*. 6:523-531.

Zhang, J., M. Betson, J. Erasmus, K. Zeikos, M. Bailly, L.P. Cramer, and V.M. Braga. 2005. Actin at cell-cell junctions is composed of two dynamic and functional populations. *J Cell Sci*. 118:5549-5562.

Zheng, Z., H. Zhu, Q. Wan, J. Liu, Z. Xiao, D.P. Siderovski, and Q. Du. 2010. LGN regulates mitotic spindle orientation during epithelial morphogenesis. *J Cell Biol*. 189:275-288.